



University of Pennsylvania
ScholarlyCommons


Publicly Accessible Penn Dissertations

2021

State Transitions Within The Cortex Are Strongly Influenced By Local Interactions Under General Anesthesia

Brenna Shortal
University of Pennsylvania

Follow this and additional works at: <https://repository.upenn.edu/edissertations>

 Part of the [Neuroscience and Neurobiology Commons](#)

Recommended Citation

Shortal, Brenna, "State Transitions Within The Cortex Are Strongly Influenced By Local Interactions Under General Anesthesia" (2021). *Publicly Accessible Penn Dissertations*. 5406.
<https://repository.upenn.edu/edissertations/5406>

This paper is posted at ScholarlyCommons. <https://repository.upenn.edu/edissertations/5406>
For more information, please contact repository@pobox.upenn.edu.

State Transitions Within The Cortex Are Strongly Influenced By Local Interactions Under General Anesthesia

Abstract

General anesthetics are a class of drugs with diverse molecular mechanisms that cause a state of unconsciousness. Generally, anesthetics are thought to exert this effect by co-opting endogenous sleep pathways within the brain, and activity patterns recorded during anesthesia resemble those recorded during natural sleep. Monitors of anesthetic depth take advantage of the relationship between brain activity patterns and anesthetic concentration to define a depth of exposure. Recovery from anesthetic-induced unconsciousness is typically assumed to be a passive, linear process that relies upon elimination of drug from the body. However, it has been shown that activity patterns undergo discrete transitions between several distinct brain states under anesthesia. Furthermore, the brain exhibits a resistance to recovery of consciousness during emergence from anesthesia. Together, these results show that emergence cannot be explained by drug elimination alone.

In this dissertation, we present evidence to suggest that stochastic fluctuations between distinct brain states account for this resistance to emergence. Furthermore, we show evidence to suggest that local cortical interactions are the principal organizing mechanism that gives rise to the brain states and state transitions recorded under general anesthesia. This mechanism is distinct from those known to drive state transitions during natural sleep. During sleep, broadly projecting modulatory pathways engage neurons throughout the thalamocortical network in coherent activity patterns and state transitions. Here, we demonstrate local heterogeneity in activity patterns and transition times within the cortex. Furthermore, our results indicate that, despite there being only weak coupling between activity patterns and transition times between different cortical regions, this coupling is sufficient to give rise to global brain states.

Altogether, the work presented in this dissertation indicates that the nature of oscillations within the cortex is strongly influenced by local interactions. This finding suggests that the mechanisms thought to give rise to state transitions during sleep are not the same as those that give rise to transitions under anesthesia. This finding that local interactions are potentially a stronger organizing mechanism for cortical activity than previously appreciated has important implications for anesthetic monitoring, clinical sleep disorders, and our basic understanding of thalamocortical activity patterns.

Degree Type

Dissertation

Degree Name

Doctor of Philosophy (PhD)

Graduate Group

Neuroscience

First Advisor

Alexander Proekt

Second Advisor

Diego Contreras

Keywords

Coherence, Cortex, Electrophysiology, Synchrony, Thalamus

Subject Categories

Neuroscience and Neurobiology

STATE TRANSITIONS WITHIN THE CORTEX ARE STRONGLY INFLUENCED BY LOCAL
INTERACTIONS UNDER GENERAL ANESTHESIA

Brenna Shortal

A DISSERTATION

in

Neuroscience

Presented to the Faculties of the University of Pennsylvania

in

Partial Fulfillment of the Requirements for the

Degree of Doctor of Philosophy

2022

Supervisor of Dissertation



Alexander Proekt, M.D., Ph.D.
Associate Professor of Anesthesiology and Critical Care

Graduate Group Chairperson



Joshua I. Gold, Ph.D.
Professor of Neuroscience

Dissertation Committee:

Diego Contreras, Ph.D., Professor of Neuroscience

Maria Geffen, Ph.D., Associate Professor of Otorhinolaryngology, Neuroscience, and Neurology

Franz Weber, Ph.D., Assistant Professor of Neuroscience

Andrew Hudson, M.D., Ph.D., Associate Professor of Anesthesiology and Perioperative Medicine

STATE TRANSITIONS WITHIN THE CORTEX ARE STRONGLY INFLUENCED BY LOCAL
INTERACTIONS UNDER GENERAL ANESTHESIA

COPYRIGHT

2022

Brenna Patricia Shortal

To Patricia Brogan, Ph.D.

You made sure I knew that whatever I wanted
was within reach.

ACKNOWLEDGMENT

To Alex, thank you for taking me on as a research technician when you had just barely started your new lab at UPenn. You were a good friend and mentor to me right after I uprooted my life and moved to a city where I didn't know a soul. Thank you for your candor as I sought your advice while I was navigating grad school applications and first year lab rotations. I knew you would have supported me no matter what I decided to do, and, in the end, it was an easy choice to come back and do my thesis work in your lab. I have benefitted enormously from your guidance and feedback and the independence you afforded to me. Thank you for giving me the opportunity to take ownership of the projects I worked on and to shape them to my interests. I am leaving your lab a better thinker and more confident communicator than I was when I entered.

To my thesis committee, thank you for your support and your interest in me as a person that was at least equal to, and I think even larger than, your interest in me as a scientist. You each made me feel supported and like I was on the right track. I wouldn't have been able to reach such a satisfying ending without you all.

To the NEURRAL group, in particular Max, Alex, and Andrew, thank you for the opportunity to be a member of the ALLiance. The three of you created a highly unusual job position for me based on your trust in a friend and my can-do attitude. I will be forever grateful, as it has led me down the path that brought me to where I am today. Thank you for taking a chance on me.

To Adeeti, thank you for being a friend and a mentor to me. You were often the voice of reason when I was struggling and a source of comfort when I needed a friend. I don't think I could have done this without you.

To the Neuroscience Graduate Group, thank you for putting so much effort into fostering close relationships between students. The community NGG has built is the most supportive graduate program I can imagine, and it was an enormous benefit to me as I progressed through the program. I am thankful to all my fellow students, the faculty, and the coordinators for making my time as a graduate student as good as it was.

Thank you, specifically, to the friends I made that will stay with me far beyond graduate school. Jess, Alexis, Leah, Mandy, and Adam, I'm not going to try and enumerate the individual debts of gratitude I owe you each. You've each been there for me when I needed friend and have shared your lives, successes, and setbacks with me. Thank you for being a friend. Ina, we became close friends during a period of transition and upheaval. I will never be able to thank you enough for your friendship. Finally, to Nitsan, my long-time roommate and friend. Thank you for being there and sharing in the day-to-day celebrations and frustrations of life with me. You brought me into your family and gave me a place while I was far away from my own.

To my family, thank you for always asking me how school was going: even though it's been going and going for half a decade now. Thank you, also, for understanding when I had to miss so many events and holidays.

To the support that came to me right when I needed it most and helped get me through the rough stops on my way to the end, thanks for being there for me.

ABSTRACT

STATE TRANSITIONS WITHIN THE CORTEX ARE STRONGLY INFLUENCED BY LOCAL INTERACTIONS UNDER GENERAL ANESTHESIA

Brenna Shortal

Alex Proekt

General anesthetics are a class of drugs with diverse molecular mechanisms that cause a state of unconsciousness. Generally, anesthetics are thought to exert this effect by co-opting endogenous sleep pathways within the brain, and activity patterns recorded during anesthesia resemble those recorded during natural sleep. Monitors of anesthetic depth take advantage of the relationship between brain activity patterns and anesthetic concentration to define a depth of exposure. Recovery from anesthetic-induced unconsciousness is typically assumed to be a passive, linear process that relies upon elimination of drug from the body. However, it has been shown that activity patterns undergo discrete transitions between several distinct brain states under anesthesia. Furthermore, the brain exhibits a resistance to recovery of consciousness during emergence from anesthesia. Together, these results show that emergence cannot be explained by drug elimination alone.

In this dissertation, we present evidence to suggest that stochastic fluctuations between distinct brain states account for this resistance to emergence. Furthermore, we show evidence to suggest that local cortical interactions are the principal organizing mechanism that gives rise to the brain states and state transitions recorded under general anesthesia. This mechanism is distinct from those known to drive state transitions during natural sleep. During sleep, broadly projecting modulatory pathways

engage neurons throughout the thalamocortical network in coherent activity patterns and state transitions. Here, we demonstrate local heterogeneity in activity patterns and transition times within the cortex. Furthermore, our results indicate that, despite there being only weak coupling between activity patterns and transition times between different cortical regions, this coupling is sufficient to give rise to global brain states.

Altogether, the work presented in this dissertation indicates that the nature of oscillations within the cortex is strongly influenced by local interactions. This finding suggests that the mechanisms thought to give rise to state transitions during sleep are not the same as those that give rise to transitions under anesthesia. This finding that local interactions are potentially a stronger organizing mechanism for cortical activity than previously appreciated has important implications for anesthetic monitoring, clinical sleep disorders, and our basic understanding of thalamocortical activity patterns.

TABLE OF CONTENTS

ACKNOWLEDGMENT	iv
ABSTRACT	vi
LIST OF TABLES	ix
LIST OF FIGURES	x
PREFACE	xii
CHAPTER 1 – General Introduction	1
CHAPTER 2 – Weak Coupling Between Spontaneous Local Cortical Activity State Switches Under Anesthesia Leads to Strongly Correlated Global Cortical States	30
INTRODUCTION	30
RESULTS	34
DISCUSSION	46
MATERIALS AND METHODS	53
FIGURES	66
CHAPTER 3 – Duration of EEG Suppression Does Not Predict Recovery Time or Degree of Cognitive Impairment After General Anesthesia in Human Volunteers	79
INTRODUCTION	79
RESULTS	80
DISCUSSION	85
MATERIALS AND METHODS	90
TABLES	99
FIGURES	105
CHAPTER 4 – General Discussion	114
REFERENCES	122

LIST OF TABLES

Chapter 3 – Duration of EEG Suppression Does Not Predict Recovery Time or Degree of Cognitive Impairment After General Anesthesia in Human Volunteers

Table 3.1 Results of linear regression model including decay time constant and overall percent suppression.....**99**

Table 3.2 Results of linear regression model including decay time constant and percent of last 15 minutes of isoflurane exposure spent in EEG suppression...**100**

Table 3.3 Statistical results of three exponential decay models. Pearson's R^2 shows similar predictive ability of each model for time of emergence from anesthesia.....**101**

Table 3.4 Analysis of correlation between the total time spent in EEG suppression and the degree of impairment in cognitive performance upon emergence.....**102**

Table 3.5 Analysis of correlation between the fraction of the last 15 minutes of isoflurane exposure spent in EEG suppression and the degree of impairment in cognitive performance upon emergence.....**103**

Table 3.6 Analysis of correlation between the time constant of elimination of isoflurane and the degree of impairment in cognitive performance upon emergence.....**104**

LIST OF FIGURES

Chapter 2 – Weak Coupling Between Spontaneous Local Cortical Activity State Switches Under Anesthesia Leads to Strongly Correlated Global Cortical States

Figure 2.1 Experimental setup.....	66
Figure 2.2 Examples of state transitions.....	67
Figure 2.3 Schematic of LFP analysis, through NMF calculation.....	68
Figure 2.4 Schematic of NMF score analysis to define state transitions and synchrony.....	69
Figure 2.5 Current source density computed for a representative V1 recording.....	71
Figure 2.6 Transition synchrony between channels in the same anatomical region is higher than between channels in different regions.....	72
Figure 2.7 Normalized mutual information (MI) between channels in the same anatomical region is higher than between channels in different regions.....	74
Figure 2.8 Canonical correlation analysis (CCA) reveals higher correspondence of overall activity between channels in the same anatomical region than between channels in different regions.....	76
Figure 2.9 Weakly correlated fluctuations in different cortical sites give rise to highly correlated cortical states.....	78

Chapter 3 – Duration of EEG Suppression Does Not Predict Recovery Time or Degree of Cognitive Impairment After General Anesthesia in Human Volunteers

Figure 3.1 End-tidal isoflurane concentration and body temperature during anesthetic exposure.....	105
Figure 3.2 Group spectrograms show canonical low frequency oscillations in the anaesthetized brain.....	106
Figure 3.3 Individual spectrograms reveal the variability of EEG activity between subjects and across time.....	107
Figure 3.4 Illustration of principal component analysis (PCA)-based method for isolating episodes of EEG suppression.....	109

Figure 3.5 The time to emerge from isoflurane (time to recovery of consciousness) is not significantly correlated with different measures of suppression.....110

Figure 3.6 The time to emerge from isoflurane (time to recovery of consciousness) is significantly correlated with the rate of isoflurane expiration.....111

Figure 3.7 Schematic of physiologically motivated model.....112

Figure 3.8 Association between amount of EEG suppression on performance speed and accuracy on both the psychomotor vigilance test (PVT) and digit symbol substitution test (DSST).....113

PREFACE

The question of the nature of consciousness has fascinated humanity for millennia. Modern scientific research has provided ample evidence to support the idea that consciousness is created by the brain itself. Sensory neuroscientists have defined intricate brain circuits that allow the us to sense, interpret, and respond to the world around us. Sleep and circadian neuroscientists have defined the circuits and chemical signals that drive sleep and wake behaviors and those that shepherd the brain between dream sleep, the various stages of deep sleep, and wakefulness at the end of the night. Computational neuroscientists have even generated models for how the brain performs complex problem-solving tasks. Along the way, the field has grown to include scientists from disciplines ranging from philosophy to physics.

Despite all this research and the high level of interest, the field still cannot define exactly what consciousness is. What is it to be me as opposed to what it is to be you? How do the circuits characterized by different subdisciplines of neuroscience work together to give rise to one single, cohesive conscious experience? The answers to these questions are not in reach quite yet, but there is evidence to suggest that consciousness is the result of an intentionally organized network within the brain. Specifically, this evidence comes from the fact that the brain is able to reassemble its own form of consciousness after perturbation. Whether it's because of sleep, trauma, seizures, coma, or anesthesia, any number of things can render the brain unconscious. However, the vast majority of the time, an individual regains consciousness to find that they are the same person as they were before losing consciousness. This suggests that the networks within the brain that allow for conscious awareness are able to reassemble themselves after being disrupted.

General anesthesia profoundly disrupts consciousness and is able to render the recipient so deeply unconscious that they do not respond to or remember stimuli including pain associated with surgery. Despite this, the vast majority of anesthetic exposures are uneventful, and the patient returns to normal soon after drug delivery stops. As a result, it is typically assumed that recovery of consciousness following anesthetic exposure is a passive process reliant only on the elimination of drug from the body. This theory posits that the deepest level of anesthesia reached by an individual sets a starting point for recovery. Once drug delivery stops, the body metabolizes drug and consciousness is restored. The latency to emergence is typically thought to depend only on how deep this starting point is and how quickly the drug is metabolized.

However, work presented in this thesis demonstrates that, in humans, knowing the starting point of recovery of consciousness for an individual does not provide information about how long it will take them to emerge. Furthermore, it has been shown in various animal models that the brain resists the transition from anesthetic-induced unconsciousness to consciousness. These data demonstrate that the process of emerging from anesthesia is not passive and relies on reorganization of neural networks within the brain. The precise mechanisms are not yet understood, but recent work suggests that they are highly structured.

Work in rodents, non-human primates, and humans has shown that activity patterns in the brain fluctuate across time, even if the concentration of drug being administered remains the same. Specifically in rats, it has been shown that these fluctuations are not random and, in fact, undergo discrete transitions between distinct, stable brain states on a timescale that is similar to switching between stages of sleep in rats. While the same activity patterns may appear during exposure to different concentrations of anesthesia,

the probability of seeing any one state changes as a function of concentration. Additionally, the activity patterns observed during these brain states under anesthesia are reminiscent of those recorded during sleep. These activity patterns have known neuronal mechanisms. Each of them is generated by the thalamocortical network via the dense, reciprocal connectivity between the cortex and thalamus.

Anesthesia and sleep are not the same. However, anesthesia is known to act by modulating endogenous sleep/wake circuitry. Specifically, anesthetics have been found to suppress wake-active neuronal populations and activate sleep-active populations. Additionally, it has been shown that anesthesia-induced unconsciousness can be disrupted via activation of the brain's endogenous arousal circuits. Taken together, these findings suggest that perhaps similar mechanisms are driving the organization and timing of transitions between the states recorded during anesthesia and those that occur naturally during sleep.

During sleep, recordings from anywhere in the cortex reveal neurons firing together in coordinated bursts of activity. The specific characteristics of this rhythmic activity depend on various currents and chemical signals in the thalamocortical network, but transitions between states are discrete. Once there is a shift between the relative influence of these various drivers, the network transitions and a new state is imposed broadly throughout the cortex. These transitions occur almost simultaneously throughout the cortex as a result of the extensive innervation of the cortex by the thalamus and hypothalamic arousal nuclei.

Additionally, this thesis presents data addressing whether similar mechanisms drive the state transitions observed during anesthesia. Experiments presented here were

designed to test whether the state transitions occur simultaneously throughout the cortex. If they do, this provides evidence for the hypothesis that state transitions under anesthesia are imposed upon the cortex by subcortical structures in a similar fashion to sleep states. Alternatively, if transitions do not occur simultaneously throughout the cortex, this suggests that brain states and state transitions under anesthesia are organized via local interactions between neurons within the cortex.

The work presented in this thesis has important implications for anesthesia and sleep. A better understanding of the mechanisms that give rise to state transitions under anesthesia has clear application to clinical anesthesia during which anesthesiologists must work within a narrow margin error between anesthetic overdose which is associated with respiratory depression or cognitive decline and underdosing which leaves the patient susceptible to intraoperative awareness. A more nuanced understanding of the relationship between brain state and likelihood to recover consciousness could help anesthesiologists better anticipate potential issues before they arise. In addition, there is a class of disorders characterized by inappropriate or incomplete transitions between sleep and wake: the parasomnias. A better understanding of the local dynamics capable of organizing brain states and state transitions could offer insight into the mechanisms that underlie parasomnias.

Finally, work in rats has shown that, in the context of sleep deprivation, spatially restricted populations of neurons are capable of entering a sleep-like state during behavioral wakefulness. The more areas that enter this sleep-like state, the worse performance in a behavioral assay of coordination becomes. This suggests that local sleep behavior could be a potential mechanism of drowsiness. It has also been shown in rats that spatially restricted areas of cortex are capable of supplementing for sleep

need in a use-dependent fashion. Together, these data suggest that our current understanding of sleep and wake states as homogenously expressed throughout the brain is incomplete. Local interactions between cortical regions may also be an essential mechanism underlying natural sleep and wake behavior that have previously been underappreciated.

CHAPTER 1 – General Introduction

This general introduction offers essential background information related to the work and interpretations presented in this thesis. It is divided into five sections outlined briefly here. (1) Anesthetic mechanisms and monitoring: This section offers a brief overview of how anesthetic drugs exert their influence over the central nervous system. It begins with an explanation of how anesthetic drugs affect brain activity patterns and how that effect is used to define anesthetic depth. The section continues with a discussion of the anesthetic drugs' cellular mechanisms of action. (2) Generation of rhythmic activity patterns: This section begins with an explanation of how brain activity patterns are recorded and the pros and cons of different methods. Then, it gives an overview of the known mechanisms that give rise to oscillatory activity patterns in the brain with special attention paid to several oscillations that will be discussed in later chapters. (3) State transitions under general anesthesia: This section covers work demonstrating that there are discrete transitions between distinct activity patterns under general anesthesia. (4) Mechanisms known to drive cortical state transitions: This section covers what is currently known about major neuronal processes that give rise to state transitions in the context of sleep and wake. Then, it covers the central question that motivated my work presented in Chapter 2. (5) Neural inertia and the resistance to state transitions: This section offers an overview of research showing that the brain resists the transition to consciousness following anesthesia and the implications for this finding. From there, it draws a connection between my work presented in Chapters 2 and 3.

Anesthetic mechanisms and monitoring

Anesthetics cause slowing of the EEG

During light anesthesia, the electroencephalogram (EEG) is dominated by relatively low-amplitude, high frequency activity. As the anesthetic dose increases, there is a progressive increase in amplitude coupled with a reduction of power in the higher frequency bands and more power concentrated near or below 1 Hz (Hagihira, 2015). Thus, higher doses of anesthesia cause the EEG to slow. At the deepest planes of anesthesia, burst suppression and even isoelectric, flat signals are observed. Burst suppression is a signal composed of transient periods of high-voltage slow waves and intervening periods of suppression which is characterized by little to no voltage fluctuations (Mircea Steriade et al., 1994). The next section offers an overview of the molecular mechanisms through which anesthetic drugs are thought to cause these effects.

Anesthetic mechanisms of action

The use of medicinal agents to blunt awareness dates back to at least 3400 BC. Ancient examples include herbal remedies, alcohol, and opium poppies. The earliest written evidence of opium and alcohol being used for their sedative properties comes from Mesopotamia (Al Ansari et al., 2019; Brook et al., 2017). Ancient Egyptian doctors used surgical equipment and are thought to have used the mandrake fruit to produce a tonic to cause a state of anesthesia (Pahor, 1992; Sullivan, 1996). Even later, substances such as cannabis and wolf's bane were used in ancient India and China to induce an anesthesia-like state (Brand and Zhao, 2017; Zhao et al., 2018). Anesthesia, as it is known today, was first used in 1846 by Dr. William T. G. Morton in the Massachusetts General Hospital Ether Dome. He used the general anesthetic ether to induce and

maintain a state of anesthesia to allow for a painless tooth extraction (Larson, 1965). Today, millions of Americans are given general anesthesia each year (Rose et al., 2015). However, the field is still far from understanding how anesthetic agents lead to loss of consciousness and how consciousness is reinstated after exposure (Mashour et al., 2005; Mashour, 2006a).

In the 19th century and up through much of the 20th, anesthetics were thought to work by disrupting cell membranes in the brain (Seeman, 1972). However, in the years since, the field has learned that the mechanisms of anesthetic action are more complicated than that. Specifically, much more is known now about how different anesthetic agents work at the molecular level. In general, anesthetics work by enhancing inhibitory activity and suppressing excitatory activity in the brain. That said, anesthetics, as a class of drugs, have diverse molecular targets, and even individual agents bind to many receptors throughout the central nervous system (CNS) (Mashour et al., 2005). Despite the vast heterogeneity of binding, a few receptors have been identified as especially relevant to anesthetics' ability to cause sedation, amnesia, and hypnosis.

The most extensively studied of these is the GABA_A receptor which is affected by nearly every anesthetic agent (Bai et al., 1999; Garcia et al., 2010). The mechanisms through which different anesthetic agents interact with this receptor vary, but these mechanisms conspire to cause an increased probability of channel opening and slow channel desensitization. Together, these actions enhance inhibition within the brain via the increased activity of the synaptic and extrasynaptic GABA_A receptors (Bai et al., 1999; Hemmings et al., 2005). In addition to GABA_A receptors, several other ligand-gated channels are thought to be potential molecular targets for anesthetic agents' effects on the CNS. Like GABA, glycine is an inhibitory neurotransmitter. Glycine receptors are

potentiated by many inhaled anesthetics (Zhang et al., 2003). This potentiation of inhibitory signaling has been implicated in anesthetic-induced immobility (Zhang et al., 2003).

The previous paragraph highlighted some of the inhibitory neurotransmitter receptors that bind anesthetics. Other neurotransmitter receptors also bind anesthetics, but these receptors tend to be inhibited rather than potentiated. Serotonin (5-HT₃) has receptors distributed throughout the nervous system (Jackson and Yakel, 1995). These receptors have been shown to be inhibited by several anesthetic agents including pentobarbital (Barann et al., 1997) and propofol (Barann et al., 2000). The effect of anesthesia on the 5-HT₃ receptors is thought to contribute to peripheral nociception (Jackson and Yakel, 1995). Nicotinic acetylcholine receptors are also widely distributed throughout the nervous system, and they are generally inhibited by anesthetic agents (Tassonyi et al., 2002). Their inhibition is thought to contribute to anesthetic amnesia, inattentiveness, and delirium (Tassonyi et al., 2002). Glutamate is the major excitatory neurotransmitter in the brain (Hudspith, 1997). Anesthetic agents are thought to inhibit glutamate receptors and cause myriad downstream affects related to anesthetic actions within the CNS (Hudspith, 1997). In particular, the anesthetic agent ketamine is thought to work, in large part, via inhibition of the glutamatergic NMDA receptor which is thought to preferentially alter NMDA receptor function on interneurons (Li and Vlisides, 2016). In addition to interneurons, NMDA receptors on cortical pyramidal cells are also suppressed by anesthetics which leads to a reduction in cortical coherence and gamma activity (Li and Vlisides, 2016).

In addition to these ligand-gated ion channels, anesthetics have well-known effects on voltage-gated ions channels. Tandem two-pore potassium (K_{2P}) channels are widely

expressed throughout the CNS and the peripheral nervous system (Steinberg et al., 2015). Anesthetic drugs, especially halogenated volatile anesthetics like isoflurane, promote opening of K_{2P} channels which enhance potassium ion currents and contribute to hyperpolarization of cell membranes and a reduction in neuronal excitability (Steinberg et al., 2015). Hyperpolarization-activated cyclic nucleotide-gated (HCN) channels are weakly selective for potassium and sodium ions and are activated by hyperpolarization, rather than depolarization (Goldstein, 2015). Upon activation, HCN channels conduct an inward current, I_h , which modulates the neuronal membrane potentials and contributes to subthreshold excitability. In this way, I_h is involved in regulating rhythmic oscillations in the nervous system (Goldstein, 2015). The anesthetic drug propofol preferentially inhibits I_h in cortical pyramidal cells which have relatively fast activation kinetics for HCN channels (Chen et al., 2005). This inhibition causes a hyperpolarizing shift in the membrane potential of cortical pyramidal cells (Chen et al., 2005). Presynaptic voltage-gated sodium channels are also targeted by some general anesthetics (Herold and Hemmings Jr., 2012). Volatile anesthetic drugs inhibit these channels thereby causing a reduction in evoked neurotransmitter release in the affected synapses (Herold and Hemmings Jr., 2012). Glutamate release is selectively inhibited which contributes to reduced excitatory transmission and CNS depression (Herold and Hemmings Jr., 2012). A variety of both inhaled and intravenous anesthetics have also been shown to modulate the activity of voltage-gated calcium channels (Hao et al., 2020). Generally, anesthetics lead to reduced neurotransmitter release via inhibition of voltage-gated calcium channels (Hao et al., 2020). However, it is not completely clear whether this reduction in neurotransmitter release is a direct of anesthetic inhibition of voltage-gated calcium channels (Hao et al., 2020).

The mechanisms reviewed here are only a brief overview of what is a rapidly expanding field. Anesthetic drugs do have specific molecular targets, but they can bind to many of them simultaneously and likely have additional targets that are yet unknown. Generally, anesthetic agents seem to work in the CNS to enhance inhibitory signaling while also suppressing excitatory signaling. Together, these effects cause profound changes in the patterns of brain activity during anesthesia, relative to wakefulness.

Monitoring anesthetic depth

Monitor of anesthetic depth take advantage of this relationship between the frequency characteristics of the electrophysiological recordings and anesthetic concentration. They rely heavily on metrics related to signal characteristics of EEG to assign a single output metric to describe anesthetic depth. For example, the bispectral index (BIS) is a statistically based, empirically generated complex parameter derived from a combination of time, frequency, and higher order bispectral features of EEG signals (Kaul and Bharti, 2002). The output of BIS is a single variable that defines the depth of sedation and hypnosis caused by an anesthetic agent, regardless of which agent was used (Kaul and Bharti, 2002). Values for the BIS output ranges from 100 (wakefulness) to 0 (isoelectric, or completely flat EEG) and correlate well with the level of responsiveness, thereby giving a good prediction of depth of anesthesia for various agents (Rampil et al., 1980).

Emergence as a progression through states of synchrony to desynchrony

When delivery of the anesthetic agent stops, the brain must reassemble its disrupted networks and achieve emergence to conscious awareness. Through this process, activity recorded from the brain progresses through activity patterns that are increasingly desynchronized, starting from the deepest point reached during anesthetic exposure.

This process has classically been conceptualized as a passive, steady bubbling up from the starting point to a state that is desynchronized enough to allow for consciousness.

Generation of rhythmic cortical activity patterns

Origins of electrophysiological signals

Scientists have been recording brain activity using electrophysiological recordings since Hans Berger invented the EEG in 1929 (Millett, 2001; Nunez and Srinivasan, 2006; Schomer and Lopes da Silva, 2018). EEG is recorded using electrodes placed on the surface of the head. The voltage fluctuations that give rise to an EEG signal are tiny (on the order of several hundred μV) and the fact that they must pass through protective tissue layers surrounding the brain, the skull, and the scalp means that EEG signals are attenuated and spatially smoothed, relative to the originating neuronal activity. As a result of this spatial smoothing and signal attenuation, more modern studies of neuronal circuits and cellular mechanisms employ recording techniques that place electrodes close to the neurons themselves. Electrocorticography (ECoG) is recorded using subdural electrodes placed on the cortical surface (Buzsáki et al., 2012). Local field potentials (LFP) are recorded using penetrating electrodes that are inserted into the brain (Buzsáki et al., 2012). Therefore, the voltage fluctuations recorded via LFP reflect the extracellular field created by the neurons within a relatively small area of tissue near the electrode. Unlike intracellular recordings, extracellular recordings like LFPs cannot be used to study cellular specific ionic mechanisms such as those described in the previous section. However, they allow for the study of populations of neurons rather than just one or two neurons at a time.

Extracellular recordings are conventionally split into two signals based on frequency. The higher frequency components of the signal reflect spikes and multiunit activity. The lower frequency components (typically < 200 Hz) constitute the LFP. Given that LFP signals are comprised mainly of the extracellular voltage fluctuations, they can be interpreted as representing the inputs to a particular area of brain tissue (Buzsáki et al., 2012). While many processes contribute to the signal characteristics of the LFP, the two main factors are the inputs to the area of brain being recorded and the biophysics of that area related to the neural architecture.

Temporally synchronous input to a population of neurons contributes significantly to the LFP because it causes large fluctuations in membrane potentials across the population (Buzsáki et al., 2012). This is because all simultaneous voltage fluctuations in an area sum up and together contribute to the extracellular field. If a population of cells is firing randomly, the positive and negative voltage fluctuations will effectively cancel out. This is why the amplitude of cortical electrophysiological signals is small during wakefulness when the cortex is engaged in many different tasks simultaneously and firing is asynchronous. If a population of neurons is depolarizing and hyperpolarizing in synchrony, those voltage changes combine to generate high-amplitude signals in the LFP. In fact, power in the different frequency components of the LFP generally follow a power law wherein power is approximately $1/f^2$ where f is the frequency band (Miller et al., 2009; Milstein et al., 2009). This relationship is related to physical properties of the dendrites. Modeling studies have shown that an extracellular signal detected in the distal dendrite following high-frequency stimulation is attenuated 100-fold at the soma, while slower signals are attenuated much less (Gold et al., 2006; Lindén et al., 2010; Pettersen et al., 2008). In addition to spatial attenuation, network features also contribute

to the power law features of LFP spectral estimates. This is due to the fact that it is more likely that many neurons will be recruited to contribute synchronously to the LFP at a lower frequency when the duration of each phase of the oscillation is longer than at a faster frequency when the phases of the oscillation are very short (Buzsáki et al., 2012).

The physical features of neurons and their physical arrangement in different brain regions also affect the extracellular fields that they generate. The cortex is composed mainly of pyramidal cells which have thick apical dendrites that generate strong dipoles with considerable separation between the poles (Buzsáki et al., 2012). As a result, pyramidal cells can generate huge ionic flow in the extracellular space and contribute substantially to the extracellular field (Buzsáki et al., 2012). In contrast, thalamocortical cells have a rounder shape with equally sized dendrites reaching in all directions. As a consequence of this geometry, thalamocortical cells make small contributions to the extracellular potential, relative to pyramidal cells (Lorente de Nó and Davis, 1947). In addition to their physical shape, the spatial arrangement of cortical pyramidal cells leaves them well-suited to generate large extracellular potentials. They are arranged so that they lie parallel to one another with their apical dendrites positioned so that the afferent inputs are perpendicular to the dendritic axis (Buzsáki et al., 2012). This arrangement is ideal for synchronously active dipoles which pyramidal cells often generate, especially during sleep and anesthesia. As a result, LFP signals from the cortex are the largest anywhere in the brain (Buzsáki et al., 2012).

Taken together, these mechanisms contribute to the generation of the extracellular field which is reflected in the LFP. LFP signals recorded under anesthesia and those recorded during wakefulness look markedly different from one another. As was mentioned earlier on, anesthetics cause slowing of electrophysiological signals by

suppressing excitatory signaling and enhancing inhibition. Higher concentrations of anesthesia are associated with slower, more synchronized signals, and emergence from anesthesia is characterized by the progression from states of synchrony to states of increasing desynchrony. The following sections present an overview of what is known about the circuits that generate the different kinds of oscillations recorded from the anesthetized brain.

Thalamocortical network

Under general anesthesia, cortical activity patterns tend to take on one of several different stereotyped oscillation patterns. These oscillations are generated by the thalamus and cortex which share dense, reciprocal connections (Mircea Steriade et al., 1993a). In this section, some of the key architectural features and connections that allow the thalamocortical network to generate these patterns will be discussed.

The cortex is where higher-order cognitive processes take place. It is organized into layers, the general purpose of which seems to be to generate a scaffold that constrains the ways in which different neurons are able to connect to one another (Rodney J. Douglas and Martin, 2004). Each layer is characterized by its inputs and outputs as well as whether it is comprised of mainly pyramidal cell bodies or their dendrites (Rodney J Douglas and Martin, 2004). The thalamus is the major relay center within the brain for information entering from the outside world (Mircea Steriade et al., 1993a). It is a collection of different nuclei which are primarily composed of excitatory neurons that do not have many excitatory reciprocal connections between themselves. Instead, thalamic nuclei send dense excitatory projections to the cortex (Halassa and Sherman, 2019). Classic literature divides thalamic nuclei based on their histological features into several groups: lateral nuclear group, medial nuclear group, and anterior nuclear group (Halassa

and Sherman, 2019). Each of the nuclei within these groups has a body of associated literature that aims to ascribe a functional output to it. While these histological distinctions are associated with function to some degree, it is clear that distinct nuclei are more often than not involved in several circuits each with their own functional output (Rikhye et al., 2018).

Another way to classify thalamic regions is to do so based on the thalamocortical projections leaving an area (Jones, 2001). Jones splits the thalamocortical cells into two populations of neurons which he refers to as the “matrix” and “core” (Jones, 2001). Matrix neurons dominate the central thalamic nuclei and send sparse, diffuse projections to superficial cortical layers (Jones, 2001). The superficial cortical layers are layers I and II/III. Layer I is composed mainly of the distal tufts of cortical pyramidal cells dendrites whose bodies are in layers III and V (Rodney J Douglas and Martin, 2004). This layer contains long-range projections between cortical neurons and is one major target of feedback connections between different cortical regions (Rodney J Douglas and Martin, 2004). Layer II/III is composed of pyramidal cell bodies that make extensive short-range arborizations, forming a network of corticocortical connections within this layer (Jones, 2009). Given the fact that matrix cells innervate cortical regions involved in both close- and long-range corticocortical communication, these neurons are well-suited to influence activity patterns throughout the cortex. Matrix neurons themselves are heavily innervated by the brainstem arousal nuclei which has been shown to be responsible for initiating desynchronized activity patterns during the transition from sleep to wake (Moruzzi and Magoun, 1949).

Core neurons have more spatially restricted and dense projections coming mainly from the lateral geniculate nucleus to innervate cortical layer IV (Jones, 2001). In the cortex,

layer IV is typically considered the principal input layer for projections from the thalamus (Jones, 2009). Layer IV sends excitatory projections to the superficial cortical layers (Gilbert and Wiesel, 1983; Gilbert, 1992). In turn, superficial layers send projections to layer V (Gilbert and Wiesel, 1983; Gilbert, 1992). Layer V has dense, lateral corticocortical connections and sends projections that drive activity in subcortical structures such as the basal ganglia and ventral spinal cord, superficial cortical layers, and layer VI (Rodney J Douglas and Martin, 2004). Layer VI sends projections back to thalamus to allow for cortical influence over thalamic activity (Gilbert and Wiesel, 1983; Gilbert, 1992).

This section so far has discussed a very brief overview of the key excitatory connections between the cortex and thalamus. It is essential to acknowledge that there are caveats and additional connections not discussed here that exist within this network (Fitzpatrick, 1996; Fitzpatrick and Raczkowski, 1990; Hirsch et al., 1998; Katz, 1987; Lund et al., 1979; Martin and Whitteridge, 1984; Muly and Fitzpatrick, 1992; Usrey et al., 1992; Usrey and Fitzpatrick, 1996). In addition to these excitatory connections, inhibition is critical for the proper functioning of the thalamocortical network. This inhibition comes mainly from the thalamic reticular nucleus which projects principally to the dorsal thalamic nuclei (Crabtree, 1996; Crabtree et al., 1998; Hale et al., 1982; Harris, 1987; Jones, 1975; Pinault et al., 1997, 1995; Pinault and Deschênes, 1998; Steriade and Deschenes, 1984; Velayos et al., 1989). The reticular thalamus receives input from both the cortex and the thalamus but sends projections only to the thalamus (Bourassa and Deschênes, 1995; Coleman and Mitrofanis, 1996; Conley et al., 1991; Conley and Diamond, 1990; Crabtree, 1992; Crabtree and Killackey, 1989; Montero et al., 1977). Reticular nucleus projections to thalamocortical neurons are GABAergic (Cucchiaro et

al., 1991; Harting et al., 1991; Montero, 1983; Montero and Scott, 1981; Ohara et al., 1980). Thalamocortical input to the reticular nucleus is glutamatergic and excitatory (Ohara and Lieberman, 1985). Cortical input to the reticular nucleus is excitatory and comes from a many different areas (Mircea Steriade et al., 1993a). Via these excitatory projections to the reticular nucleus, the cortex is well positioned to exert wide-spread influence over activity pattern in thalamus, given that the reticular neurons send inhibitory projections to a variety of thalamic nuclei (Mircea Steriade et al., 1993a). Some of the thalamic nuclei that receive inhibitory input from the reticular neurons have their own wide-spread cortical projections (Mircea Steriade et al., 1993a).

Thus, the cortex, thalamus, and reticular thalamus together form an intricate network of reciprocal excitation and inhibition that allows for each of the areas to affect activity in the others. In the next section, we will discuss how this interconnectivity generates three different well-characterized oscillation patterns that are commonly recorded during anesthesia-induced unconsciousness.

Spindle oscillation

The spindle oscillation occurs between 7 - 14 Hz and is generated by the neurons of the thalamic reticular nucleus (Steriade et al., 1985). Reticular neurons are able to spontaneously generate an oscillation in the spindle frequency due to their unique assortment of ionic currents (Avanzini et al., 1989). They generate rhythmic spike-bursts of inhibitory post-synaptic potentials (IPSPs) via low-threshold calcium spikes. These IPSPs are projected to the thalamus and cause hyperpolarization of many thalamocortical neurons (Steriade and Deschênes, 1987). Once thalamocortical neurons are hyperpolarized enough, they are removed from inactivation and fire rebound calcium spikes and associated bursts of action potentials (Steriade and Deschênes, 1987).

These depolarizing bursts are projected to the cortex via thalamocortical synapses in layer IV which, in turn, induce rhythmic excitatory post-synaptic potentials (EPSPs) that are projected back to the reticular nucleus (Contreras and Steriade, 1997). This excitatory feedback from the cortex to the reticular nucleus works to excite the reticular neurons to fire another round of IPSPs to the thalamocortical neurons thereby facilitating a rhythmic oscillation in the spindle range.

While reticular neurons are capable of generating a rhythmic oscillation at the spindle frequency on their own, reciprocal connectivity between the cortex and thalamus is required for the synchronous generation of the spindle oscillation throughout the thalamocortical network. This has been shown through a series of complementary experiments. First, it has been shown that disruption of corticocortical connections does not disrupt synchrony of spindles within the cortex (Contreras and Steriade, 1997). Therefore, the signals that drive this oscillation in spatially distinct areas of cortex must be coming from a subcortical source: in this case, the thalamus. However, thalamocortical projections alone are insufficient to generate a synchronous spindle oscillation. It has been shown that removal of the cortex disrupts spindle synchrony in the thalamus (Contreras and Steriade, 1997). In the absence of reciprocal connectivity from the cortex, spindle oscillations are still generated in thalamus. However, only nearby regions of thalamic tissue (on the order of 2 – 4 mm) express synchronous spindle oscillations (Contreras and Steriade, 1997). Therefore, corticothalamic projections, along with thalamocortical projections, are required to synchronize the spindle oscillation throughout the thalamocortical network.

Delta oscillation

The delta oscillation occurs between 1 - 4 Hz and has a more complicated origin than the spindle oscillation. There are several different mechanisms that seem to be able to generate an oscillation within the delta frequency (Steriade et al., 1990, 1971; Steriade and Deschênes, 1987). For the purpose of this thesis, only the best characterized will be discussed. This is the delta oscillation generated by the thalamocortical neurons (McCormick and Pape, 1990; Steriade and Deschenes, 1984). Thalamocortical neurons are able to generate the delta oscillation via the interplay of two intrinsic currents: the hyperpolarization-activated current (I_h) and the transient low-threshold calcium current (I_t) (Contreras et al., 1993; Jahnsen and Llinás, 1984; McCormick and Pape, 1990; Steriade and Deschenes, 1984). During unconsciousness, the reduction of excitatory input from the cortex allows the thalamocortical neurons to hyperpolarize. This hyperpolarization is sufficient to cause a spontaneous delta oscillation to begin in thalamocortical neurons (Steriade et al., 1991).

As with the spindle oscillation, reciprocal connectivity between the cortex and thalamus is required for the delta oscillation to become synchronous throughout the thalamocortical network (Steriade et al., 1991). Once thalamocortical neurons are hyperpolarized, a cortical volley is sufficient to elicit the delta oscillation in thalamocortical neurons (Steriade et al., 1991). This is true, even for thalamocortical cells that are not directly innervated by the stimulated cortical neuron (Steriade et al., 1991) Therefore, cortical input is able to drive a synchronous delta oscillation in a wide area of the thalamus. Additionally, excitatory projections from the thalamocortical neurons are thought to engage the reticular neurons and local thalamic GABAergic interneurons into the delta oscillation. These populations, then, send IPSPs to

thalamocortical neurons. In this way, thalamocortical neurons receive rhythmic inhibitory input that maintains the hyperpolarization required for generation of the delta oscillation and reinforce activity pattern (Steriade et al., 1991).

Slow wave oscillation

The slow wave oscillation occurs at frequencies below 1 Hz and is generated by cortical neurons (Mircea Steriade et al., 1993b). During non-REM sleep and anesthesia, cortical neurons periodically shift between periods of suppression and periods of bursting. The transition back and forth between these periods defines the slow wave oscillation (M. Steriade et al., 1993). Periods of suppression can, at least in part, be explained by AHPs caused by the coordinating bursting of pyramidal cells during the depolarized period of this oscillation (Buzsaki et al., 1988; Sanchez-Vives and McCormick, 2000). Various mechanisms are involved in driving this oscillation. They include the gradual decrease in extracellular calcium ions in the cortex that occurs as a result of reduced synaptic transmission during sleep and the inactivation of I_h channels.

It is known that the slow wave oscillation is generated by cortical neurons because extensive lesioning studies have demonstrated that the slow wave oscillation survives within the cortex after extensive thalamic lesions (Mircea Steriade et al., 1993b). While the cortical neurons are capable of generating the slow wave oscillation in the absence of thalamic input, synchronous firing in the cortex is a powerful driver of activity within the thalamus and reticular nucleus (Contreras et al., 1993). As a result, other thalamocortical oscillations such as the spindle and delta oscillations tend to be grouped into the depolarizing envelope of the slow wave oscillation (Contreras et al., 1993).

State transitions under general anesthesia

Despite being commonly used to fix brain activity patterns for the purpose of basic research, a growing body of literature demonstrates that, under anesthesia abrupt, spontaneous transitions occur between distinct activity patterns. This has been demonstrated in rodents (Clement et al., 2008; Hudson et al., 2014), non-human primates (Ballesteros et al., 2020a; Ishizawa et al., 2016a; Patel et al., 2020), and humans (Chander et al., 2014) exposed to various anesthetic agents with distinct mechanisms of action. Anesthesia induced with urethane is associated with fluctuations in cortical state resembling sleep stage switching in that the duration in distinct states was approximately equal to the typical duration of an individual sleep stage in a rat (Clement et al., 2008). Furthermore, this group shows that muscle tone, respiration rate, and cardiac output covary with cortical brain state which is also true during natural sleep (Clement et al., 2008). In this study, they used urethane anesthesia which is used in animal studies for its minimal effects on the cardiovascular and respiratory systems (Hara and Harris, 2002). Therefore, their results related to cardiovascular and respiratory effects cannot be explained as a drug effect.

Ishizawa et al., 2016 recorded LFP in macaques under propofol during loss of consciousness and deep anesthesia. Their results show that slow waves first appeared in recordings from the somatosensory cortex before they were visible in the frontal ventral premotor area during loss of consciousness (Ishizawa et al., 2016b). These data show that propofol-induced loss of consciousness is associated with spatiotemporal differences in oscillatory dynamics across the cortex (Ishizawa et al., 2016b). This suggests that the transitional state is not a continuous process, but rather a series of discrete neural changes (Ishizawa et al., 2016b).

In a particularly relevant study for my work, Hudson et al. exposed rats to decreasing concentrations of isoflurane in one-hour steps with time for equilibration in between. During these exposures, they recorded from the thalamus, superficial cingulate cortex, deep cingulate cortex, superficial retrosplenial cortex, and deep retrosplenial cortex. Spectral estimates of the simultaneously recorded LFP from each of these channels shows that, as isoflurane concentration gets lower, activity patterns become more desynchronized with less power in the lower in the lower frequency bands and more power in the frequency range of theta (Hudson et al., 2014). However, the spectral features from the different channels demonstrate that, even within a single step under constant isoflurane exposure, there are spontaneous transitions between distinct activity patterns, or states. The spectral features also demonstrate that emergence from anesthesia is not a graded process, as the brain is regularly switching back and forth between states that are more or less desynchronized than one another. If emergence were a linear, graded process, each transition leading towards recovery of consciousness should be from a state that is more synchronized to one that is less so. That is not true of this dataset. Additionally, this group's data shows that, while most state transitions seemed to occur simultaneously in all channels, some did not (Hudson et al., 2014).

Hudson et al. built a classifier of brain state by subjecting spectra from all simultaneously recorded channels together to principal component analysis and k-means clustering (Hudson et al., 2014). They found that brain states are characterized by discrete, stable activity patterns (Hudson et al., 2014). Furthermore, they found that each of their eight brain states is characterized by the presence of different oscillation patterns that are typically associated with the thalamocortical network during sleep and anesthesia.

Specifically, three states were associated with burst suppression, three others were associated with power concentrated in the frequency range of the delta oscillation, and the last two states were associated with power concentrated in the theta oscillation range (Hudson et al., 2014). The output of their state classifier provided a brain state classification for each window of spectra across time. When they investigated the organization of these states across the duration of their recordings and the transition probabilities between them, this group found that not all transitions were possible and there was an order to the states across time. While there are fluctuations back and forth between states with more or less synchronous activity patterns, in general, deeper anesthesia was associated with burst suppression and lighter anesthesia was associated with the theta oscillation. There was a progression in the proportion of windows in each state during each concentration step that started with virtually all windows assigned a burst suppression state in the deepest step towards the majority of windows assigned to a theta state in the lightest step (Hudson et al., 2014).

What these data establish is several important characteristics of state transitions under anesthesia. First, emergence from anesthesia relies on the reorganization of the thalamocortical network through a series of distinct brain states. Next, while progression through these discrete states on the way to emergence generally follows a path from most suppressed to least, this progression is not linear. Finally, because the thalamus was recorded during these experiments, they demonstrated that brain states during emergence from anesthesia involve activity throughout the thalamocortical network.

Mechanisms known to drive cortical state transitions

Most of what is known about cortical state transitions comes from studying sleep which is characterized by transitions between a series of sleep stages and the transition to wakefulness. Extracellular recordings collected during sleep are dominated by cortical activity (Buzsáki et al., 2012). Cortical activity during sleep exhibits the same oscillatory activity as described previously. While these oscillations are generated by the thalamocortical network, pathways ascending from the pons and the basal forebrain are known to heavily influence cortical activity during sleep (Buzsáki et al., 2012; Saper et al., 2005; M. Steriade et al., 1993; Takahashi et al., 2009; Yael et al., 2018). These ascending pathways are divided between sleep and wake promoting. Sleep and wake promoting neuronal populations exhibit self-excitation and mutual inhibition (Cho et al., 2017; Donlea et al., 2018; Sara, 2009; Scammell et al., 2017; Schwartz and Roth, 2008). Such neuronal networks are thought to give rise to a winner-take-all strategy referred to as the flip-flop switch (Saper et al., 2005). It has been hypothesized that the main purpose of the sleep flip-flop switch is to assure that the states of sleep and wakefulness do not co-exist simultaneously and to assure the stability of the states of sleep and wakefulness.

Therefore, states of sleep and wake are typically considered to be global. Similarly, transitions between sleep and wake states are also typically considered global phenomena. Transitions are driven by subcortical mechanisms that project widely throughout the cortex to elicit a global state transition. This section provides an overview of some of the key processes that mediate global transitions from a state of less synchrony to more synchrony and transitions from a state of synchrony to desynchrony during sleep.

Transitions from less synchrony to more synchrony

During wakefulness, activity patterns are desynchronized and there is extensive excitatory input passing between the cortex and thalamus. The excitatory signaling from the cortex is a powerful depolarizing force for the thalamus, as corticothalamic neurons are known to release excitatory amino acids onto their thalamic targets (Steriade et al., 1991). The activated brain state caused by this excitatory activity effectively suppresses the mechanisms that give rise to sleep states by mostly inactivating an ionic current that has an important role in the generation of these sleep states: the low-threshold calcium current (I_t) (Steriade and Llinás, 1988).

I_t is inactivated by depolarization of the cellular membrane. Therefore, hyperpolarization of cell membranes is a critical feature of the sleeping brain. I_t is generated by the T-type calcium channels which are found on neurons throughout the brain, including the thalamus where these channels are highly expressed. Once sleep begins, the cells of the thalamocortical network become hyperpolarized, and T-type calcium channels become available for opening (Cain and Snutch, 2010). Once a neuron is hyperpolarized, small membrane depolarizations are sufficient to cause the T-type calcium channel to open and allow extracellular calcium ions to enter the cell (Iftinca, 2011). This rush of positive calcium ions further depolarizes the cell membrane and causes the neuron to fire a burst of action potentials. As discussed in a previous section, this current is partially responsible for generating the delta oscillation.

In addition to allowing for the cellular mechanisms that drive the delta oscillation, hyperpolarization of the thalamocortical network seems to be essential for the generation of all synchronous oscillations associated with sleep (Steriade et al., 1991). This has been shown in experiments during which cortex was stimulated while thalamocortical

cells were held at different membrane potentials (Steriade et al., 1991). At resting membrane potential (-55 mV), cortical stimulation elicited a spindle oscillation in the thalamocortical neuron. When the thalamocortical cell was held at a hyperpolarized membrane potential (-63 mV), cortical stimulation induced a delta oscillation (Steriade et al., 1991). These results suggest that progressive hyperpolarization of the thalamocortical network during sleep may be responsible for the activity patterns generated by the thalamocortical network during subsequent stages of sleep (Steriade et al., 1991).

Transitions from synchrony to desynchrony

As discussed earlier, the thalamocortical oscillations characteristic of sleep and anesthesia generalize to engage the entire thalamocortical network, and they are each self-sustaining. How, then, does the sleeping brain awaken and reenter a depolarized, desynchronized brain state that is capable of supporting consciousness? The answer to this lies in the reticular formation of the brainstem. The reticular activating system is a system of ascending relays whose direct stimulation is sufficient to desynchronize activity in the cortex (Moruzzi and Magoun, 1949). This desynchronizing effect occurs in all areas of cortex simultaneously and is mediated, in part, by the diffuse projections from thalamus to cortex (Moruzzi and Magoun, 1949). It should be noted that the brain must be in a hyperpolarized state for the reticular activating system to have an effect. Identical stimulation was shown to be effective at inducing desynchrony in both a drowsy and anesthetized cortex but had no effect on activity in an already desynchronized cortex (Moruzzi and Magoun, 1949).

Various studies have demonstrated that each of the thalamocortical oscillations discussed above are susceptible to disruption via the reticular activating system. The

spindle oscillation was blocked by a stimulation to the parabrachial nucleus of the reticular formation in anesthetized and naturally sleeping cats (Hu et al., 1989). Specifically, the reticular neurons are reliably inhibited by parabrachial stimulation. In accordance with Moruzzi and Magoun's foundational work, inhibition of reticular neurons was only observed if the cell was already sitting at a membrane potential favorable for sleep (Hu et al., 1989). Hyperpolarization of reticular neurons by the reticular activating system prevents them from sending rhythmic IPSPs to thalamocortical neurons and thereby effectively ends the spindle oscillation (Steriade et al., 1985).

Similarly, the delta oscillation is also reliably disrupted by parabrachial stimulation (Steriade et al., 1991). Simultaneous cortical EEG recordings show an activation response in the cortical recordings after parabrachial stimulation (Steriade et al., 1991). This activation response is seen as the cessation of a pronounced delta oscillation and beginning of desynchronized, low amplitude signal. These results demonstrate that, like the spindle oscillation, the delta oscillation depends on hyperpolarization in the thalamocortical network and that short depolarizing input from the reticular activation system is sufficient to destabilize this oscillation and induce a state of desynchrony. Finally, stimulation of two other reticular nuclei, pedunculopontine tegmental cholinergic nucleus and locus coeruleus, blocked a slow wave oscillation at about 0.3 Hz in cortical neurons (Mircea Steriade et al., 1993b).

In sum, the reticular activating system is a subcortical collection of brain regions that collectively innervate the entirety of the cerebral cortex and are capable of destabilizing the synchronous oscillations of sleep and anesthesia so that a state of wakefulness may be established (Mircea Steriade et al., 1993a). These nuclei release various excitatory neurotransmitters including acetylcholine, norepinephrine, serotonin, histamine, and

glutamate onto their cortical targets (Steriade and McCarley, 1990). There is growing recognition of the fact that many of these neurotransmitters are also effective in destabilizing the anesthetized state and driving emergence (Aston-Jones et al., 2001; Kelz et al., 2008; Luo and Leung, 2009; Solt et al., 2011). The effect of this excitatory input is to cause depolarization of the cortical neurons which, in turn, depolarize the thalamus via extensive corticothalamic projections. By relieving the synchrony and order imposed by hyperpolarization, the reticular activating system allow the thalamocortical network to again receive and process information from the environment and regain a state of consciousness.

Why do transitions occur? Two alternatives

The question at the core of my thesis work is related to why it is that the brain undergoes state transitions under general anesthesia. Given that anesthetic-induced unconsciousness is an unnatural state of the brain characterized by a disconnection from the outside environment and wide-spread suppression of neurons, it would perhaps be more intuitive to assume that there should not be different brain states or discrete transitions. This was certainly the assumption of basic neuroscientists and anesthesiologists until very recently. However, given the results of the studies highlighted in the previous sections, it is clear that there are indeed discrete state transitions during anesthetic-induced unconsciousness. For my thesis work, I set out to investigate the mechanisms driving these state transitions.

State transitions during states of sleep and wake are generated subcortically via modulation of excitatory tone within the thalamus or by the reticular activating system. Through dense innervation of the cortex via either the thalamus or the reticular activating system, a central signal to change activity patterns is projects widely throughout the

cortex which gives rise to discrete, global state transitions. In order to test whether state transitions under anesthesia are generated by similar mechanisms, we laid out two potential, experimentally distinguishable mechanisms. The first is that transitions are like sleep transitions and are coordinated throughout the cortex by a single, central signal that is simultaneously projected to the entirety of the cortex. Such a signal would need to come from a subcortical structure that sends dense, wide-spread connections to the cortex. Evidence to support this hypothesis would be that recordings from spatially distinct areas of cortex undergo state transitions at the same time. The alternative hypothesis is that state transitions under general anesthesia are local and that local cortical interactions are what organize spatially restricted, stable brain states. If this mechanism were true, it would imply that corticocortical interactions are what give rise to states. Evidence in support of this hypothesis would be spatial heterogeneity between brain states and transition times between recordings collected from different areas of cortex.

Neural inertia and the resistance to state transitions

Regardless of the specific mechanisms that give rise to state transitions under anesthesia, brain activity patterns under anesthesia fluctuate back and forth between states of more or less synchrony (Hudson et al., 2014). This demonstrates that emergence from anesthesia is not a linear process during which elimination of drug allows the brain to ascend from its deepest point of anesthesia back to consciousness. These data provide a potential explanation for what has been a curious phenomenon that is gaining more attention in the field of anesthesia: anesthetic hysteresis.

Until very recently, it was assumed by basic scientists and anesthesiologists alike that emergence from anesthesia was the simple inverse of induction. If this were true, there should be a simple mapping between brain state and anesthetic concentration. Consequently, it should be possible to predict how long it will take an individual to reach emergence based on the deepest plane of anesthesia that they experienced, and there should be a one-to-one relationship between probability of reaching emergence and anesthetic concentration. However, data collected from several model organisms as well as humans demonstrates the relationship between brain state and anesthetic depth is not linear.

First, it has been shown that the anesthetized brain resists the transition to consciousness. In rodents, one way to assess emergence is to place them in a supine position. If an animal is anesthetized, they are not able to right themselves from this vulnerable position. If they are sleeping or conscious, they will immediately right themselves. This righting reflex is commonly used to identify deep anesthetic depth in rodents. If you expose mice to progressively higher concentrations of isoflurane or halothane general anesthesia in long exposure steps with equilibration time in between and assess the righting reflex at each step, you are able to get a percentage of mice at each concentration that retain the righting reflex. As expected, the percentage of mice that retain the righting reflex at each concentration step decreases as a function of anesthetic dose during induction (Friedman et al., 2010). However, during emergence when the steps of fixed anesthetic concentration become progressively smaller, the dose response curve is not the same as for induction. There is a leftward shift, meaning that the percentage of mice capable of righting themselves at each step is consistently lower

than the percentage of mice capable of righting themselves during the same concentration step during induction (Friedman et al., 2010).

These results were also shown in *Drosophila melanogaster* in the same study using percent of flies active during a window of time as the output metric (Friedman et al., 2010). A trivial explanation of these results could be that the lipophilic property of anesthetic drugs causes drug to accumulate in the brain's fatty tissue and that, while the delivered concentration of drug was the same at two steps, the actual concentration experienced by the organism was higher during emergence because there is still residual drug accumulated in the tissues. To dispel this possible explanation, Friedman et al. measured the concentration of the delivered anesthetic in the brain tissue (for mice) or whole organism (for *Drosophila*) and found that the concentration of anesthetic drug in the tissue at EC_{50} was higher during induction than emergence (Friedman et al., 2010). Therefore, the trivial pharmacokinetic explanation of these data cannot be true. Rather, these results demonstrate that there is a hysteresis between induction and emergence dose-response curves such that the brain resists the emergence to consciousness (Friedman et al., 2010). This hysteresis shows the emergence cannot be explained simply as the reverse of induction.

The same study also sought to characterize a potential mechanism for this phenomenon. They show results that implicate the endogenous sleep/wake circuitry in driving emergence from anesthesia. The locus coeruleus is one of the nuclei of the reticular activating system and is the main source of norepinephrine in the brain (Aston-Jones et al., 2001). To test for the involvement of endogenous arousal circuits, mice with a global knockout of norepinephrine and epinephrine were assayed (Thomas et al., 1995). When these mice were tested alongside heterozygous controls, there was a slight

leftward shift in the induction curve: indicating that the homozygous knockouts were slightly hypersensitive to anesthesia. However, the effect on the emergence curve was far more dramatic. Without norepinephrine and epinephrine, the emergence curve was dramatically left shifted: indicating that these mice had enormously delayed emergence times, compared to controls (Friedman et al., 2010). Furthermore, reinstating norepinephrine and epinephrine in the CNS was sufficient to rescue the wildtype dose-response curves (Friedman et al., 2010). Similar results were collected using drosophila mutants with a mutated potassium channel (Friedman et al., 2010). In wild type flies, this potassium channel decreases neuronal activity and promotes sleep. *Shaker* mutants in which this channel has been genetically disrupted, have reduced sleep and resist induction with anesthesia (Cirelli et al., 2005). When the induction and emergence dose response curves for these mutants were compared to wild type controls, hysteresis in the *Shaker* mutants had collapsed (Friedman et al., 2010). Wild type dose response curves were rescued in these mutants with CNS-specific reinstatement of adrenergic signaling (Friedman et al., 2010).

What these data show is that emergence from anesthesia is not the simple inverse of induction. There is no simple mapping between the dose of anesthetic drug delivered and the state of the brain. If it were, there should be an equal probability across a population of retaining the righting reflex at a specific anesthetic concentration, regardless of whether it is during induction or emergence. Furthermore, the same lab has shown that, even for a single individual mouse, the time it takes to reach emergence from anesthesia, given the exact same exposure to anesthesia, is highly variable. This, along with the findings drug concentration in the tissue is higher at EC₅₀ during induction than during emergence, demonstrates that a pharmacokinetic explanation of these

results is insufficient. Instead, these findings provide evidence to support the statement that emergence from anesthesia involves complicated, structured mechanisms of reorganization within the cortex as it reassembles consciousness. These data also implicate the endogenous arousal systems of the brain in anesthetic emergence. Disruption of this system substantially delays emergence. This suggests that the same circuitry involved in awakening plays a role in emergence from anesthesia. This is an important finding because it indicates that the process of reaching emergence relies on neuronal mechanisms and not the simple washout of drug.

Goals of thesis

The aim of this thesis is to present my work in support of a potential mechanism for state transitions under anesthesia and evidence that suggests emergence from anesthesia is a complex process in humans. In Chapter 2, I will present my work in investigating the cortical mechanisms that give rise to state transitions under anesthesia. I show that stable brain states and transitions between them are organized by local cortical interactions and that weak interactions between distinct cortical regions are sufficient to give rise to coherent, global brain states. In Chapter 3, I will present work showing that time to emergence from anesthesia cannot be predicted by depth of anesthetic exposure alone in humans. These findings suggest that humans, like mice and drosophila, likely resist the transition to consciousness following anesthetic exposure. This would imply that our own cortices must engage in a careful, complex reorganization process in order to achieve emergence.

CHAPTER 2 – Weak Coupling Between Spontaneous Local Cortical Activity State Switches Under Anesthesia Leads to Strongly Correlated Global Cortical States

INTRODUCTION

Brain activity arises as a result of interactions amongst billions of neurons and synapses. Each component in this vast network exhibits complex nonlinear dynamics (Hodgkin and Huxley, 1952; Pan and Zucker, 2009). Generically, such complex nonlinear dynamical systems can dramatically change their collective behavior after small changes in parameters or perturbations to their ongoing activity (Canavier et al., 1993; Destexhe et al., 1994; Ermentrout, 1998; Izhikevich, 2007; Strogatz, 2015). Furthermore, because nonlinear systems generally have multiple steady state behaviors, there is no guarantee that after a dramatic perturbation, the system will recover to its previous state once the perturbation subsides.

These considerations suggest that brain activity ought to be quite fragile and unable to withstand dramatic perturbations. Contrary to this intuition, there is ample evidence that the brain is remarkably robust to perturbations. Seizures, for instance, are a paradigmatic example of aberrant brain activity, being characterized by extreme synchronization in neuronal firing and subthreshold voltage fluctuations (Timofeev et al., 2004). While seizures can be followed by a transient postictal period characterized by abnormal brain activity and function (Fisher and Engel, 2010), normal brain function is eventually restored. Another classic example of the brain's ability to recover from an extreme perturbation is general anesthesia (Brown et al., 2010). Every year, millions of patients undergo general anesthesia. While some patients experience aberrant brain

activity, which manifests as delirium upon emergence (Saczynski et al., 2012), most eventually recover normal brain activity and cognitive function. During general anesthesia, the brain may exhibit dramatically abnormal activity patterns, such as burst suppression, which is caused by the hyperpolarization and silencing of more than 90% of cortical neurons (Amzica, 2009; Civillico and Contreras, 2012; Contreras and Steriade, 1997). Occasionally, complete isoelectric electroencephalogram (EEG) is observed in surgeries requiring circulatory arrest (Stecker et al., 2001). Nevertheless, once anesthetic delivery is stopped, the brain regains normal function. Given this and the fact that anesthetic delivery can be precisely controlled, general anesthesia is a good model system to address the general question of how the brain is able to restore normal activity patterns after a dramatic perturbation.

Several converging lines of evidence strongly argue that recovery from anesthesia cannot be explained by anesthetic washout alone. The first is that recovery of consciousness after anesthesia occurs at a lower anesthetic concentration than induction of anesthesia across taxa, from *Drosophila* (Joiner et al., 2013) to mice (Friedman et al., 2010) and humans (Warnaby et al., 2017). Furthermore, this neural inertia can be modulated by factors altogether unrelated to the concentration of anesthetic, such as single gene mutations (Friedman et al., 2010) and manipulations of specific neuronal populations (Kelz et al., 2008; Reitz et al., 2021; Zhou et al., 2018). Together, these results strongly argue that recovery from anesthesia is not simply the byproduct of anesthetic washout. They do not, however, directly shed light on the mechanisms that allow the brain to recover after general anesthesia.

In order to recover from anesthesia, the brain must follow a path through the state space that begins in the deeply anesthetized state and eventually leads back to the pre-anesthetic conditions. The neurophysiological processes that allow the brain to navigate this path efficiently have been addressed by Hudson et al. (Hudson et al., 2014). Specifically, they show that *en route* to recovery of consciousness, brain activity is constrained to a low-dimensional space. In this space, most activity is confined to a small number of discrete activity patterns, and the transitions between these patterns are highly structured. In sum, these mechanisms greatly constrain the number of possible paths through the activity space that can lead to wakefulness and allow the brain to recover consciousness on a physiological time scale. Abrupt transitions between discrete activity states have been observed in rodents (Hudson et al., 2014), non-human primates (Ballesteros et al., 2020b; Ishizawa et al., 2016a; Patel et al., 2020) and human patients (Chander et al., 2014) after exposure to a variety of anesthetics with distinct mechanisms of action. Abrupt transitions between different activity patterns at a fixed anesthetic concentration are observed not only at the level of the local field potentials (e.g., Hudson et al., 2014), but also in the activity of individual cortical neurons (Lee et al., 2020). These discrete activity patterns and structured transitions between them serve as a scaffold that guides the brain back towards normal patterns of activity after it has been profoundly disrupted by anesthetics.

Given that state transitions are critical for reinstating consciousness, it is of fundamental importance to determine the neuronal mechanisms that give rise to transitions between discrete activity states during recovery from a dramatic perturbation. Previous work on anesthesia (Chander et al., 2014; Hudson et al., 2014; Ishizawa et al., 2016a) and sleep (Gervasoni et al., 2004) defined different activity patterns on the basis of oscillatory

activity observed in the local field potentials (LFPs) of firing of individual neurons (Lee et al., 2020). Much of this oscillatory activity is coordinated via thalamocortical loops (Contreras and Steriade, 1997; Liu et al., 2015; Schiff, 2008; Mircea Steriade et al., 1993b). An extensive body of work shows that the thalamocortical circuitry is modulated by the arousal pathways ascending from the brainstem and basal forebrain to produce oscillations at different characteristic frequencies (Destexhe et al., 1994; Jones, 2003; Mircea Steriade et al., 1993a). Indeed, during constant anesthetic concentration, fluctuations in the firing rates of individual neurons within these arousal nuclei co-vary with fluctuations in the spectra of cortical LFPs (Gao et al., 2019). Direct manipulations of neuronal activity within the reticular activating system can elicit profound changes in the oscillations observed in the cortical LFP (Gao et al., 2019; Moruzzi and Magoun, 1949; Mircea Steriade et al., 1993a; Vazey and Aston-Jones, 2014). Thus, one distinct possibility is that the discrete oscillatory patterns of activity observed under fixed anesthetic concentration are imposed onto the thalamocortical networks by fluctuating modulatory tone. If this is the case, because modulatory systems project broadly across the thalamus and cortex (Jones, 2003), we expect to find that abrupt transitions between distinct oscillations occur in close temporal proximity across the different cortical layers and regions. Alternatively, it is possible that the oscillatory activity in different cortical regions is largely coordinated through short-range thalamocortical and cortico-cortical interactions. In this case, we expect to find that transitions between different oscillatory patterns are largely local.

Here, we provide direct experimental evidence for this latter possibility by simultaneously recording abrupt transitions between different states across cortical layers and across distant cortical areas at a constant anesthetic concentration. Using a complementary

combination of analytic techniques, we show that state transitions across different cortical sites are only weakly coupled. Furthermore, we demonstrate that state transitions in layer 4 (L4)—the layer that directly receives input from the thalamus—are particularly decoupled from state transitions observed in other layers. This suggests that cortico-cortical interactions rather than fluctuations in the broad modulatory tone play a crucial role in controlling state transitions under anesthesia. Remarkably, we also show that the multitude of weak pairwise interactions between local state transitions is sufficient to constrain the overall brain activity to just a few states embedded in a low-dimensional space. Thus, our results suggest that the highly coordinated, low-dimensional macroscopic brain dynamics that allow the brain to recover from a dramatic perturbation emerge as a consequence of a multitude of weak pairwise interactions between different cortical sites.

RESULTS

State transitions under constant anesthetic can be local

We sought to determine whether state transitions under a fixed concentration of isoflurane (1% atm.) occur simultaneously across different cortical regions and across layers within the same cortical region. This concentration was chosen based on previous work (Hudson et al., 2014) showing that burst suppression is not likely to occur at this concentration, but that state transitions in the spectral characteristics of the LFP are frequently observed. Here we focused on the local field potentials (LFPs) recorded using two laminar probes that sampled signals across all cortical layers. In half of the experiments, both electrodes were inserted into the right hemisphere: one in the primary visual area (V1) and the other in the motor cortex (M1) ($n = 3$) (**Figure 2.1A**). In the other

half of experiments, bilateral V1 recordings were performed ($n = 4$). Postmortem localization of electrodes (Methods) in a representative experiment is shown in **Figure 2.1B**. Consistent with previous findings (Hudson et al., 2014), at 1% isoflurane, the power spectrum of the LFP fluctuated between several discrete states (**Figure 2.1C**).

State transitions can be readily identified in the raw LFP (**Figure 2.2**). The top and bottom LFP traces show one minute of recordings from a single M1 and V1 electrode, respectively. The accompanying spectra were calculated using a multitaper spectral estimate. These spectra were averaged across two second windows of LFP with a one second step size, sampled either from eight to two seconds prior to transition (black, pre-transition) or from two to eight seconds after the transition (red, post-transition). Spectral estimates are shown as mean \pm 95% confidence interval computed from 1000 bootstraps. In some instances, state transitions occur approximately simultaneously in the motor and visual cortices (**Figure 2.2A**). However, this was not always the case. For instance, **Figure 2.2B** shows an example of a state transition that occurs first in the visual cortex and, only after a delay of approximately 10 seconds, is seen in the motor cortex. Thus, abrupt changes in the LFP characteristics need not occur simultaneously in different brain regions. **Figure 2.2C** shows a more extreme example of this phenomenon. A state transition is clearly seen in the motor cortex, but in the visual cortex, the LFP characteristics remain unchanged. These observations suggest that, while some state transitions may indeed be global, there is a previously unappreciated degree of independence between state fluctuations observed in the cortex during fixed anesthetic administration.

Multitaper analysis and non-negative matrix factorization extract states and their transitions across cortical layers and regions

To quantify the degree of coupling between state transitions at different recording sites, we developed a methodology to automatically detect state transitions at the level of individual channels (Methods). We then deployed this methodology to determine the degree to which transitions in different cortical sites are coupled. **Figure 2.3** is a flowchart of the initial analysis steps. The first step in the analysis is to compress the LFP recording into a low-sample-rate, low-dimensional matrix that accurately captures fluctuations in oscillatory activity. The right side of the figure presents an example five-minute window of data from one recording site to demonstrate the outcome of each step. Briefly, wideband data were filtered between 0.1 and 300 Hz to extract the LFP signal. (**Figure 2.3A**) LFP signals were converted to frequency domain using multitaper spectral analysis, (**Figure 2.3B**). Raw power spectra were then normalized such that the power contained in each frequency band was mapped onto a value between 0 (smallest observed power) and 1 (largest observed power) (**Figure 2.3C**). Non-negative matrix factorization (NMF) was used to further decompose the signal into a set of loadings and associated scores across time (**Figure 2.3D-E**).

NMF can be thought of as a “soft” clustering algorithm. Previous work on state transitions under anesthesia (Hudson et al., 2014) and sleep (Gervasoni et al., 2004) used k-means clustering of the spectrograms to assign the state of the brain. Our first approach to state assignment used a similar strategy—the index of the NMF component with the highest score in each time window was defined as the state of the LFP at each recording site (Methods). This assumption was relaxed in subsequent stages of the analysis (see below). **Figure 2.4A** shows the score matrices for two different channels

recorded simultaneously from two contacts along the same electrode in the motor cortex. The upper matrix is the same as **Figure 2.3E**, and the lower matrix was generated from data collected by a contact 140 μm deeper inside the cortex. Notice that these matrices resemble one another but are not identical. **Figure 2.4B** shows state classifications for 18 channels of simultaneously recorded data: nine from an electrode in V1 and nine from an electrode in M1. Note again that some state transitions are observed around the same time in most of the electrodes. There are, however, many instances where state transition is observed in just a subset of the recording sites.

One way to characterize the coupling between state transitions is to quantify the propensity of state transitions to occur simultaneously across different recording sites. Brain state transitions were defined as time points at which consecutive windows from the same channel have different brain state assignments (Methods). **Figure 2.4C** shows an example of this analysis. There are many transitions that appear in only one or very few channels, while others appear to be more global. **Figure 2.4C** is a raster plot of transitions. The color of each line shows the synchrony score of that transition with all other channels (Methods). Consistent with the observations in **Figure 2.2** and **2.4C**, the synchrony score reflects the fact that most state transitions are localized to a small subset of electrodes.

As we show below, coupling between state transitions depends on the cortical layer. Layer assignment in V1 was performed using current source density (CSD) analysis computed immediately following brief light stimulus (Methods). **Figure 2.5** shows a representative example of CSD in V1 showing the stereotypical pattern of response to visual stimuli. The first current sink occurs approximately 33 ms following stimulus presentation in L4. A short time after, additional sinks and sources appear above and

below, revealing interlaminar communication. The channel where the initial sink occurred was defined as the center of L4. The dashed black lines in this figure mark the approximate boundaries of L4 based on the average thickness of this layer in rats and the spacing between channels (Einevoll et al., 2013; Quairiaux et al., 2011; Self et al., 2013). In the motor cortex, we did not estimate the location of cortical layers directly. Instead, we estimated the depth of each recording electrode relative to the cortical surface.

State transitions in different cortical sites exhibit weak synchrony

We used three different analytical techniques to quantify the tendency of oscillatory states and the transitions between them to be coordinated across recording sites. Each technique relies on a different set of assumptions and was performed on a different feature of the data. First, we quantified the synchrony of transitions, as demonstrated in **Figure 2.4** (Methods). **Figure 2.6A-B** shows the cumulative distribution of synchrony scores (red curves) computed over all channel pairings and across all animals (M1/V1: 3 animals, 16–18 electrodes/animal, median of 99 transitions/electrodes/animal; bilateral V1: 4 animals, 15–19 electrodes/animal, median of 175.5 transitions/electrode/animal).

In order to compare the synchrony scores (**Figure 2.6A-B**) to those expected by chance, we generated shuffled datasets constrained to have the same state transition statistics. This was accomplished by simulating a Markov process defined by the state transition probability matrix derived from state assignments for each recording (Methods). This control preserves the statistics of each recording site, while destroying any coordination between them. The cumulative distributions of the synchrony scores obtained in these shuffled controls are shown in **Figure 2.6A-B** (blue curves; shading shows 95% confidence intervals computed over 1000 shuffled datasets). Both in the experiments

involving M1 and V1 (**Figure 2.6A**) and in those involving bilateral V1s, we find that the synchrony score is consistently higher than expected by chance ($p < 0.001$, z-test based on means of shuffled datasets). Despite this large deviation from the null hypothesis, state transitions do not typically occur at the same time in different cortical sites (mean synchrony score ≈ 0.35 for both M1/V1 and bilateral V1 recordings). This implies that while state transitions observed across different cortical sites are not completely independent, coupling between channels is weak.

Data in **Figure 2.6A-B** aggregate the transition synchrony scores calculated between all channel pairs—both pairs of channels in the same cortical region and those located in different cortical sites. We hypothesized that, because most cortical connectivity is local, nearby electrodes would tend to have a higher propensity to change state at the same time. **Figure 2.6C-F** shows that state transitions are indeed more synchronous between electrodes within a cortical region than between regions. **Figure 2.6C-D** shows synchrony scores between all channel pairs in a representative pair of experiments: an M1/V1 experiment (**Figure 2.6C**) and a bilateral V1 experiment (**Figure 2.6D**). Pairs with scores that did not reach significance compared to the shuffled datasets, after Bonferroni correction for multiple comparisons, are shown in gray. Across all experiments, 57.0% of channel pairs from M1/V1 experiments and 80.2% of pairs from bilateral V1 experiments had significantly synchronous transitions at the corrected $p < 0.05$ level. The synchronization scores for all channel pairs from all experiments are quantified in **Figure 2.6E-F**, for M1/V1 and bilateral V1 experiments respectively. Both panels show the synchrony scores for within-region channel pairs (red) and between-region channel pairs (blue). In both types of recordings, within-region pairs had significantly larger synchrony

scores than between-region pairs ($p = 1e-7$ for M1/V1 and $p = 2e-7$ for bilateral V1, compared to 10^7 random permutations of the relevant channels (Methods)).

L4 is the thalamic input layer and has fewer horizontal connections than the supragranular or infragranular layers, which are rich in horizontal connections (Zilles and Palomero-Gallagher, 2017). To test whether layer organization affects transition synchrony, from each V1 recording (in which L4 was identified using CSD), we separated channel pairs in which one channel was in L4 from pairs in which neither channel was in L4. **Figure 2.6G** presents synchrony scores from all channel pairs from all experiments in which one channel was in L4 and the other was not (purple) and all channel pairs from all experiments in which neither channel was in L4 (orange). In **Figure 2.6E** and **F**, the specific channel pairs that were included in the “L4” and “non-L4” groups are outlined in purple and orange, respectively. We found that synchrony between channel pairs with one channel in L4 tended to be lower than between pairs in which neither channel was in L4 ($p = 0.015$, compared to 10^7 random permutations of the relevant channels (Methods)). Therefore, transition times in channels from L4 tend to be relatively uncoupled from the specific timing of transitions in channels from other layers. This observation suggests that it is unlikely that thalamocortical input is the principal driver of state transitions in the cortex. If it were, one would expect that the thalamic input layer (L4) would transition in synchrony with the rest of the cortex. Therefore, these results imply different mechanisms, such as cortico-cortical interactions, are likely responsible for the timing of these spatially localized transitions.

Our final analysis using synchrony scores was performed to build upon these L4 results and determine whether the type of subcortical input to a cortical region has an influence on transition synchrony. It is typically assumed that switches of the oscillatory activity in

the cortical LFP critically involve interactions with the thalamus (Contreras and Steriade, 1997; Herrera et al., 2016; Liu et al., 2015; Schiff, 2008; Mircea Steriade et al., 1993a, 1994). In light of this, one may expect two regions receiving similar thalamic input to exhibit greater synchrony of state transitions than two regions that interact with the thalamus in different ways. Therefore, we tested whether between-region comparisons for the bilateral V1 experiments had higher synchrony scores than the between-region comparisons for the M1/V1 experiments. Contrary to our hypothesis, we were not able to detect any increase in synchrony scores calculated between the bilateral V1s relative to M1/V1 experiments ($p = 0.35$, percentile bootstrap over channels (Methods)).

Discrete states in different cortical sites have weak correspondence

Until this point, our analysis was based on transition synchrony, a measure that is sensitive to the timing of transitions but not the identities of the states. In what follows, we shift our focus away from the timing of state transitions and quantify the consistency of LFP-defined states at different sites. We accomplish this using normalized mutual information (MI), a measure of the amount of information obtained about one random variable by observing another random variable (Methods). In our case, these random variables are the time series of discrete states of two channels. High MI between these time series represents a large reduction in uncertainty about the state in channel j given the state in channel i . Two channels do not need to be in the same brain state to have high mutual information; indeed, since states are defined for each channel independently, there is no definition of different channels being in the “same” state. Rather, there must only be a consistent mapping from the states in one channel to those in the other. For example, if channel i is always in state A whenever channel j is in state D, one can predict the state of channel i from the state of channel j , and the MI between

these channels would be high. As noted in the Methods, we normalized MI by the total entropy of the state distributions in the two channels over time in order to obtain a measure that was comparable across channels with different state distributions.

Figure 2.7A-B shows the normalized MI between all channel pairs in the same representative M1/V1 and bilateral V1 experiments as those in **Figure 2.6C-D**. 81.9% of channel pairs from M1/V1 experiments and 96.9% of pairs from bilateral V1 experiments had normalized MI that was significantly higher than for shuffled data, after Bonferroni correction for multiple comparisons (z-test based on distribution of shuffled data). The summary of normalized MI across all animals is shown in **Figure 2.7C-D**, for M1/V1 and bilateral V1 experiments respectively. In both types of recordings, within-region channel pairs had significantly higher normalized MI than between-region pairs ($p = 1e-7$ for M1/V1 and $p = 1e-7$ for bilateral V1, compared to 10^7 random permutations of the relevant channels (Methods)). Note that, while for most channel pairs MI was higher than for a shuffled dataset, the amount of information about the state of one channel contained in the state of another was small. Normalized mutual information varies between 0 and 1, where 1 denotes that the two channels carry identical information. Yet, even in a pair of channels within a single cortical region, the mean MI is about 0.3. One way to interpret this statistic (Methods) is that no more than 15% of the combined information carried by the states of any two channels is redundant. Thus, most of the information about the state of one channel cannot be extracted from observing the state of a nearby channel in the cortex.

As with transition synchrony, we did not detect a higher mean normalized MI in left/right V1 channel pairs compared to M1/V1 channel pairs ($p = 0.70$, percentile bootstrap over channels (Methods)). Additionally, as with the transition synchrony analysis, pairs

including a channel in L4 did have lower normalized MI than pairs where neither channel was in L4 ($p = 0.002$, compared to 10^7 random permutations of the relevant channels (Methods)). These results show, not only that channels from the same brain region are more likely to undergo transitions at the same time, but also that the broader structure of these state assignments across the entire recording is more similar in channels from the same region. Furthermore, the conclusions regarding the differences between L4 and other cortical layers are consistent between synchrony and mutual information analyses.

Full compressed spectrograms of different sites have moderate correspondence, depending on distance and cortical layer

In the previous analyses, to generate a single-value description of activity across time, we defined brain state as the NMF loading with the highest score in each time window. This method was convenient for comparing synchrony of transitions and mutual information of state sequences. Parcellation of the LFP signals into discrete states is also supported by previous work (Hudson et al., 2014) However, reducing the LFP to a single value eliminates much of the information in the original signal. In order to incorporate more of this information, rather than collapsing the LFP signal to a single value, we used the vector of NMF scores for the LFP in each temporal window directly. Each score vector, once multiplied through by the appropriate loading matrix (Methods and **Figure 2.3**), yields a good approximation of the actual spectrum of the LFP in that time window.

To test for correlated fluctuations in the spectral features of LFPs at different cortical sites, we applied canonical correlation analysis (CCA) to the pair of score matrices derived from each pair of channels. High canonical correlation indicates a close linear relationship between two sets of variables. The mean of the vector ρ of canonical

correlations between all pairs of canonical variables was calculated to give a measure of overall state similarity that is invariant to invertible linear transformations of each channel's state space. This method of taking the average across ρ is explained further in Alpert and Peterson (1972). **Figure 2.8A-B** shows the CCA similarity measure for all channel pairs from the same representative M1/V1 and bilateral V1 experiments that have been shown previously. All channel pairs from both M1/V1 and bilateral V1 experiments had significantly higher CCA similarities than for shuffled data, after Bonferroni correction for multiple comparisons (z-test based on distribution of shuffled data). The summary of CCA similarity across all animals is shown in **Figure 2.8C-D**. These results are very similar to those for transition synchrony and normalized MI and show that in both types of recordings, within-region channel pairs had significantly higher CCA similarities than between-region pairs ($p = 1e-7$ for M1/V1 and $p = 1e-7$ for bilateral V1, compared to 10^7 random permutations of the relevant channels (Methods)). Furthermore, as with the previous measures, channel pairs including a channel in L4 had lower CCA similarities than pairs in which neither channel was in L4 ($p = 0.001$, compared to 10^7 random permutations of the relevant channels (Methods)). We did not detect a higher mean CCA similarity in left/right V1 channel pairs compared to M1/V1 channel pairs ($p = 0.12$, percentile bootstrap over channels (Methods)).

Global brain state is low-dimensional, despite weak pairwise interactions

All results shown up until this point were calculated on pairs of channels for which state assignments were computed independently. What we have shown is that channels within the same cortical region tend to be more similar in their activity patterns and state transition times than channels from different cortical regions. However, close inspection of the results shows that, even for the channel pairs within the same cortical region, only

about one third of the information contained within the discrete state sequences is shared between channels (**Figure 2.7C**). For channel pairs from different cortical regions, the amount of mutual information in state sequences is even lower. This weak coupling between channels could imply that spatially restricted regions of the brain act independently of one another and there is no discernable global state of the brain at any given time. Alternatively, it is possible that this weak coupling between channels, *en masse*, gives rise to a complex, global state of activity that is differently expressed in the oscillation patterns of spatially restricted regions of cortex. In this final analysis, we sought to directly distinguish these possibilities by characterizing the global brain state. In a key distinction from the previous work, rather than defining the global state on the basis of the concatenated spectra from all recordings, we attempted to identify global macroscopic dynamics from the simplified dynamics observed at each recording site. This was accomplished by first concatenating the NMF score vectors from all simultaneously recorded channels at each timepoint into a single vector that encodes the joint state of all channels. The resulting full matrix of joint states over time was then subjected to principal component analysis (PCA).

We found that all but one recording required 10 or fewer components to account for 80% of the variance in the concatenated NMF score matrices, which ranged in dimensionality from 91 to 136. The recording that required greater than 10 required 15 components to reach the same threshold. This is far outside the 95% confidence interval of expected cumulative explained variance, computed on Markov-shuffled controls which ignore weak pairwise correlations between fluctuations in different channels (**Figure 2.9A, D**). These results demonstrate that widespread weak coupling is sufficient to give rise to a highly correlated global state. **Figures 2.9B** and **E** show the loadings onto channels and

frequencies (mapped back from corresponding NMF loadings) for the top two principal components of a representative M1/V1 and bilateral V1 recording, respectively. These data offer qualitative evidence that the global state is differentially reflected in different regions and layers of the cortex. For example, the loadings of the second principal component (PC2) of the M1/V1 recording in **Figure 2.9B** show that, while there is high power in the higher frequencies for the V1 channels, the same is not true in the M1 channels. In contrast, **Figure 2.9E** shows that the loadings of PC1 of the bilateral V1 recording onto all channels of both electrodes are fairly uniform, except for in channels near L4 where there is higher power in the lowest frequency bands. **Figures 2.9C** and **F** show histograms of all samples from these representative recordings projected onto the first two principal components. Although more than two dimensions would be necessary to fully visualize the landscape of the global dynamics, even in this limited projection, a clustered pattern is visible, similar to previous results (Hudson et al., 2014). These data suggest that global brain states comprise regionally distinct oscillation patterns that are weakly coupled with one another. Remarkably, these results show that discrete transitions between global cortical states (Ballesteros et al., 2020b; Hudson et al., 2014; Patel et al., 2020) under a fixed anesthetic concentration arise from the multitude of weakly coupled local fluctuations.

DISCUSSION

Here we set out to determine how abrupt transitions between global thalamocortical states arise at a fixed anesthetic concentration. Using several complementary analysis methods, we demonstrate that correlated fluctuations in the oscillatory behavior observed at different cortical sites are widespread, but that each pairwise interaction is

weak. Thus, for instance, the ability to infer the current state of one channel by observing the state of a nearby channel in the cortex is limited. Remarkably, we provide evidence that abrupt transitions between discrete macroscopic cortical activity patterns (Ballesteros et al., 2020b; Chander et al., 2014; Hudson et al., 2014; Ishizawa et al., 2016a; Lee et al., 2020; Patel et al., 2020) emerge naturally from the multitude of these quasi-independent local fluctuations. We also demonstrate that the strength of the interactions between recording sites depends on the inter-electrode distance and on the cortical layer. Specifically, we find that fluctuations in L4, the thalamic input layer, tend to be less congruent with those in other layers. Altogether, these results argue that abrupt global state transitions are not imposed on the thalamocortical networks by changes in the activity of broadly projecting modulatory arousal systems, but rather are strongly influenced by the local cortico-cortical interactions.

It has been conjectured that structured transitions between discrete states constrain the space of possible brain activity patterns and thereby allow the brain to efficiently recover its normal waking state after a dramatic perturbation (Hudson et al., 2014). The idea that, in order to recover from a perturbation, the space of possible activity states must be constrained by stabilization of a few discrete activity patterns is not specific to recovery from anesthesia *per se*. For instance, pharmacologically provoked recovery of consciousness in the setting of brain injury is also characterized by abrupt transitions between quasi-stable activity patterns (Victor et al., 2011). Sleep is also well known to consist of discrete activity patterns (e.g., Gervasoni et al., 2004). Thus, it appears that abrupt state transitions among discrete activity states accompany recovery of normal consciousness in a variety of settings.

It is thus of great interest to determine how such state transitions arise and how they are coordinated across thalamocortical networks. Here, in keeping with previous work (e.g., Gervasoni, 2004; Hudson et al., 2014), we defined the state of each local recording site on the basis of the power spectrum of the LFP. Since we focused on state transitions observed in the anesthetized brain, most fluctuations occurred in the slow oscillations (< 1 Hz) (Mircea Steriade et al., 1993b), delta oscillations (1-4 Hz), and the spindle range of 8-14 Hz (Purpura, 1968). Multiple distinct neurophysiological mechanisms contribute to the generation and coordination of the various brain oscillations observed in the anesthetized brain. Slow oscillations, for instance, are thought to be primarily generated through local synaptic mechanisms in the cortex (Sanchez-Vives and McCormick, 2000; Mircea Steriade et al., 1993b). Thalamocortical and thalamic reticular neurons reflect these slow oscillations and are phase locked to them (Mircea Steriade et al., 1993b). However, the fact that slow oscillations are abolished in the thalamus of decorticated animals (Timofeev and Steriade, 1996) but are observed in the cortex of athalamic animals (Mircea Steriade et al., 1993b) strongly argues for the cortical origin of slow oscillations. Corticocortical interactions are thought to underlie not just the generation of slow waves, but also the synchronization of these waves across the cortex. Pharmacologic and surgical lesions of intra-cortical connections disrupt the synchrony of slow waves (Amzica and Steriade, 1995).

The observation that slow oscillations are coordinated primarily through corticocortical interactions is consistent with our results. Many of the state transitions under isoflurane involve fluctuations in the power of slow oscillations. Using three distinct analysis methods, we consistently find that state fluctuations in L4 are relatively dissimilar to those observed in the infra- and supragranular layers. L4 neurons are most directly

affected by spatially localized inputs from the thalamus, whereas supra- and infra-granular neurons are primarily driven by corticocortical connections and matrix projections from the thalamus (Jones, 2001). While anesthetics suppress both core and matrix thalamocortical inputs, their dominant effect is specifically suppressing corticocortical connectivity (Raz et al., 2014). It is thus likely that the local nature of state transitions in the slow oscillation range is a consequence of both weakened thalamocortical and corticocortical interactions in the anesthetized brain.

Transitions between slow (< 4Hz) and faster EEG oscillations, occasionally observed even in the anesthetized brain (e.g., **Figure 2.2**), are thought to arise as a result of the interaction of the thalamocortical networks with neuromodulatory projections from cholinergic neurons in the brainstem and basal forebrain (Steriade, 2004). Noradrenergic neurons (Vazey and Aston-Jones, 2014) and other brain stem and basal forebrain nuclei also contribute to the modulation of the oscillations exhibited by the thalamocortical networks (Jones, 2003). Activity within the various arousal promoting nuclei is coordinated by a group of medullary neurons, activation of which can trigger prompt awakening from deep states of anesthesia (Gao et al., 2019). In the anesthetized brain, fluctuations in the firing rate of these medullary neurons co-varies with the fluctuations in the spectral characteristics of the cortical LFP (Gao et al., 2019). Thus, it is possible that the spontaneous fluctuations of the LFP characteristics between the slower and faster oscillations are in part mediated by fluctuations in the activity of the nuclei that modulate the thalamocortical networks. However, most arousal nuclei have broad projections to the thalamus and the cortex (Jones, 2003). Thus, if the fluctuations in the state of the LFP were entirely driven by the fluctuations in the activity of the modulatory projections, one would expect that the state of the LFP would fluctuate coherently across the cortex.

Instead, we observe that fluctuations in state of the LFP are only weakly coupled between different cortical sites. This implies that the influence of the modulatory nuclei on the power of specific cortical oscillations, within the physiological range, is not absolute. Rather, activation of the modulatory systems likely biases the cortex towards a particular oscillatory state. The overall pattern of activity at each cortical site, however, is strongly influenced by interactions within the thalamocortical networks.

The experiments performed here cannot directly address the cellular and synaptic mechanisms that give rise to local state transitions and their coordination across the cortex. They do, however, offer clear insights into network mechanisms of global state transitions. Here, rather than attempting to simplify the dynamics of the global signals directly (Hudson et al., 2014), we embedded the dynamics of the local signals into a low-dimensional space. This analysis revealed only weak interactions between local signals. Remarkably, assembling just the low-dimensional projections of the local signals into a state vector recapitulated the low-dimensional dynamics and discrete global cortical states. Thus, we show that the global states and abrupt transitions between them arise because of weak coupling between local state fluctuations.

We are not the first to note that weak coupling among local fluctuations can give rise to coherent macroscopic states. In the retina, weak correlations in spike timing co-exist with a conspicuously high probability of certain large ensembles of neurons firing in synchrony (Schneidman et al., 2006). It may seem that a network with weakly correlated nodes can be well approximated by a collection of completely independent nodes, but this is not the case. Weakly coupled elements can yield highly correlated macroscopic states if the weak interactions are prevalent enough throughout the network. Indeed, we

find that while the correlations between different cortical sites were weak, they were present and statistically significant for most electrode pairs.

The emergence of highly correlated global states from weak pairwise interactions has been investigated extensively in statistical mechanics using Ising models. It has been shown that an Ising model is mathematically equivalent to a maximum entropy models of the statistics of neural firing that are constrained only by the experimentally observed firing probabilities of individual neurons and their pairwise correlations (Schneidman et al., 2006; Tkačik et al., 2006). The maximum entropy approach has proven successful in diverse systems (Ohiorhenuan et al., 2010; Tang et al., 2008; Tkačik et al., 2014; Yu et al., 2008). Although Ising models have traditionally been applied to binary state spaces, such as the presence or absence of an action potential within a small time window, the maximum entropy approach can be generalized to continuous variables (Bialek et al., 2012), such as local fields. In this work, we did not explicitly attempt to construct a maximum entropy model of local field fluctuations, as we are recording only a tiny fraction of all cortical signals. Future work may sample of local field fluctuations more densely to determine whether an Ising-type model suffices to explain the fluctuations of the global state of the brain under anesthesia, or whether other mechanisms in addition to pairwise interactions are needed (Ohiorhenuan et al., 2010; Tang et al., 2008). Regardless of the specific details of such a model, however, we directly demonstrate that widespread weak correlations in local field fluctuations give rise to coherent global cortical states. This conclusion is strongly supported by the observations that locally defined cortical states yield highly correlated global behavior despite weak pairwise interactions, whereas the shuffled controls do not.

There are multiple parallels between our characterization of state transitions in the anesthetized brain and those observed during slow wave sleep (NREM). While sleep and anesthesia are clearly distinct phenomena, the neurophysiological mechanisms that give rise to oscillations in the thalamocortical circuitry under anesthesia and during natural sleep share some essential similarities (Mircea Steriade et al., 1993b; Steriade and Amzica, 1998). Many diverse anesthetics promote activity in the sleep active subcortical nuclei and suppress activity in the wake active ones (Jiang-Xie et al., 2019; Moore et al., 2012; Nelson et al., 2002; Zhang et al., 2015). Furthermore, both sleep and anesthesia consist of several discrete states, each characterized by a distinct pattern of oscillations in the cortex and thalamus (Saper et al., 2010). Based on the original recordings at the microscopic level of single isolated neurons or, alternatively, on the macroscopic level using EEG, it has long been hypothesized that sleep stages are brain-wide phenomena and that the neurophysiological mechanisms that give rise to sleep stage switching specifically prevent multiple sleep stages or sleep and wakefulness from coexisting at the same time in different brain regions (Lu et al., 2006; Saper et al., 2010). Interestingly, at the mesoscopic level of neuronal populations and local fields, sleep state transitions, much like in this work, can be local (Nir et al., 2011; Poulet and Petersen, 2008; Vyazovskiy et al., 2011). Furthermore, it has been suggested that antecedent neuronal activity driven by a specific task can increase the propensity of a population of cortical neurons to exhibit local sleep-like slow oscillations (Huber et al., 2004), implying that transitions between different oscillatory modes are strongly influenced by local synaptic interactions. The degree of synchrony between cortical locations across naturally observed state transitions, such as those between different sleep stages or between sleep and wake, has not been directly quantified in a systematic fashion. Because sleep is strongly influenced by both homeostatic and

circadian influences, it will be challenging to disentangle these global influences from the local interactions between different sites in the cortex. However, analysis of cortical state transitions in the brain anesthetized with a fixed anesthetic concentration is free from these complications. This analysis shows that the apparently global coordinated shifts in cortical activity arise naturally out of weakly interacting local state switches.

MATERIALS AND METHODS

Animals

All experiments were performed using ten male Sprague-Dawley rats, each two to three months of age (250–350 g) (Charles River Laboratories, Wilmington, MA). Two animals were excluded from further analyses because of excessive burst suppression or noise, respectively. One additional animal was excluded after current source density analysis revealed that the V1 probe was inserted too deeply to clearly identify cortical L4 and the supragranular layers. Rats were housed under a conventional 12:12 h, light:dark cycle and given food and water *ad libitum*. All experiments were performed in accordance with the Institutional Animal Care and Use Committee at the University of Pennsylvania and conducted in accordance with the National Institute of Health Guidelines.

Surgery

All surgeries were performed under aseptic conditions. Each animal was weighed immediately prior to surgery. Animals were induced with 2.5% isoflurane in oxygen and secured in a stereotaxic frame (Kopf Instruments, Los Angeles, CA) in the prone position. Core body temperature was maintained at 37 (\pm 0.5) °C using a temperature controller (TC-1000 Temperature Controller, CWE, Incorporated, Ardmore, PA). Prior to

surgery, isoflurane concentration was reduced to 1.5% (flow rate 1 L/min), and dexamethasone (0.25 mg/kg) was delivered subcutaneously. Bupivacaine (5 mg/mL) was injected under the scalp to provide local anesthesia. Throughout the surgery, the lack of response to a toe pinch was used to assess proper anesthetic depth.

The scalp was retracted and two 2 x 2 mm craniotomies were performed using a dental drill: one centered over -5.52 mm AP, 4 mm ML of bregma and another centered over -1.26 mm AP and 1.55 mm ML of bregma for V1 and M1 sites respectively. Dura was removed and Gelfoam (Pfizer, New York, NY) was placed on the exposed cortical tissue to prevent the tissue from desiccating. Prior to insertion, both linear probes (Cambridge NeuroTech, Cambridge, UK; H3 acute 64-channel linear probe) were dipped in Dil to allow for subsequent track tracing and lowered to 1.2 mm into the brain. Prior to electrode insertion, Dura Gel (Cambridge NeuroTech) was applied to each craniotomy and isoflurane concentration was lowered again to 1% (flow rate 1 L/min) for recordings. Immediately following electrophysiological recordings, animals were perfused transcardially with 4% paraformaldehyde under 4% isoflurane. Brain was harvested and processed for electrode track tracing.

Histological confirmation of recording sites

Brains were sectioned at 80 μ m on a vibratome (Leica Microsystems, Wetzlar, Germany). Sections were mounted with medium containing a DAPI counterstain (Vector Laboratories, Burlingame, CA). Electrode tracks were manually identified and localized using epifluorescence microscopy (Olympus, Tokyo, Japan; BX41) at 4x magnification.

Electrophysiology and Preprocessing

All recordings were performed at 1% isoflurane, after allowing the anesthetic concentration to equilibrate for at least 30 minutes. Signals were amplified and digitized on an RHD2132 headstage (Intan, Los Angeles, CA) and streamed to a PC using an Omniplex acquisition system (Plexon, Dallas, TX) at a rate of 40,000 samples per second per channel. All recordings were performed using a ground skull screw as reference. Local field potentials (LFP) were extracted from raw signals online using the bandpass filter with a passband of 0.1-300 Hz. Offline, LFP were decimated to 1 kHz and filtered using a custom acausal FIR 0.1–200 Hz bandpass filter. Noisy channels were removed by visual inspection of the signals. Before subsequent analyses, data were re-referenced to the mean computed over all clean channels on the laminar probe. All data analysis was completed using custom built MATLAB (MathWorks, Natick, MA) code unless otherwise stated. In total, 29.88 hours of recordings were used to generate all data in this manuscript.

Current Source Density and Channel Selection

In order to facilitate cortical layer localization, a series of 10 ms light flash stimuli was presented from a green LED positioned about one inch from the eye contralateral to the craniotomy over V1. Interstimulus intervals were drawn from a uniform distribution between 3 and 5 seconds to prevent stimulus entrainment. Current source density (CSD) analysis was then applied to the post-stimulus LFP to identify layers in V1. The CSD C_t at time t was calculated by computing a smoothed second spatial derivative (a representative example is shown **Figure 2.5**):

$$C_t(z) = V_t(z) * K(z) \quad (2.1)$$
$$K(z) = \frac{z^2 - \sigma^2}{\sigma^5 \sqrt{2\pi}} \exp\left(\frac{-z^2}{2\sigma^2}\right)$$

55

Here, z is the channel depth, $\sigma = 280 \mu\text{m}$ is the distance along the electrode from z at which the kernel changes sign, V_t is the mean voltage over all light flash trials at time t relative to flash onset, and $*$ indicates convolution. The electrode closest to the center of L4 was identified manually from the CSD as the earliest current sink. Once L4 was identified, supra- and infragranular channels were selected for analysis at $140 \mu\text{m}$ intervals above and below L4.

Time-Frequency Analysis

Spectrograms of selected channels were calculated from LFP signals using the multitaper method with 17 Slepian tapers and time-bandwidth product $(NW) = 9$. A 6-second sliding window with a step size of 100 ms was used. Windows containing signal artifacts were identified and removed using a combination of automatic burst suppression detection based on the root-mean-square of LFP in a moving exponential window and manual inspection of multitaper spectrograms. Each window was zero-padded to 65.536 s to increase the frequency resolution and input a power-of-2 number of samples to the Fourier transform. In order to sample frequencies of greater interest more densely, 279 frequencies were selected from 0.14 to 300 Hz, spaced on a log scale from 0.14 to 10 Hz and on a linear scale above 10 Hz. The multitaper spectrograms were then smoothed over frequencies with a median filter spanning 10 frequency steps (up to 17.5 Hz) and over time with an exponential (Poisson) window spanning 2 minutes. In order to remove baseline differences in power across frequencies (such as power-law scaling) and emphasize temporal fluctuations, each spectrogram was rank-order normalized along the time axis. At each frequency bin, the time window with the highest power was given the value of one. Each other window was given the value of $(r-1)/(N-1)$, where r is that window's sorted index among the N

windows. Thus, the smallest power value at each frequency was represented as zero, and the largest as one.

Dimensionality Reduction

Dimensionality reduction was performed on each channel's spectrogram individually, in order to obtain high reconstruction accuracy and ensure that any characteristic differences in activity patterns between sampled regions and cortical depths were preserved. Non-negative matrix factorization (NMF) (Lee and Seung, 1999; Mankad and Michailidis, 2013) was used to compress the rank-ordered spectrograms. The NMF output represents the signal at each time as a short vector of K non-negative coefficients (scores) that weight a sum of corresponding frequency components (loadings) to reproduce the original spectrum. Given a spectrogram A of size $279 \times N$, NMF produces a loading matrix U of size $279 \times K$ and a score matrix V of size $N \times K$. The product UV^T reconstructs A with some error E , quantified relative to the norm of A as:

$$E = \frac{\|A - UV^T\|_F}{\|A\|_F} \quad (2.2)$$

Where $\|\cdot\|_F$ is the Frobenius norm. To select an appropriate number of components (K) for each channel, a cross-validation approach was employed (Owen and Perry, 2009). First, spectrograms were downsampled across time by a factor of 20, for computational efficiency. Then, a random subset of 20% of the rows and columns were selected to be withheld. Starting with $K = 1$ and increasing to 15, NMF was applied to the downsampled matrix after the random subset of rows and columns had been removed. This iteration provides both a loading and score matrix. Next, NMF was run again on the data with only the pre-selected rows withheld. In this iteration, the loading matrix from the first round was fixed and only a new score matrix was calculated. In the third and final run of

NMF, NMF was run on the data with only the pre-selected columns removed, fixing the score matrix from the first round and calculating only a new loading matrix. Finally, the loading and score matrices produced in the second and third run of NMF, respectively, were multiplied to generate an estimate of the original dataset and calculate error as a function of K . This procedure was repeated for five replicates for each value of K , and the optimal K was chosen such that increasing K by one would reduce mean reconstruction error by less than 1%. In our dataset, the optimal value for K ranged from five to nine for different channels. After the cross-validation procedure, each channel's full, normalized spectrogram was subjected to NMF using the channel's optimal K , resulting in a mean reconstruction error of 14.8% across all channels (~85% of the variance captured by NMF for each spectrogram). Note that NMF does not constrain the relative scales of the loading vectors: for any invertible diagonal $K \times K$ matrix D , $UV^T = UD(VD^{-1})^T$. To remove these degrees of freedom, U and V were rescaled by a matrix D such that the rescaled loadings had unit L_2 norm.

Transition and Discrete State Identification

The rescaled score matrix VD^{-1} is the basis for defining each channel's state over time. For each channel, at each time point, the component with the highest score was taken as the state of the brain near that channel's recording site, and samples where the state changed were marked as local transition times. In order to prevent an arbitrarily high number of transitions during periods when two or more components had similar scores, transitions that were likely to reflect transient fluctuations were ignored and the state assignments between them were updated accordingly. Specifically, suppose one time segment between two transitions was assigned state "A" and either the previous or next segment was assigned state "B." If the first segment was less than 100 seconds long

and, within the first segment, the mean score for NMF component A was less than 1.1 times the mean score for component B (*i.e.*, if the state assignment was sufficiently ambiguous), the transition between the two segments was ignored and the combined segment was assigned state B. If a segment could be merged with either the previous or next segment, the tie was broken by ignoring the transition with a smaller magnitude of change in the full NMF score vector from the 3 seconds before the transition to the 3 seconds following it. A matrix of state transition frequencies was computed by tabulating how often each discrete state followed each other state over the duration of the recording using the table of discrete state transitions for each channel.

Markov-based Shuffled Null Model

When testing whether pairs of channels are synchronized in the sense that they preferentially occupy certain combinations of discrete states, apparent synchrony could arise due to the channels' individual NMF score distributions, independent of the relative timing of transitions. To control for this possibility, a discrete-time Markov chain (the "null model") was fit to the transition frequencies of each channel independently. The channel's null model was then used to simulate 1000 new discrete state sequences of the same length as the original data. For each pair of channels, these "null" state sequences were then used to fit distributions of transition synchrony and normalized mutual information (see corresponding sections below). This distribution reflects the probability of observing a given state synchrony and mutual information under the assumption of complete independence between different recording sites. To obtain a null distribution of canonical correlation-based synchrony (see below), full score matrices were generated from each channel's null state sequences as follows: for each of the K states k , at each sample with null discrete state assignment k , the corresponding row of

the null score matrix was randomly drawn from the set of rows of the original data score matrix where the original discrete state was equal to k . These random sequences for all pairs of channels were then subjected to canonical correlation analysis.

After fitting normal distributions for each of the three channel pair interaction measures (transition synchrony, normalized mutual information, and canonical correlations) to the shuffled surrogates, the values obtained for the real data were tested against these distributions to estimate whether they would be expected by chance, given the statistics of the data (see “Statistical Tests” below).

Transition Synchrony

To quantify how frequently channels transitioned together we employed the SPIKE-synchronization score (“synchrony score”), a method for quantifying synchrony between two simultaneously recorded sequences of events (Kreuz et al., 2015). At its core, this method is a coincidence detector in which the coincidence window is derived from the dataset. The adaptive definition of the coincidence window means that this method for quantifying synchrony is equally well-suited for state transitions as it is to spike trains. Each transition r is assigned a local window length $\tau(r)$, which is defined as half the smaller of the inter-transition intervals directly before and after r . For a pair of channels i and j , if transition r_j in j was the closest transition to transition r_i in i and vice versa, and the time between r_i and r_j is less than $\min(\tau(r_i), \tau(r_j))$, both transitions have a synchrony score of 1. All other transitions have a score of 0. This measure is extended to the multi-channel case by assigning each transition a synchrony score equal to its mean pairwise synchrony score with the nearest transitions in all other channels. Both pairwise and all-channel synchrony scores were computed for all discrete state transitions in each

recording, and then averaged over all transitions to obtain pairwise and global mean synchrony measures.

Normalized Mutual Information

Mutual information of discrete states was used to quantify the synchrony of states themselves rather than just the timing of their transitions. Specifically, this measure was implemented to quantify how well one could predict the state in one channel, given the state of another channel at the same time point. Since NMF was performed separately on each channel, states labeled with the same index in different channels are not necessarily the same with respect to the frequency characteristics of the signal. Regardless, mutual information is able to reveal temporal relationships between channel pairs because it does not assume any particular relationship between the state assignments of the different channels and is, therefore, agnostic to the assignments themselves.

Mutual information $I(X; Y)$ between two channels X and Y with N observations and sets of classes K_X and K_Y was computed pointwise as follows:

$$I(X; Y) = I(Y; X) = H(Y) - H(Y | X) \quad (2.3)$$

$$H(Y) = - \sum_{k \in K_Y} P(Y = k) \log_2 P(Y = k)$$

$$H(Y | X) = - \sum_{j \in K_X} P(X = j) \sum_{k \in K_Y} P(Y = k | X = j) \log_2 P(Y = k | X = j)$$

$$P(Y = k) = \frac{|\{t | Y[t] = k\}|}{N}$$

$$P(Y = k | X = j) = \frac{|\{t | X[t] = j, Y[t] = k\}|}{|\{t | X[t] = j\}|}$$

Mutual information is not a pure measure of the predictability of one variable given the other; it also increases with the entropy of each variable. For example, if channels X and Y each occupy a wider distribution of states and, as a result, have higher entropy than both channels W and Z , then $I(X; Y) > I(W; Z)$. This is true even if the state of X is perfectly predictable given Y , Y given X , W given Z , and Z given W . In order to control for this, mutual information was normalized by the sum of the entropies of the two channels, giving the normalized mutual information, or symmetric uncertainty (Witten et al., 2011):

$$U(X, Y) = 2 \frac{I(X; Y)}{H(X) + H(Y)} \quad (2.4)$$

Using another definition for mutual information in terms of the individual and joint entropies of X and Y , we can write:

$$U(X, Y) = 2 \frac{H(X) + H(Y) - H(X, Y)}{H(X) + H(Y)} \quad (2.5)$$

Thus, normalized mutual information can be understood as twice the fraction of the sum of individual entropies, $H(X) + H(Y)$, that exceeds (is redundant to) the joint entropy $H(X, Y)$ due to mutual information between X and Y . For example, if X and Y are identical, $U(X, Y) = 1$ and 50% of $H(X) + H(Y)$ is redundant, as only one of the variables carries unique information.

Canonical Correlation

Both the transition synchrony and normalized mutual information measures assume that LFP signals at each channel form discrete states and that the sequence of NMF components with the largest magnitude at each time point is informative about this state. However, there may be cases where multiple components must be considered. For instance, consider a situation in which NMF component A in channel i is characterized

by strong activity in two frequency bands, and components B and C in channel j are characterized by strong activity in one of those frequency bands each. If only the “top” component determines the discrete state, there could be artificially low synchrony and mutual information between channels i and j . This is because, during a bout of state A in channel i , there could be frequent switching between states B and C in channel j , even though the overall signal characteristics in channel j remain largely static. To address this kind of ambiguity and compute a state synchrony measure that softens the artificially sharp boundaries between “discrete states,” canonical correlation analysis (CCA) was applied to the NMF score matrices of pairs of channels. Intuitively, CCA allows each score matrix to be linearly transformed to optimally match components between channels. CCA maximizes the correlations between the matched, transformed components. These correlations are used to derive a measure of state similarity.

The procedure for computing CCA-based synchrony is as follows: let $V \in \mathbb{R}^{N \times L}$ and $W \in \mathbb{R}^{N \times M}$ be the NMF score matrices two channels, and let $K = \min(L, M)$. At each step i from 1 to K , CCA finds coefficient vectors a_i and b_i to maximize the correlation $\rho_i = \text{corr}(Va_i, Wb_i)$, with the constraints that a_i is uncorrelated with all previous vectors a_1, \dots, a_{i-1} , and likewise for b_i . The MATLAB function *canoncorr* was used to perform this algorithm and the canonical correlation coefficients ρ_1, \dots, ρ_K were averaged to obtain a state similarity measure.

Statistical Tests

This section describes the procedure used to establish the statistical significance of interactions between recordings sites as measured by the synchrony score, normalized mutual information, and canonical correlation analysis. For each channel pair under consideration and each of these three interaction measures, the measure was computed

both on the experimental dataset and on a set of 1000 null-model datasets generated from discrete Markov models of each channel's transition statistics, as described above. The values of each measure were approximately normally distributed across null-model datasets. To test statistical significance, the deviation of each measure obtained in the experimental dataset from those generated from null-model datasets was expressed as a z-score. The one-tailed p -value was then directly computed from the z-score. The significance threshold was set at $\alpha=0.05$. Bonferroni correction was applied to account for multiple comparisons over all channel pairs in each animal. The percentage of pairs for which each interaction measure was different from chance after Bonferroni correction is reported in the manuscript, and non-significant pairs are grayed out in **Figures 2.6-8**.

To compare interaction measures between different sets of channel pairs, special consideration must be paid to the statistical dependence between observations. In a recording with n channels, for any channel k , one would not in general expect the values of a distance-like measure on the pairs $(k, 1), \dots, (k, k-1), (k, k+1), \dots, (k, n)$ to be independent. For example, if channel k were an outlier, all $n-1$ pairs would take extreme values due to what is statistically only one extreme observation. If pairwise statistics were compared naively, e.g., using a two-sample t -test, these dependencies would result in an overestimation of effective sample size and thus significance. Instead, a Monte Carlo permutation procedure was used to establish null distributions for comparisons of pairwise measures between groups of channel pairs. This procedure randomly shuffled group assignments while preserving the dependency structure inherent in the matrix of pairwise measures by only shuffling rows and columns. For each such comparison, 10^7 permutations of only the channels of each recording that were included in that comparison were conducted, and the difference of group means

was computed after each permutation. The frequency with which these null differences exceeded the difference of means of the unpermuted groups was taken as the p -value of the comparison.

Finally, when comparing the interaction measures for between-region channel pairs in M1/V1 recordings to those in bilateral V1 recordings, the method of permuting channel labels cannot be used because there are no data for pairs of channels that mix different recordings. Instead, the distribution for the difference of means of the measure over pairs between the two sets of recordings was estimated by bootstrapping over channels. Specifically, each group in such a comparison consists of a set of rectangular matrices, containing values of the measure for each pair of one channel along the rows and one channel along the columns. By resampling both rows and columns with replacement in each such matrix, the dependencies along rows and columns were preserved, but the variance in the mean could be estimated thanks to the principles of bootstrapping. A total of 10^6 bootstrapped estimates of the group mean difference were computed in this manner for each interaction measure and used to obtain a p -value for the one-tailed hypothesis that the measure is greater on average between hemispheres of V1 than between M1 and V1.

FIGURES

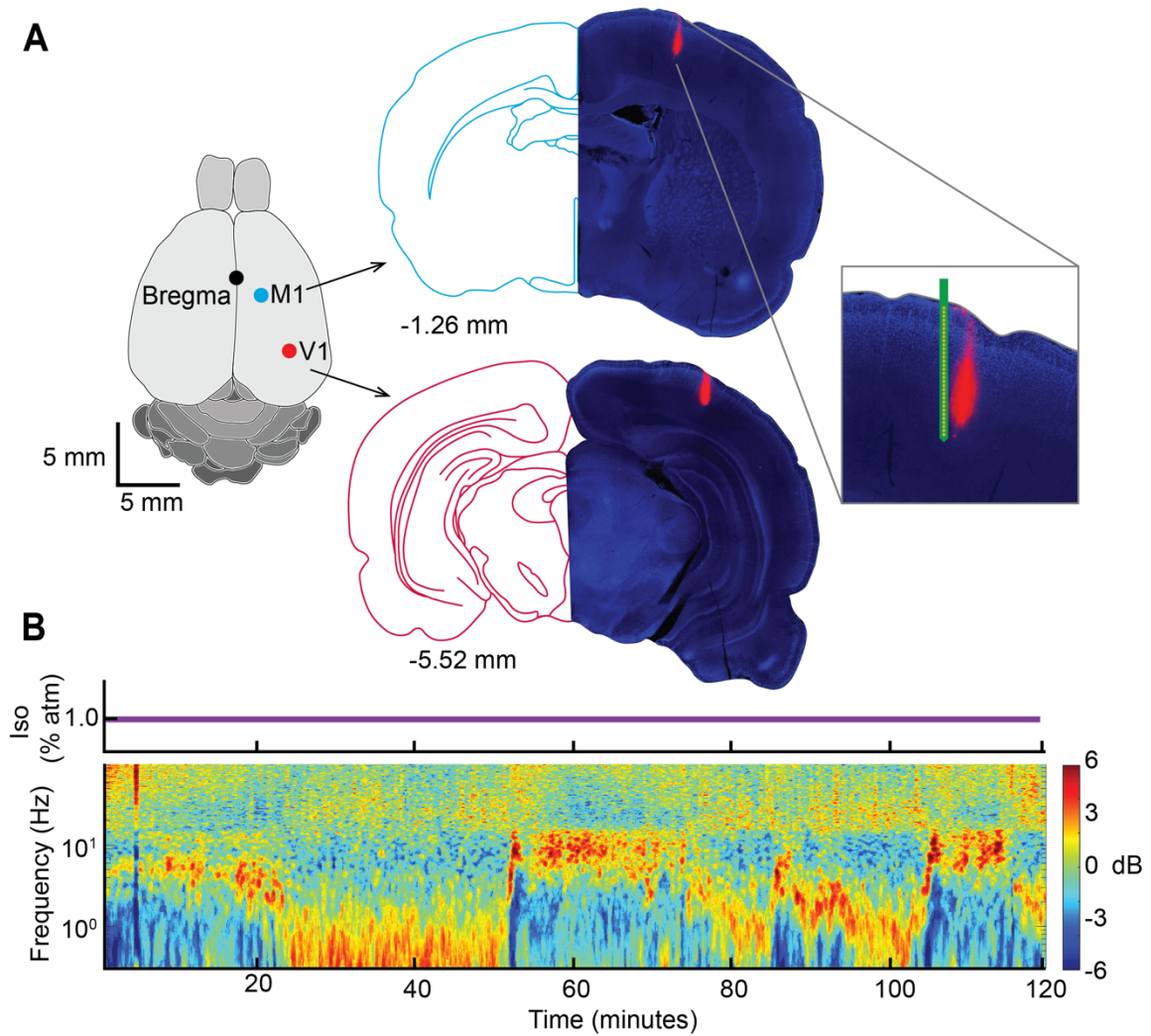


Figure 2.1: Experimental setup. (A) Verification of Electrode placement into V1 and M1. DAPI-stained histological section showing tracks of the Dil-dipped electrode (right) juxtaposed with the corresponding section from the rat brain atlas (left). The zoomed cutout includes an image to show electrode channel layout. (B) Time-resolved spectrogram recorded from V1 under 1% isoflurane general anesthesia (concentration shown above spectrogram).

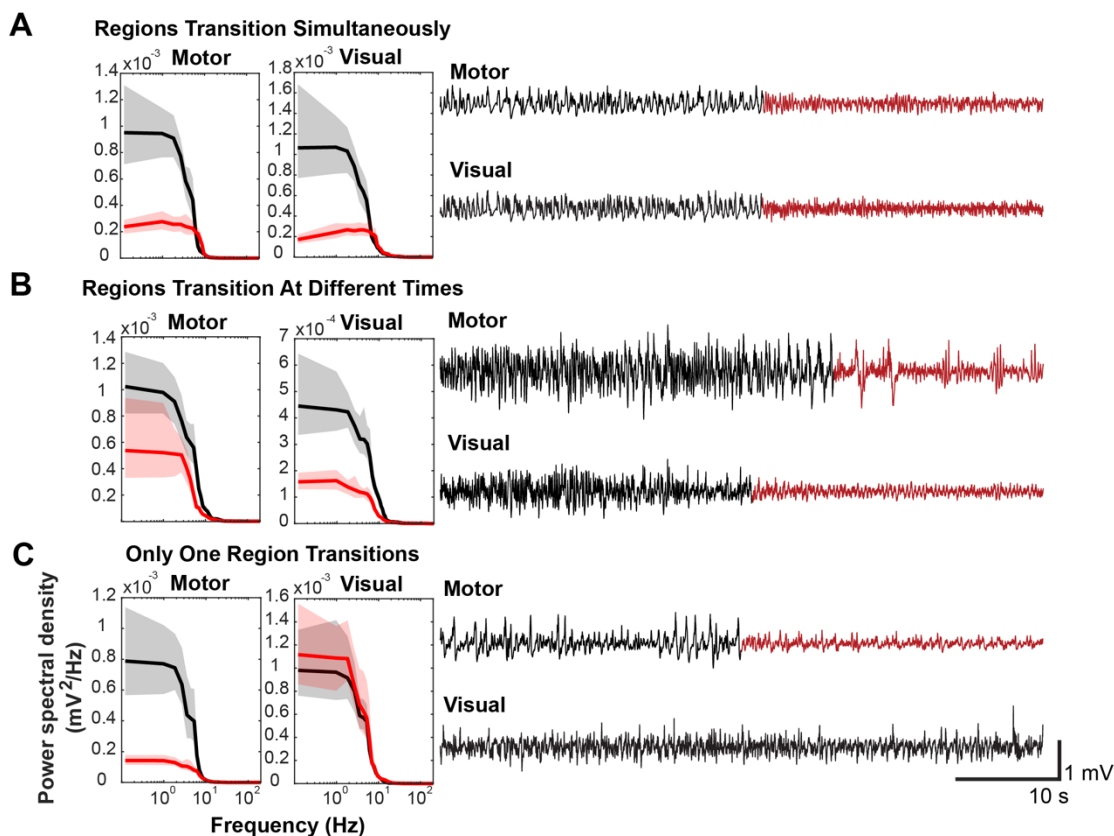


Figure 2.2: Examples of state transitions. (A – C) Right: LFP traces (1 minute) recorded simultaneously from right M1 and V1. Visually apparent abrupt transitions in the character of the LFP are indicated by shifts of color from black to red. Left: spectra computed from the red and black time periods respectively to indicate that the abrupt switches in the features of the signals are associated with changes in the spectra. (A) An example where both M1 and V1 LFPs appear to change state simultaneously. (B) An example where both M1 and V1 signals change states but with an appreciable time delay (~ 10 s). (C) An example where a state transition is observed in M1 but not in V1. In this case for the purposes of computing the spectrum (left, red) in V1, the time segment highlighted in red for the M1 electrode was used.

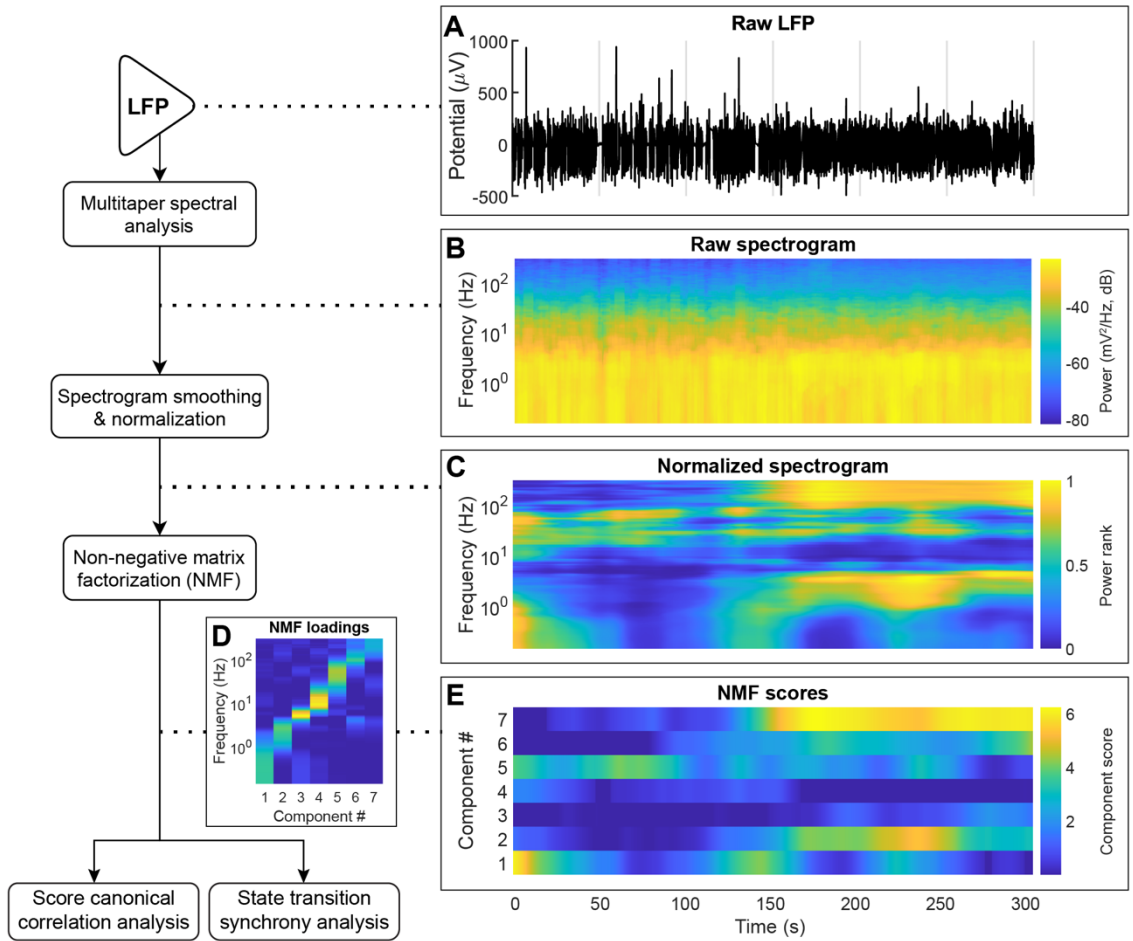


Figure 2.3: Schematic of LFP analysis, through NMF calculation. Left: Flowchart of analysis steps. Right: (A) Five minutes of raw LFP signal centered around a state transition. (B) Power spectrogram of LFP, computed using the multitaper method. (C) The spectrogram from panel B after smoothing and rank-order normalization across time (Methods). (D – E) The loading (D) and score (E) matrices generated using NMF showing the spectral characteristics of each component and its relative contribution to the signal across time, respectively. The number of NMF components was optimized individually for each channel (Methods).

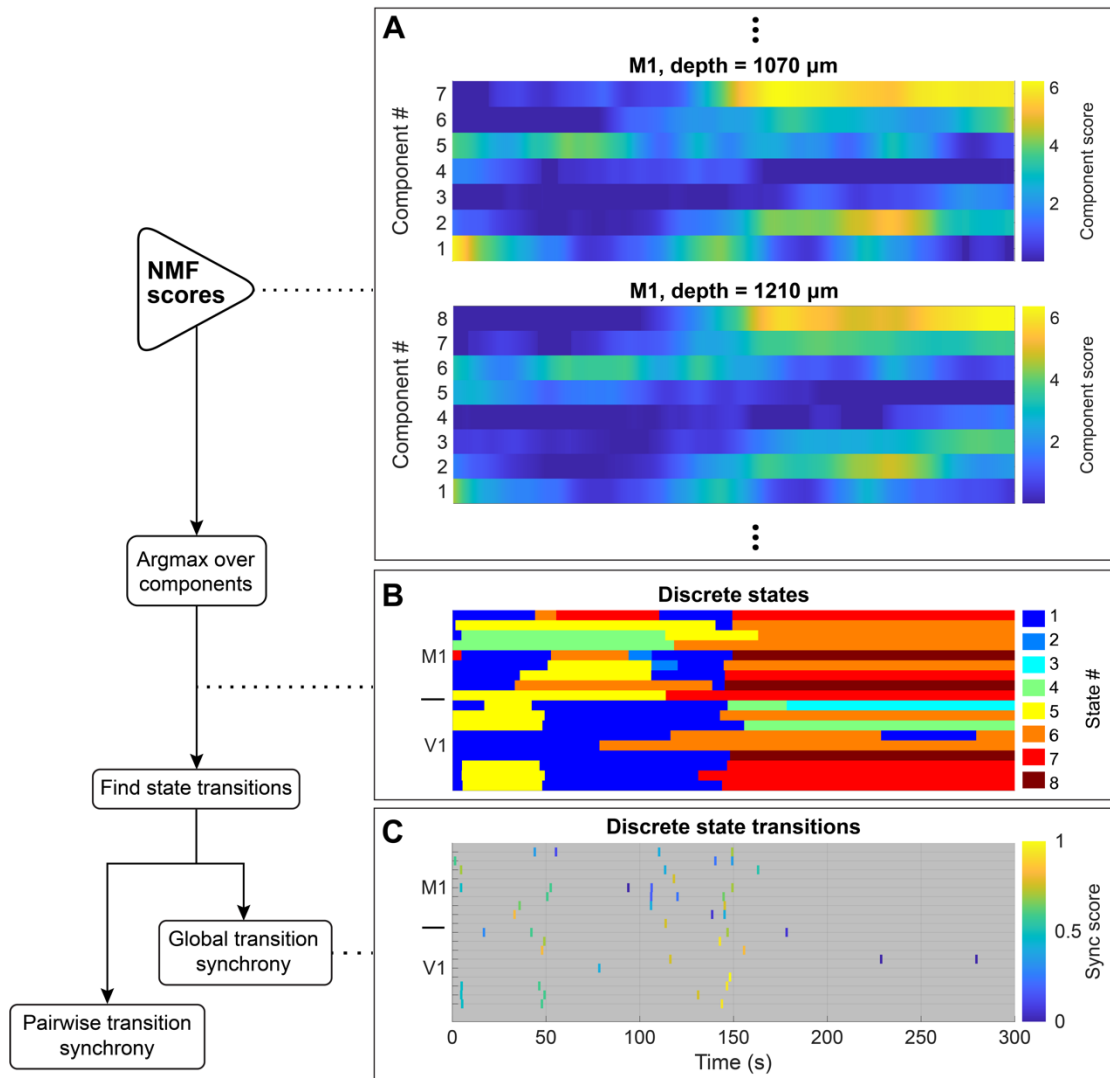


Figure 2.4: Schematic of NMF score analysis to define state transitions and synchrony. Left: Flowchart of analysis steps. Right: (A) The NMF score matrix presented in **Figure 2.3E** (upper) and another NMF score matrix from simultaneously collected LFP from a neighboring channel(lower). Note that while nearby channels share similar characteristics across time, they are not identical. Also, the two channels have different optimal number of components, since NMF was performed and optimized (Methods)independently for each channel. (B) State assignments across example time window from 18 simultaneously recorded signals: 9 signals from an M1 (top rows) electrode and 9 from V1 (bottom rows). State # indicates the NMF component with the highest score in each time window, after removing state segments that were both short and ambiguous due to small score fluctuations (Methods). (C) Raster plot of all transition times from the channels presented in panel B. Transitions are colored according to their synchrony (sync score) with transitions in all other channels (Methods).

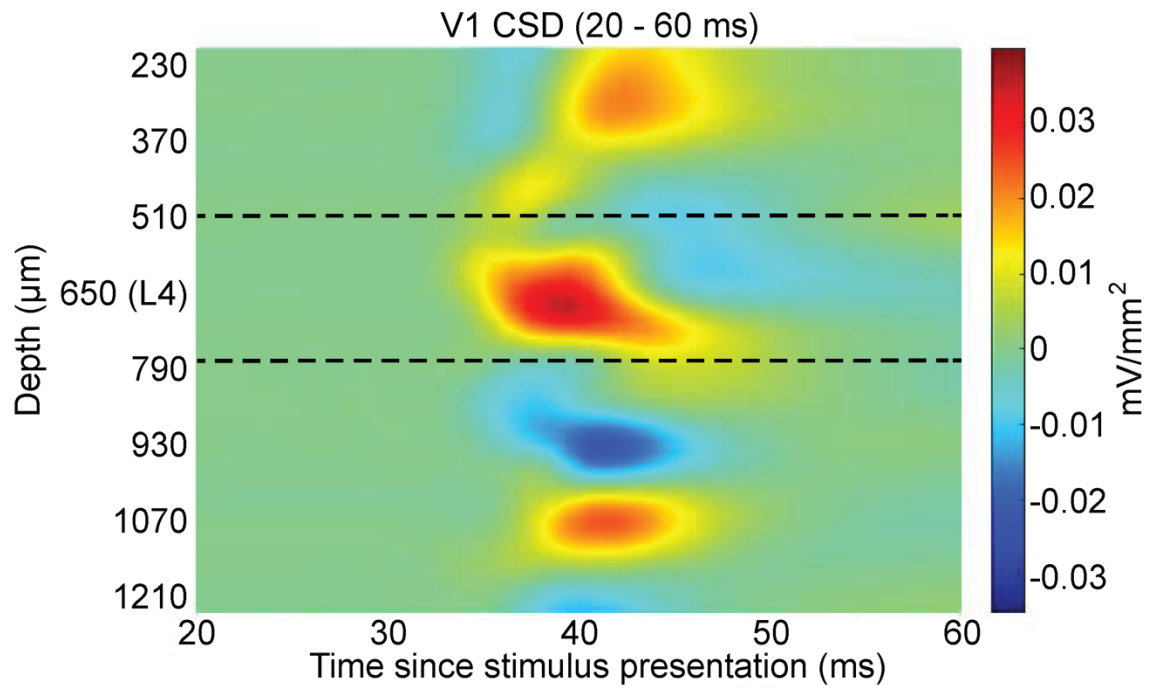


Figure 2.5: Current source density computed for a representative V1 recording. Evoked potential was elicited using a brief green LED flash (Methods). Dotted lines indicate the approximate boundaries of L4. Depth denotes estimated depth from the cortical surface.

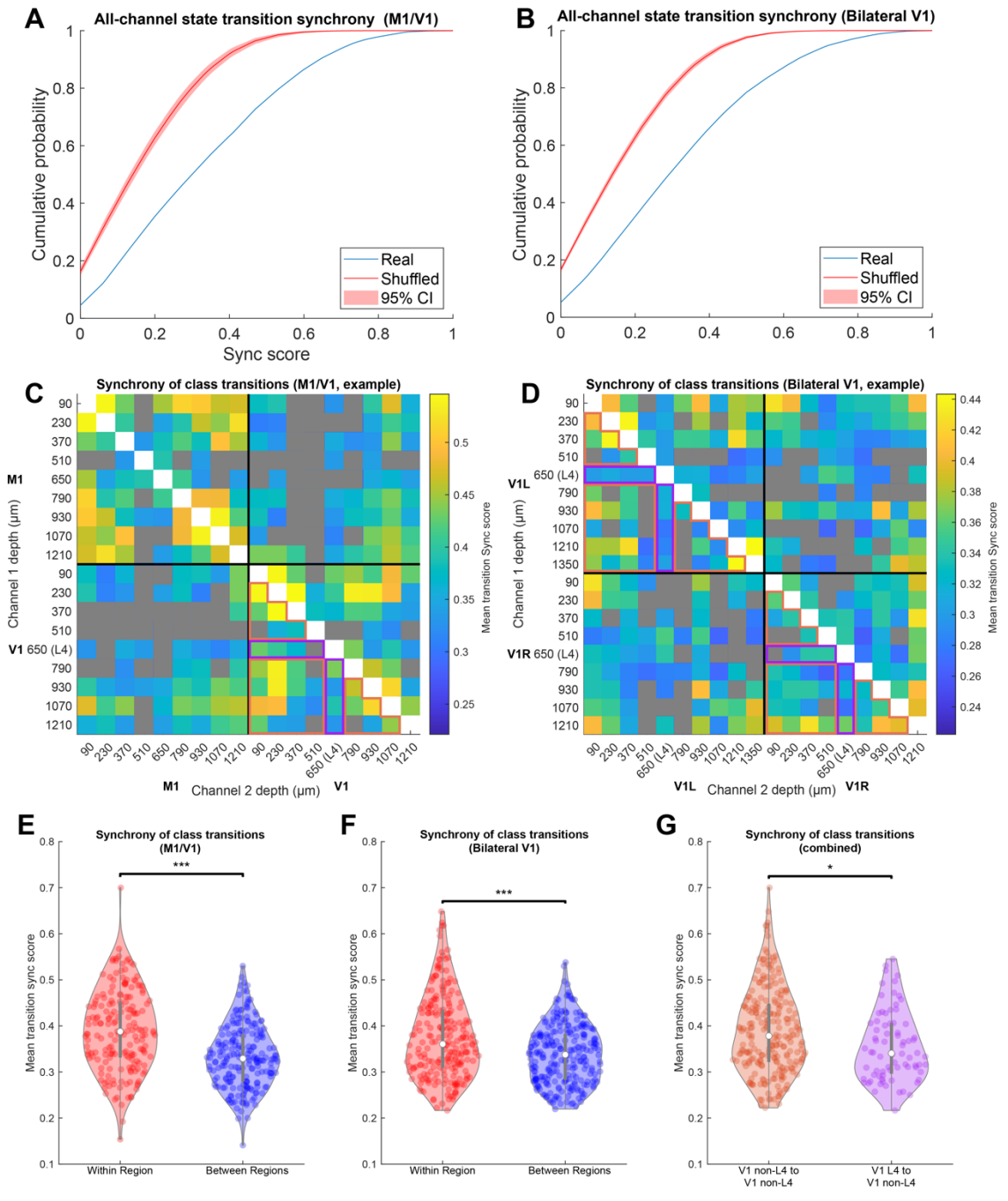


Figure 2.6: Transition synchrony between channels in the same anatomical region is higher than between channels in different regions. (A – B) The cumulative distribution of SPIKE-synchronization (synchrony) scores across all channels, in real recordings (blue) and the median \pm 95% CI of 1000 shuffled recordings (red), for M1/V1 experiments (A) and bilateral V1 experiments (B). (C – D) Mean synchrony score across transitions for all channel pairs from a representative M1/V1 (C) and bilateral V1 (D) recording. Channel pairs whose synchrony scores were not significantly different from shuffled controls after Bonferroni correction are colored gray. (E – F) Channel pairs in which both channels are in the same region (red) have higher synchrony scores than those in which the channels are in different regions (blue) for M1/V1 (E, $p = 1e-7$, permutation test) and bilateral V1 (F, $p = 2e-7$, permutation test) recordings. (G) Channel pairs in which one channel was within L4 and the other was not had lower synchrony scores than pairs in which neither channel was in L4 ($p = 0.015$, permutation test). Data included in these comparisons for the representative experiments are outlined in orange and purple, respectively, to highlight that only data from V1 electrodes were used.

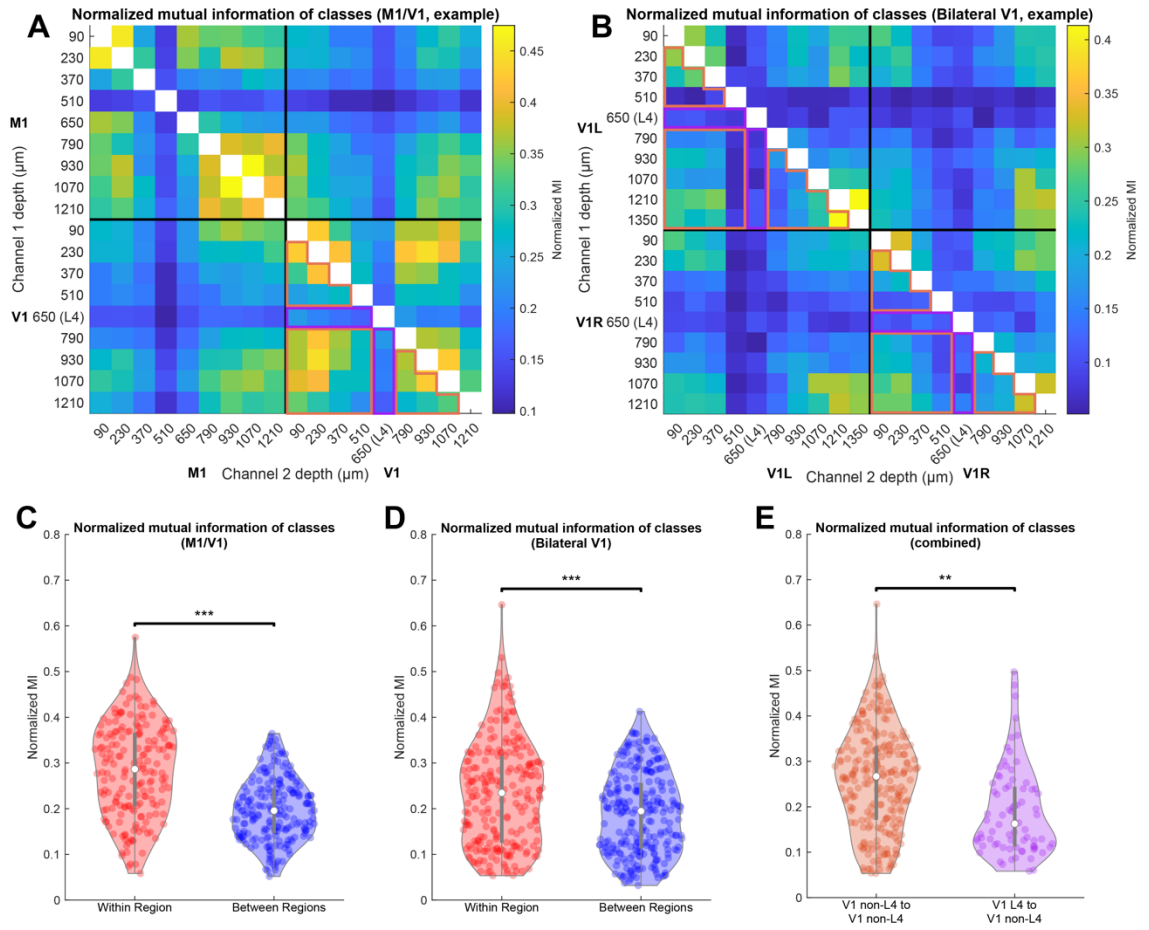


Figure 2.7: Normalized mutual information (MI) between channels in the same anatomical region is higher than between channels indifferent regions. (A – B) Normalized MI between state assignment vectors for all channel pairs from a representative M1/V1 (A) and bilateral V1 (B) recording. All normalized MI values are significantly different from shuffled controls after Bonferroni correction. (C – D) Channel pairs in which both channels are in the same region (red) have higher normalized MI than those in which the channels are in different regions (blue) for M1/V1 (C, $p = 1e-7$, permutation test) and bilateral V1 (D, $p = 1e-7$, permutation test) recordings. (E) Channel pairs in which one channel was within L4 and the other was not had lower normalized MI than pairs in which neither channel was in L4 ($p = 0.002$, permutation test). Data included in these comparisons for the representative experiments are outlined in orange and purple, respectively, to highlight that only data from V1 electrodes were used.

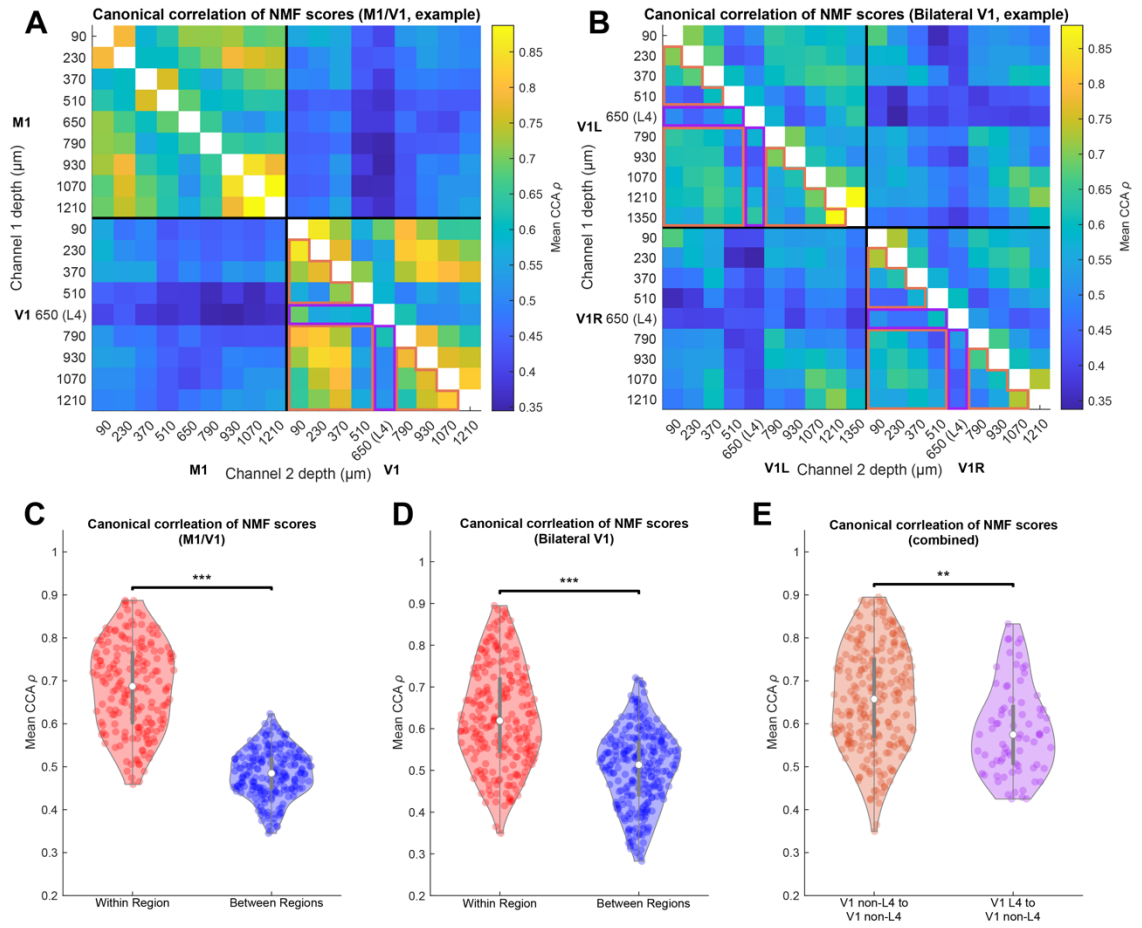


Figure 2.8: Canonical correlation analysis (CCA) reveals higher correspondence of overall activity between channels in the same anatomical region than between channels in different regions. (A – B) CCA measure on NMF scores for all channel pairs from representative M1/V1 (A) and bilateral V1 (B) recordings. (C – D) Channel pairs in which both channels are in the same region (red) have higher NMF score correspondence than those in which the channels are in different regions (blue) for M1/V1 (C, $p = 1e-7$, permutation test) and bilateral V1 (D, $p = 1e-7$, permutation test) recordings. (E) Channel pairs in which one channel was within L4 and the other was not had lower NMF score correspondence than pairs in which neither channel was in L4 ($p = 0.001$, permutation test). Data included in these comparisons for the representative experiments are outlined in orange and purple, respectively, to highlight that only data from V1 electrodes were used.

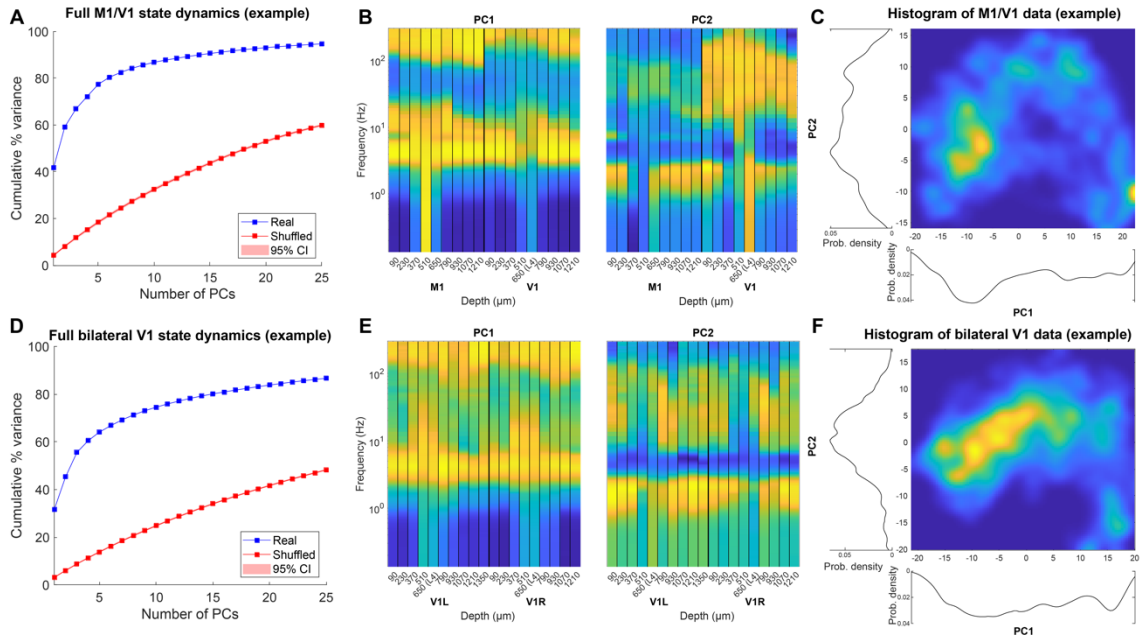


Figure 2.9: Weakly correlated fluctuations in different cortical sites give rise to highly correlated cortical states. NMF scores from all recorded channels were concatenated into a single state vector (median dimension across recordings = 106) and subjected to PCA. Fraction of total variance as a function of number of PCs is shown in (A) and (D) for M1/V1 and bilateral V1 example recordings respectively (blue). Shuffled surrogates (Methods) were subjected to the same analysis (red). (B) and (E) show loadings of the top 2 principal components, mapped back from each channel's NMF components to frequencies, for the two representative recordings. This projection reveals consistent differences between M1 and V1 (B) but is relatively consistent across bilateral V1s (E). In both instances, Layer 4 is distinct from supra-and infragranular layers. C and F show histograms of the data projected onto the top two PCs for the representative M1/V1 (C) and bilateral V1 (F) recordings. In both instances, the distribution of data is multimodal, suggesting the presence of discrete global cortical states.

CHAPTER 3 – Duration of EEG Suppression Does Not Predict Recovery Time or Degree of Cognitive Impairment After General Anesthesia in Human Volunteers

INTRODUCTION

As an experimental tool, general anesthesia provides a valuable opportunity to study how a healthy brain recovers from a dramatic perturbation that disrupts consciousness (Hudson et al., 2014). EEG features under general anesthesia have been extensively studied and used to quantify anesthetic depth for decades (Mashour, 2006b). Burst suppression is one well-known EEG activity pattern traditionally associated with deep anesthesia. This pattern is characterized by periods of isoelectric EEG punctuated by bursts of electrical activity and is induced at high concentrations of various general anesthetics with different mechanisms of action (Akrawi et al., 1996). During burst suppression, 95% of cortical neurons are hyperpolarized (M. Steriade et al., 1994), excitatory transmission is greatly diminished (Ferron et al., 2009), inhibitory postsynaptic potentials are completely abolished (Ferron et al., 2009), and cerebral metabolic rate is reduced (Woodcock et al., 1987).

Outside of the domain of anesthesia, burst suppression is observed during states of profound cerebral dysfunction, including encephalopathy (Ohtahara and Yamatogi, 2003) and coma (Cloostermans et al., 2012). Furthermore, burst suppression has been hypothesized to be a poor prognostic indicator for recovery after brain injury (Hofmeijer et al., 2014). Burst suppression has been associated with adverse outcomes such as delirium and death in post-surgical (Fritz et al., 2016; Radtke et al., 2013; Soehle et al., 2015) and intensive care (Andresen et al., 2014) settings (Sessler et al., 2012; Watson

et al., 2008). Yet, the fundamental physiology of burst suppression as a determinant of recovery from anesthesia has not been established.

We hypothesized that greater duration of EEG suppression during anesthesia would be associated with increased time to emergence, defined as time to recovery of consciousness after discontinuation of the anesthetic. Contrary to our hypothesis, the addition of metrics of EEG suppression in a model built to predict time to emergence did not sufficiently improve the predictive ability of the model. We also hypothesized that a longer duration of EEG suppression would be correlated with greater cognitive impairment at emergence from anesthesia. The assumption that suppression would predict cognitive impairment also proved false. Thus, while burst suppression is thought to reflect the deepest plane of general anesthesia, EEG suppression is not a good predictor of prolonged recovery time or degree of impairment of cognition in healthy human volunteers.

RESULTS

Individual variability in EEG characteristics during constant anesthetic administration

The end-tidal isoflurane concentration (**Figure 3.1A**) was maintained near 1.3 age-adjusted MAC. Temperature (**Figure 3.1B**) was maintained in the physiologic range. The population mean (**Figure 3.2A**) and median (**Figure 3.2B**) spectrogram exhibited a canonical high power of low frequency oscillations during isoflurane administration. Yet, both the mean and median spectrograms conceal two important sources of variability: inter- and intra-subject variability (**Figure 3.3**). In the absence of surgical stimulus, and

despite a constant isoflurane concentration, the spectra of EEG fluctuate as a function of time. Four examples of this variability are highlighted in **Figure 3.3**. One subject (**Figure 3.3A**) had two periods of prolonged isoelectric EEG in the first hour of isoflurane administration. During the remaining two hours, no significant suppression was observed, but the frequency of α oscillations waxed and waned. In contrast, another subject (**Figure 3.3B**) exhibited short periods of EEG suppression throughout the 3-h administration of isoflurane, and another (**Figure 3.3C**) had EEG dominated by suppression interrupted by a consolidated period of non-suppressed period. Finally, a fourth subject (**Figure 3.3D**) did not exhibit any appreciable EEG suppression at all. Thus, the population mean and median spectrograms do not reflect individual EEG dynamics under anesthesia in healthy human volunteers undergoing constant isoflurane exposure. In the remainder of the manuscript, we will focus on one aspect of EEG activity—EEG suppression—to determine whether it is associated with a longer time to recovery of consciousness or greater impairment of cognition at emergence.

The first two principal components separate suppression from non-suppression

Periods of suppression are characterized as flat-lined, or isoelectric EEG, which is associated with a dramatic decrease in cortical activity. In the frequency domain, this is seen as a broadband decrease in power (blue regions in the spectrograms in **Figure 3.3**).

Because EEG suppression is associated with a broadband decrease in EEG power, we reasoned that projecting the spectra onto the first principal component should separate periods of suppressed EEG into a distinct cluster. In 21 out of 25 subjects with burst suppression, assessed by visual inspection, the null hypothesis that the distribution is unimodal was rejected ($P < 0.05$ after multiple comparison correction).

Consistent with the results of the Hartigan dip test, spectrograms projected onto a plane spanned by the first two PCs formed two clusters (**Figure 3.4A**). Points were assigned to each cluster using a standard *k-means* algorithm and overlaid on the spectrogram to demonstrate the accuracy of cluster assignments (**Figure 3.4B**).

Visual inspection suggested that all episodes of suppressed EEG were assigned to a single cluster. To verify that this was the case, we concatenated all epochs of the EEG assigned to the suppressed and the non-suppressed cluster (**Figure 3.4C**).

EEG suppression is not independently associated with increased time to recovery of consciousness

As demonstrated in **Figure 3.3**, the suppression patterns varied over all 27 subjects, including two subjects who failed to exhibit any EEG suppression. Variability occurred in the total amount of suppression, number of distinct suppression episodes, dwell time of suppression episodes, and the organization of suppressed episodes during isoflurane administration.

Of the 25 subjects exhibiting suppression, the cumulative percentage of suppression ranged from 1.1 to 67.9% (average: 25%; SD: 21) of the recording. The maximum length of suppression ranged from 0.28 to 13 min (average: 3.5; SD: 3.3 min). The number of transitions between suppression and non-suppression ranged from six to 412 (average: 150.8; SD: 120.2). We also calculated the percentage of suppression during the last 15 min of isoflurane administration, as this might be a better indicator of whether a subject is likely to recover consciousness more quickly or more slowly than their suppression over the entire 3 h of isoflurane administration. Fourteen subjects showed no

suppression during the last 15 min of isoflurane administration. In the remaining subjects, the average suppression duration was 2.9 min (2.3 SD).

None of the four suppression-derived measures were individually correlated with time to emergence (percent suppression: $R^2=0.03$, $P=0.40$, longest suppressed episode: $R^2=8\times 10^{-4}$, $P=0.89$, number of suppressed episodes: $R^2=0.02$, $P=0.51$, percent suppression in the last 15 min: $R^2=0.02$, $P=0.44$) (**Figure 3.5**).

We investigated the relationship between time to emergence and three measures derived from the age-adjusted isoflurane MAC values. Two showed no relationship with time to emergence (MAC in the first 30 min: $R^2=9\times 10^{-5}$, $P=0.96$ and mean MAC from 50 to 180 min: $R^2=0.02$, $P=0.53$). The third isoflurane-derived measure κ is the exponential decay rate for the end-tidal isoflurane starting from the moment isoflurane was shut off (Eq. 3.1). As expected, the decay rate constant was strongly correlated with time to emergence ($R^2=0.39$, $P=5\times 10^{-4}$), but accounted for less than 40% of the variance (**Figure 3.6**). Therefore, the rate constant, κ , was included in all subsequent models that predict the time of emergence and impairment of cognition.

We start with the conventional approach using linear regression. The regression models incorporated the isoflurane decay rate constant, κ , and either the percent of total time in suppression or percent of the last 15 min of isoflurane exposure spent in suppression. Both of these models demonstrated statistical significance (**Table 3.1**, **Table 3.2**). Yet, neither the fraction of total time spent in suppression nor the fraction of the last 15 min of isoflurane exposure spent in suppression showed a statistically significant association with time to emergence. Furthermore, no statistically significant interaction was found between the isoflurane decay rate constant and EEG suppression.

We, next, turn to a more physiologically motivated modelling approach graphically illustrated in **Figure 3.7**. We model recovery of consciousness as a process that starts from some anesthetic depth observed at the time when isoflurane is turned off (ω). As the anesthetic is eliminated, the system gradually evolves towards a threshold (Ω) at the rate dictated by the elimination rate constant (κ). We model the percent of time spent in suppression as an additive anesthetic depth (σ), as we expect that the brain with more EEG suppression should take longer to recover. To test this intuition, we determine whether the ability to predict the time of emergence is significantly improved by incorporating the fraction of time spent in suppression.

The ability of each model to predict time of recovery is shown in **Table 3.3** as the Pearson correlation coefficient between the model and the time to emergence of each subject. Notice that each model has a similar correlation coefficient. To select the best one among the considered models, we computed the AIC for each. From the AIC, we computed the probability that each model minimizes loss of information relative to the other models considered (Burnham and Anderson, 2003). From an information theoretic standpoint, the model with the highest probability is chosen as the most appropriate model. Using this approach, we conclude that the model without any measure of EEG suppression is the most appropriate model. In the interest of testing the consistency of the AIC and the associated relative probabilities, we bootstrapped our calculation of corrected AIC values. This was accomplished by randomly selecting (with replacement) a set of 27 subjects. Each model was then fit to this subset. The best model was selected for each such subset as the one that maximizes relative probability. The model that did not include a measure of burst suppression was chosen in 86% of the 1000 bootstraps.

EEG suppression is not associated with impairment in cognitive task performance at emergence

Having established that there is no statistically significant relationship between EEG suppression and recovery of consciousness, we asked whether increased EEG suppression is associated with greater impairment of cognitive function at this time point. For this purpose, we turned to estimates of changes in cognitive performance on the DSST and the PVT at emergence. Performances on both the PVT and DSST, in terms of both accuracy and response time, were impaired immediately upon recovery of consciousness. We hypothesized that subjects exhibiting more burst suppression would exhibit greater impairment relative to baseline. Additionally, we hypothesized that slower elimination kinetics of isoflurane would result in greater impairment. Yet, we found no evidence that the duration of EEG suppression is associated with greater impairment in accuracy or response time for both the PVT and DSST (**Figure 3.8 and Table 3.4, Table 3.5**). Likewise, the time constant of isoflurane elimination was not correlated with estimates of impairment at emergence for either cognitive task, in terms of accuracy or response times (**Table 3.6**).

DISCUSSION

The results of this study do not reveal an association between EEG suppression and time to recovery from general anesthesia. Furthermore, we failed to find an association between the amount of EEG suppression and the degree of impairment in cognitive performance at emergence, as measured using two independent cognitive tests. Anesthetic exposure profoundly impeded performance on both of these tests. Burst

suppression, however, did not confer any additional decrement in cognitive function after anesthesia.

Absence of evidence is clearly not evidence of absence. However, our findings reduce the probability of a strong relationship between EEG suppression and recovery of consciousness or impairment of cognition in healthy subjects. Here we defined recovery of consciousness as the time when the subject was first able to follow instructions to squeeze either the right or left hand twice. The ability to follow this command implies that the subject is capable of parsing a simple sentence, has an elementary conception of numbers, and the ability to communicate via the execution of a simple motor task. Thus, recovery of consciousness as defined herein, signifies return of at least rudimentary cognition. In an attempt to discover a relationship between the time it takes to recover consciousness and EEG suppression, we used several complementary modelling approaches. None reveals a significant association between EEG suppression and time to recovery of consciousness. This conclusion is further reinforced by the finding that subjects whose EEG exhibited significant suppression were no more impaired in performance time or performance accuracy of two cognitive tests that assess distinct neurobehavioral processes (Basner et al., 2015, 2011) than those without any suppression of the EEG. This is a counterintuitive observation, as isoelectric EEG is universally considered to be the deepest attainable state of anesthesia.

Animal studies have established previously that EEG suppression is not necessarily associated with prolonged recovery (Hambrecht-Wiedbusch et al., 2017). For example, Hambrecht-Wiedbusch and colleagues (Hambrecht-Wiedbusch et al., 2017) added ketamine to an isoflurane anesthetic, which induced burst suppression but nevertheless accelerated emergence time. Our findings here are distinct from those of

Hambrecht-Wiedbusch and colleagues (Hambrecht-Wiedbusch et al., 2017) as we demonstrated that burst suppression induced in humans with a single anesthetic agent is not associated with longer time to recovery of consciousness.

Although the effect of various anesthetics on the EEG has been extensively studied in humans (Blain-Moraes et al., 2014; Cimenser et al., 2011; Gibbs et al., 1937; John et al., 2001; Lee et al., 2013), most studies present EEG characteristics averaged across subjects and time. When group averages (e.g. **Figure 3.2**) and individual EEG recordings (e.g. **Figure 3.3**) are compared, it becomes clear that the population and time averaging fail to represent the behavior of any individual subject. We exploited this natural inter- and intra-subject variability to isolate the effect of EEG suppression on the timing of subsequent recovery of consciousness and impairment of cognition without the confounds of variably noxious surgical stimuli, changing anesthetic concentrations, or complex polypharmacy commonly used in the operating room. Yet, we were unable to discover any statistically significant association between features of EEG suppression and 1) restoration of consciousness or 2) cognitive impairment at this time point.

A major limitation of the study was that only a single anesthetic and a single concentration were evaluated. Full exploration of the possible activity patterns of the EEG and their dependence on the anesthetic agent and concentration will require additional investigation. Further, it is likely that EEG activity patterns and the dynamics of switching among them could be dramatically altered by clinically relevant factors such as brain pathology, surgical stimulation, and the addition of opioids. Yet, this study in a healthy volunteer population establishes that, even when many variables are constrained, variability in EEG activity does not vanish in the anesthetized brain.

The surprising results from this study indicate that no aspect of EEG suppression assessed here (cumulative time in suppressed EEG, longest epoch of suppressed EEG, percent of time in suppressed EEG during the penultimate 15 minutes before discontinuing the anesthetic, and the frequency with which the anesthetized brain transitions into and out of the suppressed state) correlate with the time to emerge from anesthesia. Furthermore, features of EEG suppression were not significantly associated with estimates of cognitive impairment on the PVT and DSST at emergence. Such a result, while not definitive, is clearly consistent with the notion of a non-linear depth of anesthesia, a dissociation between the dynamics governing the state of anesthesia and recovery from anesthesia. It also instructs the clinician that heretofore unrecognized factors underlie the variable fluctuation between states of EEG suppression and non-suppression in the presumptively healthy human brain.

In the clinical literature, burst suppression has received much attention because of its reported association with adverse outcomes in surgical and ICU patients. Monk and colleagues (Monk et al., 2005) showed in a prospective study that increased cumulative deep anesthesia time was associated with increased mortality after noncardiac surgery. While they did not directly study burst suppression, bispectral index below 45—defined as deep anesthesia by Monk and colleagues (Monk et al., 2005)—is typically associated with burst suppression (Bruhn et al., 2000). Watson and colleagues (Watson et al., 2008) found that burst suppression is associated with increased mortality in the ICU patient population. In addition to mortality, burst suppression has been reported to be associated with delirium in ICU (Andresen et al., 2014) and in surgical patients (Chan et al., 2012; Fritz et al., 2016; Radtke et al., 2013; Soehle et al., 2015). One interpretation of these findings is that administering excessive doses of anesthetics may have

deleterious effects on the brain. This view is consistent with the multiple lines of evidence demonstrating potentially neurotoxic effects of anesthetics (reviewed by Vutskits and Xie (Vutskits and Xie, 2016)).

In studies on surgical and ICU patients, it is difficult to delineate why certain patients had more burst suppression than others. One possibility is that patients with more burst suppression received higher doses of anesthetics and sedatives. Another possibility is that some patients are more sensitive to the effects of anesthetics, and therefore are more likely to exhibit burst suppression at anesthetic doses that do not typically elicit burst suppression in others. As all subjects in our study were exposed to similar anesthetic concentrations, it is tempting to speculate that subjects who exhibit more suppression are more sensitive to the effects of isoflurane. If so, one would expect that more sensitive subjects should take a longer time to recover from anesthesia and experience greater cognitive impediment. We find no evidence to support this hypothesis. Instead, we find that a parsimonious measure of deep anesthesia— isoelectric EEG—is not useful in predicting the time to recovery of consciousness or subsequent decrement in cognitive function. While our findings do not invalidate the previously published association between suppressed EEG and cognitive outcomes (Hesse et al., 2019), they illustrate that burst suppression *per se* may not be an important determinant of the recovery of consciousness and cognition. Indeed, none of the subjects in this cohort exhibited delirium based on the standard confusion assessment method for the intensive care unit (CAM-ICU) assessment. However, it is possible that EEG suppression is associated with subtle cognitive deficits upon recovery in normal subjects that were not captured in our study. This relationship will require further investigation, but results herein suggest that EEG suppression *caeteris paribus* is

not associated with significantly greater impairment of cognition or increased time to recovery in healthy adults.

MATERIALS AND METHODS

All data were collected as a part of the ReCCognition (NCT01911195) study after appropriate institutional review board approval: University of Pennsylvania, Philadelphia, PA, USA (Protocol #818401), University of Michigan, Ann Arbor, MI, USA (Protocol #HUM0071578), and Washington University in St. Louis, St. Louis, MO, USA (Protocol #201308073). To be eligible to participate, all subjects gave written informed consent in accordance with the Declaration of Helsinki. Details of the study design and eligibility and exclusion criteria are previously described (Maier et al., 2017).

Anesthetic administration

EEG was recorded in 30 healthy (ASA patient status 1 and 2) (Vacanti et al., 1970) volunteers (12 women and 18 men, 22–39.5 yr), with 10 subjects recorded at each of three sites: University of Michigan, Washington University, and University of Pennsylvania. EEG was sampled at 500 Hz using the Electrical Geodesics, Inc. (Eugene, OR, USA) EEG system with either a 32 (20 subjects), 64 (one subject), or 128 (nine subjects) channel montage referenced to Cz. Sessions began with baseline cognitive testing. After pre-oxygenation using a face mask, anesthesia was induced with a stepwise increasing infusion rate of propofol: $100 \mu\text{g kg}^{-1} \text{min}^{-1} \times 5 \text{ min}$, increasing to $200 \mu\text{g kg}^{-1} \text{min}^{-1} \times 5 \text{ min}$, and then to $300 \mu\text{g kg}^{-1} \text{min}^{-1} \times 5 \text{ min}$. After 15 min of propofol administration, we administered isoflurane 1.3 age-adjusted MAC, delivered via

a laryngeal mask airway, for three hours. Subjects breathed spontaneously with pressure support adjusted to attain tidal volumes 5–8 ml kg⁻¹.

During anesthetic administration, vital signs and other data (ECG, noninvasive BP, pulse oximetry, end-tidal carbon dioxide and isoflurane concentration, and nasopharyngeal temperature) were monitored and recorded in an electronic anesthetic record and analyzed *post hoc*. Surface warming blankets were applied to maintain body temperature in the normal range. BP was maintained within 20% of starting values by intermittent boluses or infusions of phenylephrine. I.V. ondansetron (4 mg) was administered 30 min before discontinuation of isoflurane.

At the discontinuation of isoflurane, an audio command loop, issued every 30 seconds, asked the subject to squeeze either the right or left hand twice. Emergence was defined by the initial time at which participants responded correctly to two consecutive commands. Recovery time was defined as the period between isoflurane discontinuation and emergence.

Cognitive testing battery

Upon emergence, a cognitive testing battery was administered at 30-min intervals. Six tasks from the computerized Cognition test battery (Basner et al., 2015) were used to serially assess cognitive task performance with high temporal resolution. Here, we focused on two robust cognitive tests in order to reduce the number of statistical comparisons. We first used the digit symbol substitution test (DSST), a test of cognitive throughput and visual scanning previously used to characterize cognitive recovery in surgical patients recovering from general anesthesia (Ibrahim et al., 2001; Larsen et al., 2000; McLeod et al., 1982). The DSST requires participants to select keys based upon a

menu of nine matching symbols and numbers displayed on the screen. We additionally used the psychomotor vigilance test (PVT), a measure of vigilance and attention resistant to learning effects with repeat administration (Basner and Dinges, 2011). The PVT measures reaction time (Basner et al., 2011) by requiring the space bar to be pressed as quickly as possible after the appearance of a counter with incrementing numbers.

Tests were administered on a 14" LCD Dell Latitude E4530 laptop computer (Dell, Round Rock, TX, USA). Test order was randomized between participants. Alternate forms of cognitive tests were used at each administration to reduce practice effects. In considering a speed-accuracy trade-off (Wickelgren, 1977), we analyzed median response times and performance accuracy separately for each test.

EEG analysis

The analyses presented herein were performed on the EEG recorded during the 3 h of isoflurane administration at 1.3 MAC. Artifacts attributable to noise or movement were rejected manually. *K-means* clustering was performed on the number of minutes of clean data for all 30 subjects, resulting in the exclusion of three subjects. These three excluded subjects had only 92.2 (± 12 min) (~51% of recorded data) of clean data compared with the 158.8 (± 9.8 min) (~88% of recorded data) of clean data for the remaining 27 subjects (nine women, 22–39.5 yr). Thus, only the 27 subjects with longer clean EEG recordings were used in all subsequent analyses.

Data were high pass filtered at 0.1 Hz using a 4th order Butterworth filter. Spectrograms were computed on lead F3 for each subject using the Thomson's multitaper method (Thomson, 1982) implemented in MATLAB using the following parameters: 10 s window

length, 1 s step size, time-bandwidth product $NW=9$, and number of tapers $K=5$. Power estimates were computed for frequencies up to 50 Hz. In order to expose fluctuations around the mean spectrogram, the temporal mean spectrogram was computed by averaging across all 10 second windows during the three hour isoflurane administration. This mean spectrum was subtracted from the original spectrum obtained in each 10 second window, after a *log* transformation. For the group mean and median spectrograms, the individual spectrograms were not normalized. All subjects' spectrograms were truncated to the length of the shortest clean spectrogram, 124.35 min.

Many methods exist for detecting suppressed EEG (e.g.(Chemali et al., 2013; Leistriz et al., 1999; Särkelä et al., 2002). Here, we sought to separate periods of suppression in the EEG using the methodology similar to that described by Hudson and colleagues such that the EEG spectrum of the signal in each window is a vector. Each element of the vector specifies the power estimate at each frequency. To reduce the dimensionality of this vector, we subjected the matrix consisting of spectral estimates at each 10 second window to principal component analysis performed on each subject individually. To determine whether distribution of the data projected onto first principal component (PC1) was unimodal, we used Hartigan's dip statistic (1000 bootstraps) (Hartigan and Hartigan, 1985). For every subject, if the null hypothesis of unimodality was rejected, *k-means* clustering was performed on their data projected onto the first two principal components. In the subjects with burst suppression, this procedure resulted in suppressed epochs grouped into a single cluster. Thus, each one of the 10-s windows of the spectrogram was effectively categorized as either EEG suppression or non-suppression.

Statistical analysis

To determine how time to emergence is related to experimental variables, we began our statistical analyses by constructing linear regression models for each of three isoflurane-derived measures and four suppression-derived measures with time to emergence. These isoflurane and suppression measures are described in further detail below.

For all 27 subjects, end-tidal isoflurane values were collected and analyzed (**Figure 1A**). The three predictors derived from isoflurane measures were: 1) the summation from 1 to 30 min; 2) the mean value from 50 to 180 min; and 3) the rate constant of exponential decay of a curve fit to the measured isoflurane concentration after discontinuation of anesthesia at 180 min until time of emergence. This rate constant was calculated for each subject individually using the following equation:

$$[isoflurane] = ae^{-\kappa t} \quad (3.1)$$

where t is the time in minutes since isoflurane was shut off. Parameters a and κ were fit to the data using the least-squares method. The only isoflurane-derived variable that had a significant relationship with time to emergence was the exponential time constant for isoflurane expiration, κ .

Several measures of suppression were also considered in our initial analyses: fraction of total time spent in suppression, longest single episode of suppression, number of distinct suppression episodes, and the fraction of time spent in suppression during the last 15 min of isoflurane administration. Given the limited number of subjects included in this study, we chose to focus subsequent analyses on the fraction of total time spent in suppression and the fraction of time spent in suppression in the last 15 min at isoflurane 1.3 MAC.

To further investigate the relationship between suppression and time to emergence, we tested for independence between the rate of isoflurane expiration and durations of EEG suppression. To assess this, we constructed a pair of linear regression models with time to emergence as the dependent variable and independent variables κ and one of two suppression measures (either the fraction of total time spent in suppression or the fraction of suppression in the last 15 min of isoflurane exposure) in addition to an interaction term between κ and the suppression measure.

In order to test the hypothesis that the inclusion of information about the amount of EEG suppression improves model predictions of emergence time, we generated three additional models. Each model was built to estimate the emergence time based on measured and fitted parameters. The general intuition we used in construction of these models was that isoelectric EEG can be thought of as the deepest state of anesthesia. Recovery of consciousness can then be conceptualized as the gradual evolution of the brain state from its starting point towards some threshold brain state at which emergence occurs. We modelled this trajectory as an exponential decay from the starting brain state at which anesthetic was turned off to brain state at which emergence is observed. This model is mathematically expressed as follows:

$$\Omega = Ae^{-\kappa t_{wake}} \quad (3.2)$$

where Ω is the threshold brain state at which emergence occurs, κ is the rate constant obtained by fitting decay of expired isoflurane to an exponential (Eq. 3.1) and A is the initial brain state at the time of isoflurane shut-off. Finally, t_{wake} is the time of emergence in minutes. The equation can be solved for t_{wake} and rewritten as:

$$t_{wake} = -\left(\frac{1}{\kappa}\right) \ln\left(\frac{\Omega}{A}\right) \quad (3.3)$$

In order to determine whether the amount of EEG suppression can predict t_{wake} , A was constructed in three different ways; models 1 and 2 each include a different measure of EEG suppression (σ), while model 3 does not contain any information concerning suppression of the EEG. The variable σ is percent of total time in suppression during the 3-h exposure, in model 1. In model 2, σ is percent of time in suppression during the last 15 min. In models 1 and 2, $A=\sigma+\omega$ where ω is an offset that ensures A is never equal to Ω . This offset allows us to deal with subjects that had no suppression. Model 3 does not include a suppression variable and $A=\omega$.

We estimated Ω and A using least-squares fitting of Eq. 3.2 to the observed emergence times and measured parameters. Using the fitted parameters, we obtained three different sets of predictions for the time to emergence, \hat{t} : one from each model.

The ultimate question we aim to address in this study is whether incorporating a measure of EEG suppression (σ) into a model of emergence from anesthesia improves predictions. To answer this question, we use a model selection strategy grounded in information theory—Akaike Information Criterion (AIC) (Bozdogan, 1987). The best model is not necessarily the one that minimizes residuals. This is because models with more parameters will generally fit data better than models with fewer parameters, regardless of how relevant the additional parameters are. To ensure that there is not a bias for models with more parameters, AIC assigns a penalty for each additional parameter used in a model. With correction for a finite sample size, AIC was implemented according to the following equation:

$$AIC = 2n - 2\ln(\hat{L}) + \frac{2n^2 + 2n}{N - n - 1} \quad (3.4)$$

where, n is the number of parameters in the model, L is the log likelihood of the residuals, and N is the total number of subjects. L is calculated using the following equation:

$$L = -\frac{N}{2} \ln\left(\frac{SS}{N}\right), \text{ where } SS = \sum_{i=1}^N (t_{wake_i} - \hat{t}_i)^2 \quad (3.5)$$

Models 1 and 2 include suppression and have two parameters (κ and σ). whereas model 3 has only one parameter (κ). AIC can be converted to the probability that the i^{th} model, out of a set of considered models, is preferred. This probability is computed according to the following equation (Burnham and Anderson, 2003):

$$P_i = e^{\frac{AIC_{min} - AIC_i}{2}} \quad (3.6)$$

In order to maximize reproducibility, we bootstrapped our calculation of AIC probabilities (1000 bootstraps).

Analysis of cognitive task performance

Accuracy and response time measures for the PVT and DSST were standardized as z-scores based upon the distribution of pre-intervention baseline scores from the study sample. The standardized scores were expressed as differences from individuals' baseline performance before anesthesia (Maier et al., 2017). Cognitive task performance as a function of time was fit using non-linear mixed effects model using a damped exponential function:

$$Y_i(t) = \Phi_{1,i} e^{-\phi_{2,i} \cdot t} + \Phi_3 \quad (3.7)$$

where i is the subject index and t represents time after recovery of consciousness. Φ_{1-2} were modelled as random effects that were fit for each subject independently, while Φ_3 was treated as a fixed effect and accounted for differences relative to baseline. The sum of $\Phi_{1,i}$ and Φ_3 was used to model the change in cognitive performance at the

time of emergence (t_0). This accounted for the variability in the timing of DSST and PVT task administration and allowed cognitive task performance to be compared at a common time point across participants. As the modelled cognitive task measures at time of emergence were not normally distributed, Spearman's rank-order correlation was used to assess for relationships between measures of burst suppression and impairment in task performance at emergence.

Non-linear mixed effects modelling of cognitive task performance was performed in SAS (SAS Institute Inc., Cary, NC, USA). All further analyses were performed in R or in Matlab R2017a using customized scripts. All errors are shown in terms of standard deviation (SD) unless otherwise indicated.

TABLES

Linear Regression with Elimination Time Constant and Overall Percent Suppression		
Overall Significance (F-statistic: 6 on 3 and 23 DF)	Adjusted R ² : 0.37	P-value: 0.004*
Isoflurane Elimination Time Constant (κ)	0.79 (0.6)	P-value: 0.18
Percent Suppression (overall)	0.23 (0.3)	P-value: 0.46
Interaction	0.02 (0.01)	P-value: 0.27
Asterisk denotes statistical significance at the level defined as $p < 0.05$.		

Table 3.1: Results of linear regression model including decay time constant and overall percent suppression. Overall suppression is not significantly associated with time to recovery and fails to show statistically significant interaction with the isoflurane elimination time constant.

Linear Regression with Elimination Time Constant and Percent Suppression in the last 15 minutes		
Overall Significance (F-statistic: 5.35 on 3 and 23 DF)	Adjusted R ² : 0.33	P-value: 0.006*
Isoflurane Elimination Time Constant (κ)	1.4 (0.4)	P-value: 0.003*
Percent Suppression (overall)	22.8 (51.8)	P-value: 0.66
Interaction	-0.49 (2.9)	P-value: 0.87
Asterisk denotes statistical significance at the level defined as $p < 0.05$.		

Figure 3.2: Results of linear regression model including decay time constant and percent of last 15 min of isoflurane exposure spent in EEG suppression. EEG suppression is not significantly associated with time to recovery and fails to show a statistically significant interaction with the isoflurane elimination time constant.

	Model with % Suppression	Model with % Suppression in last 15 minutes	Model with no Suppression Term
R²	0.41	0.40	0.39
P-value	3x10 ⁻⁴	4x10 ⁻⁴	5x10 ⁻⁴
No. of Parameters	2	2	1
AIC Probability	0.24	0.19	0.58

Table 3.3: Statistical results of three exponential decay models. Pearson's R² shows similar predictive ability of each model for time of emergence from anesthesia. Probabilities based on Akaike information criteria indicate the probability that a single model is the best one to fit experimental data, given the set of models being considered. AIC, Akaike Information Criterion.

Association between EEG Suppression and Cognitive Performance		
	Spearman's Rho	P-value
DSST Reaction Time	-0.0519	0.7971
DSST Accuracy	0.036	0.8584
PVT Reaction Time	0.3444	0.078
PVT Accuracy	0.1105	0.5832

Table 3.4: Analysis of correlation between the total time spent in EEG suppression and the degree of impairment in cognitive performance upon emergence. No significant relationship was observed between total duration of suppression and change in cognitive metrics relative to baseline. DSST, digit symbol substitution test; PVT, psychomotor vigilance test.

Association between EEG Suppression in the last 15 Minutes and Cognitive Performance		
	Spearman's Rho	P-value
DSST Reaction Time	-0.1656	0.409
DSST Accuracy	-0.0165	0.9351
PVT Reaction Time	0.2754	0.1645
PVT Accuracy	0.3007	0.1275

Table 3.5: Analysis of correlation between the fraction of the last 15 min of isoflurane exposure spent in EEG suppression and the degree of impairment in cognitive performance upon emergence. As with the measure of total duration of suppression, suppression in the last 15 min of anesthetic exposure was not significantly correlated to initial cognitive task performance at emergence. DSST, digit symbol substitution test; PVT, psychomotor vigilance test.

Association between Isoflurane Elimination Time Constant and Cognitive Performance		
	Spearman's Rho	P-value
DSST Reaction Time	-0.3291	0.0941
DSST Accuracy	-0.3065	0.1201
PVT Reaction Time	-0.0122	0.9527
PVT Accuracy	0.1099	0.5839

Table 3.6: Analysis of correlation between the time constant of elimination of isoflurane and the degree of impairment in cognitive performance upon emergence. The time constant of elimination was not significantly associated with any of the cognitive task measures. DSST, digit symbol substitution test; PVT, psychomotor vigilance test.

FIGURES

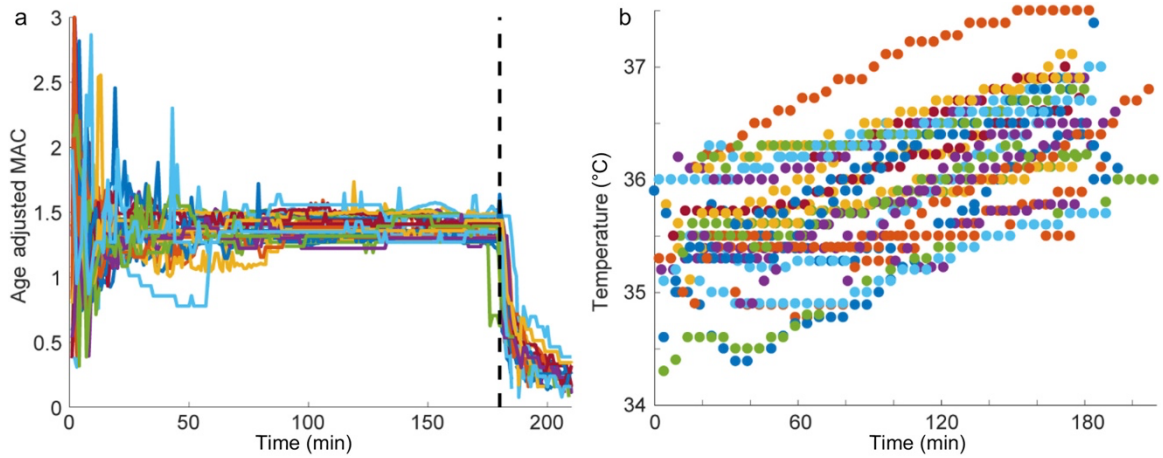


Figure 3.1: End-tidal isoflurane concentration and body temperature during anesthetic exposure. (A) Age-adjusted isoflurane minimum alveolar concentration (MAC) from the start of isoflurane administration (time 0) to the discontinuation of isoflurane at 180 min (vertical dotted black line) for all 27 subjects. (B) Temperature is presented in °C over the three hours of isoflurane administration.

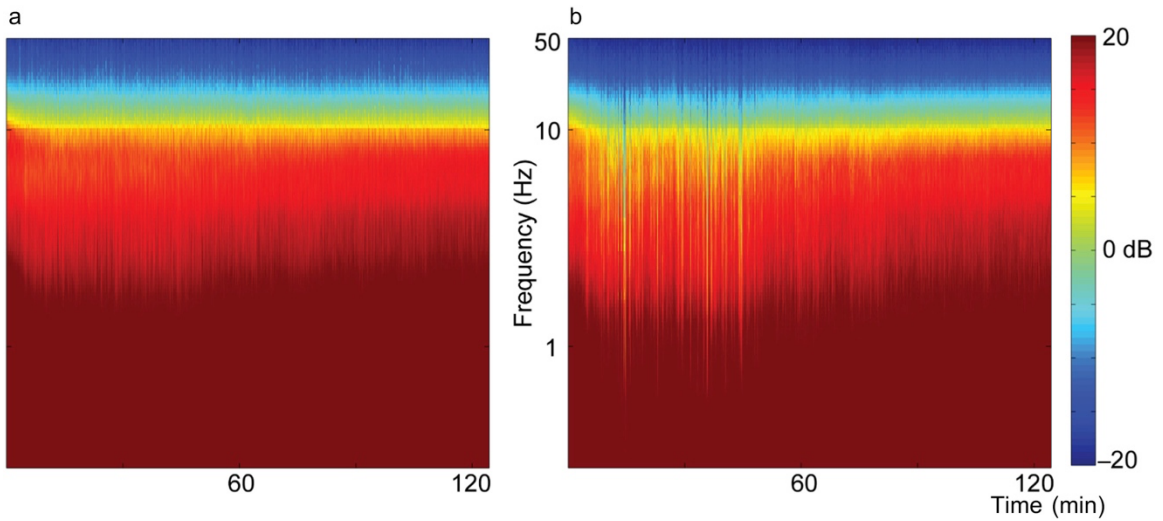


Figure 3.2: Group spectrograms show canonical low frequency oscillations in the anesthetized brain. Spectrograms measured from F3 combined over all 27 subjects. Spectra are computed for the last two hours of isoflurane administration (starting one hour into the administration). (A) The mean spectrogram computed over all subjects shows consistent power over all frequencies for the duration of anesthetic exposure after equilibration. (B) The median spectrogram computed over all subjects shows similar results to the mean spectrogram. Both ways of combining the data across subjects show the well-known slow oscillations in the EEG under anesthesia.

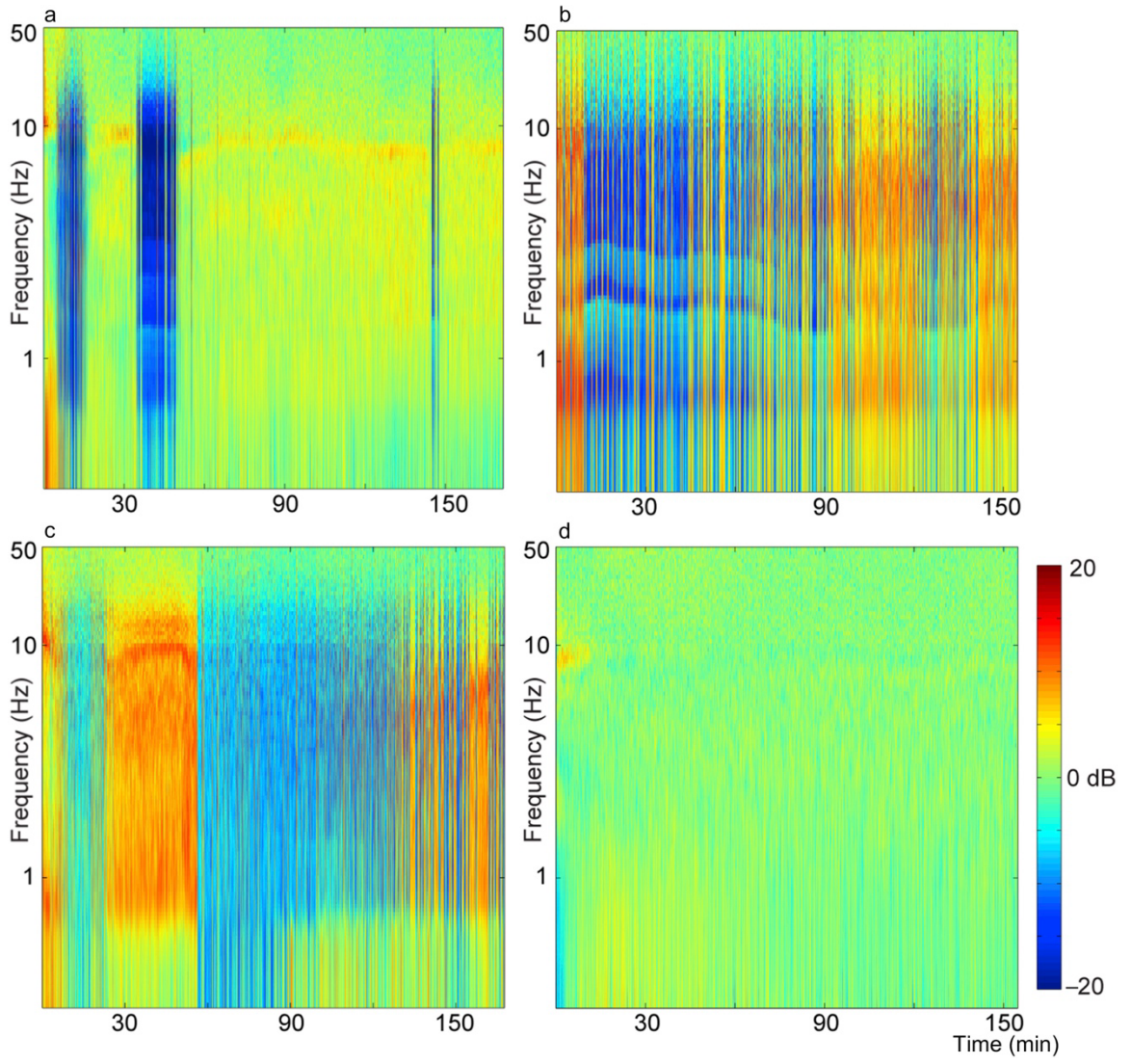


Figure 3.3: Individual spectrograms reveal the variability of EEG activity between subjects and across time. (A - D) Spectrograms of four individual subjects computed over the entire three hour isoflurane administration. To better expose fluctuations in the spectral content, the mean of the spectrum across three hours is subtracted. Periods in which there is suppressed EEG appear in the spectrogram as vertical blue lines, as these periods have decreased spectral activity across all frequencies. There is individual variability in the overall amount of suppression that occurred during the recording, the number of times a subject transitioned between suppressed and non-suppressed states, and the duration of a suppression period. (A) Suppression condensed into distinct periods. (B) Suppression occurring intermittently throughout the recording. (C) Suppression dominating the recording but interrupted by a period without suppression. (D) No suppression. A lack of suppression was seen for two subjects (data not shown).

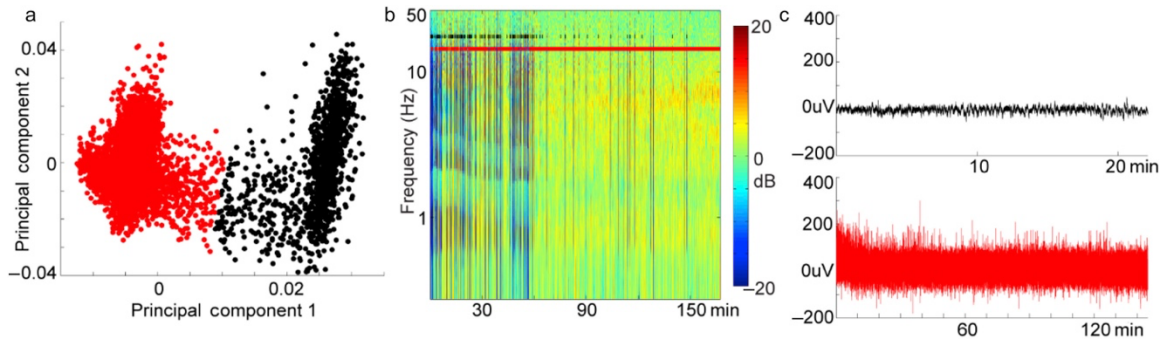


Figure 3.4: Illustration of principal component analysis (PCA)-based method for isolating episodes of EEG suppression. (A) Projection of the spectrogram in (B) onto its first two principal components reveals two well-separated groups of points. These data were subjected to k-means clustering which revealed two distinct clusters (red and black). (B) Suppression-classified times (black) and non-suppression-classified (red) times are shown over the spectrogram. Suppression times do indeed correspond to periods of broadband power decreases. (C) To illustrate that PCA and k-means reliably separate periods of suppressed EEG from non-suppressed periods, all EEG time periods classified as suppressed (black) were concatenated. Note that almost no detectable voltage oscillations are observed. In contrast, EEG epochs classified as non-suppressed (red) exhibit sustained activity.

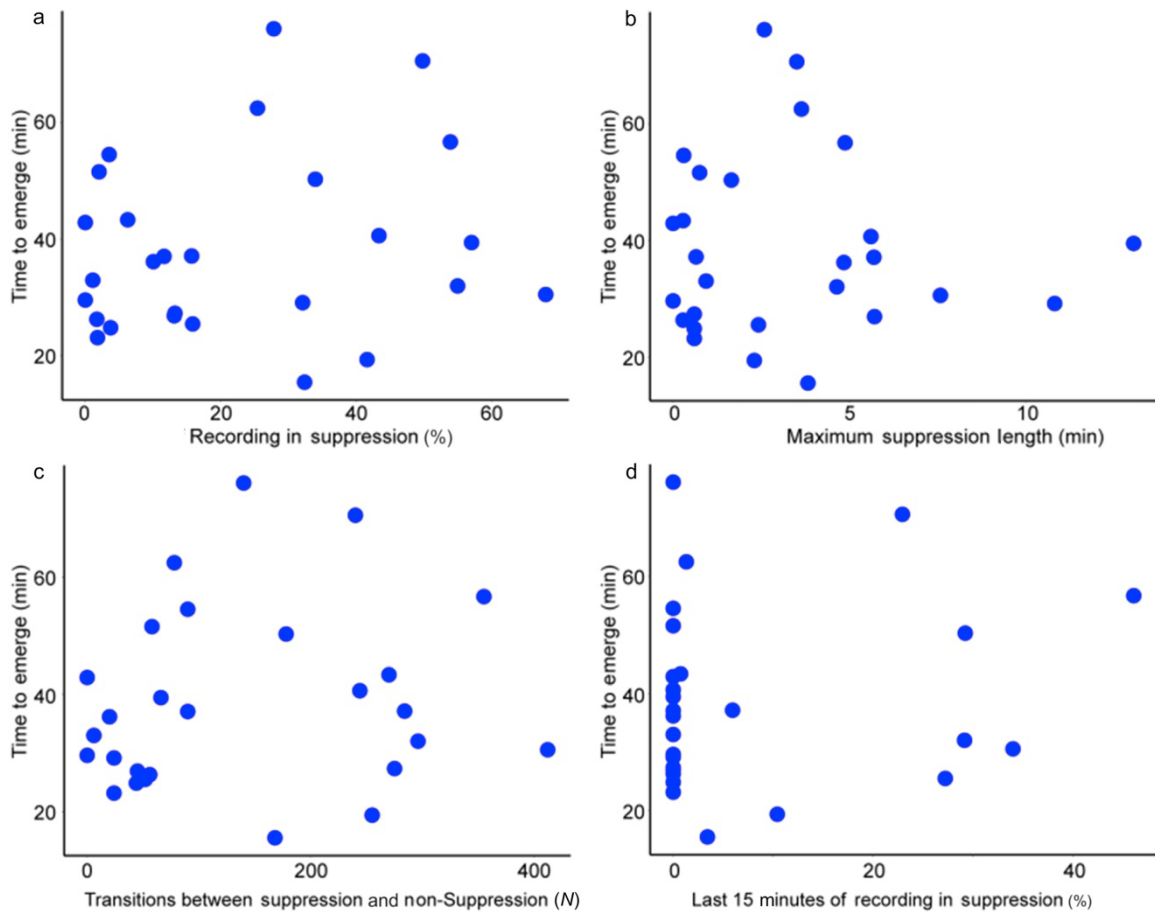


Figure 3.5: The time to emerge from isoflurane (time to recovery of consciousness) is not significantly correlated with different measures of suppression. (A) The cumulative percentage of the recording spent in suppression ($R^2=0.03$, $P=0.40$); (B) the longest period of continuous suppression ($R^2=8\times 10^{-4}$, $P=0.89$); (C) the number of transitions between suppression and non-suppression ($R^2=0.02$, $P=0.51$); and (D) the cumulative percentage of the last 15 minutes of the recording before isoflurane is discontinued spent in suppression ($R^2=0.02$, $P=0.44$).

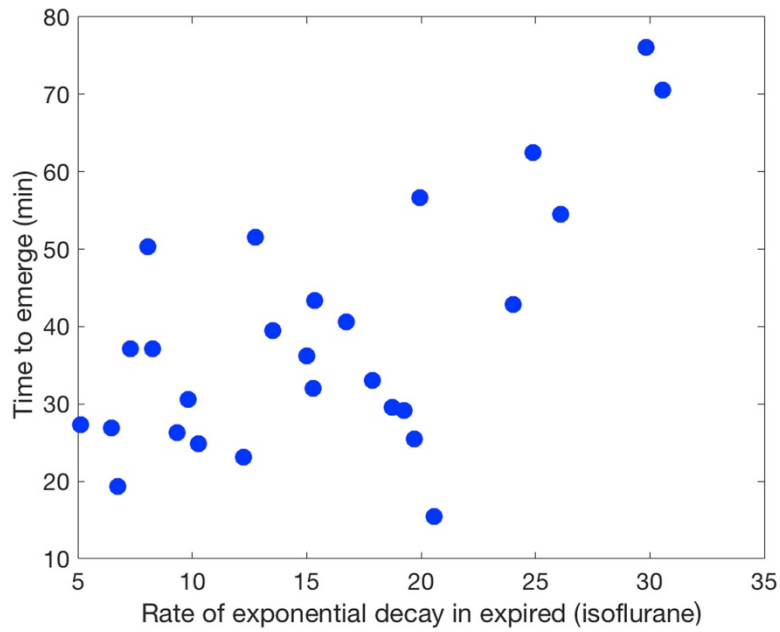


Figure 3.6: The time to emerge from isoflurane (time to recovery of consciousness) is significantly correlated with the rate of isoflurane expiration.

The subjects that clear isoflurane more rapidly tend to be those that recover consciousness more quickly after discontinuation of isoflurane anesthesia ($R^2=0.39$, $P=5 \times 10^{-4}$).

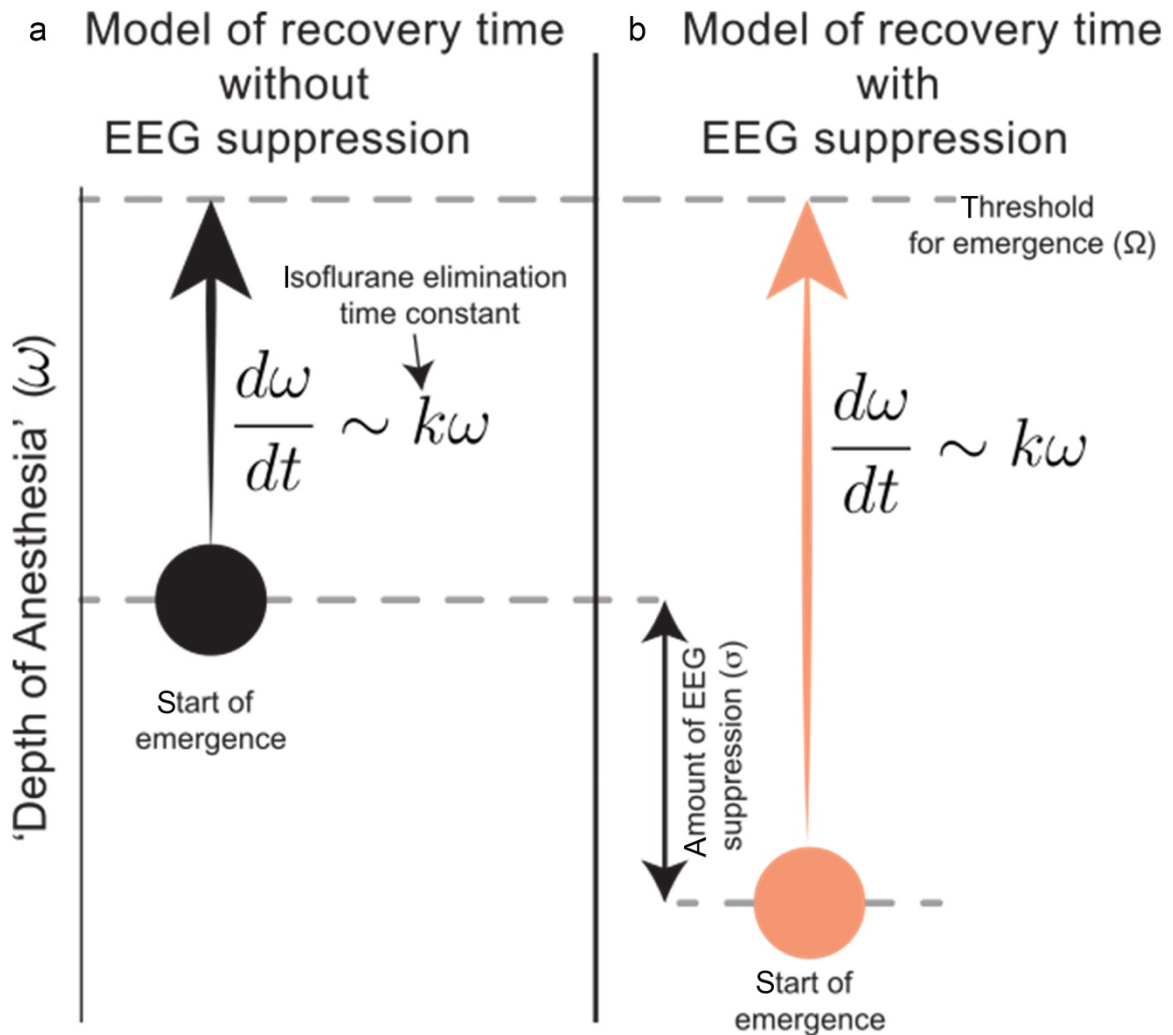


Figure 3.7: Schematic of physiologically motivated model. Emergence occurs as the progression from initial brain state to a threshold brain state (Ω) at which consciousness is regained. The rate of this progression is defined by the rate of exponential decay in expired isoflurane (k). Suppressed EEG (σ) is modelled as increased anesthetic depth in (A). The motivating hypothesis for this model is that increased anesthetic depth is expected to be correlated with increased time to emergence (B).

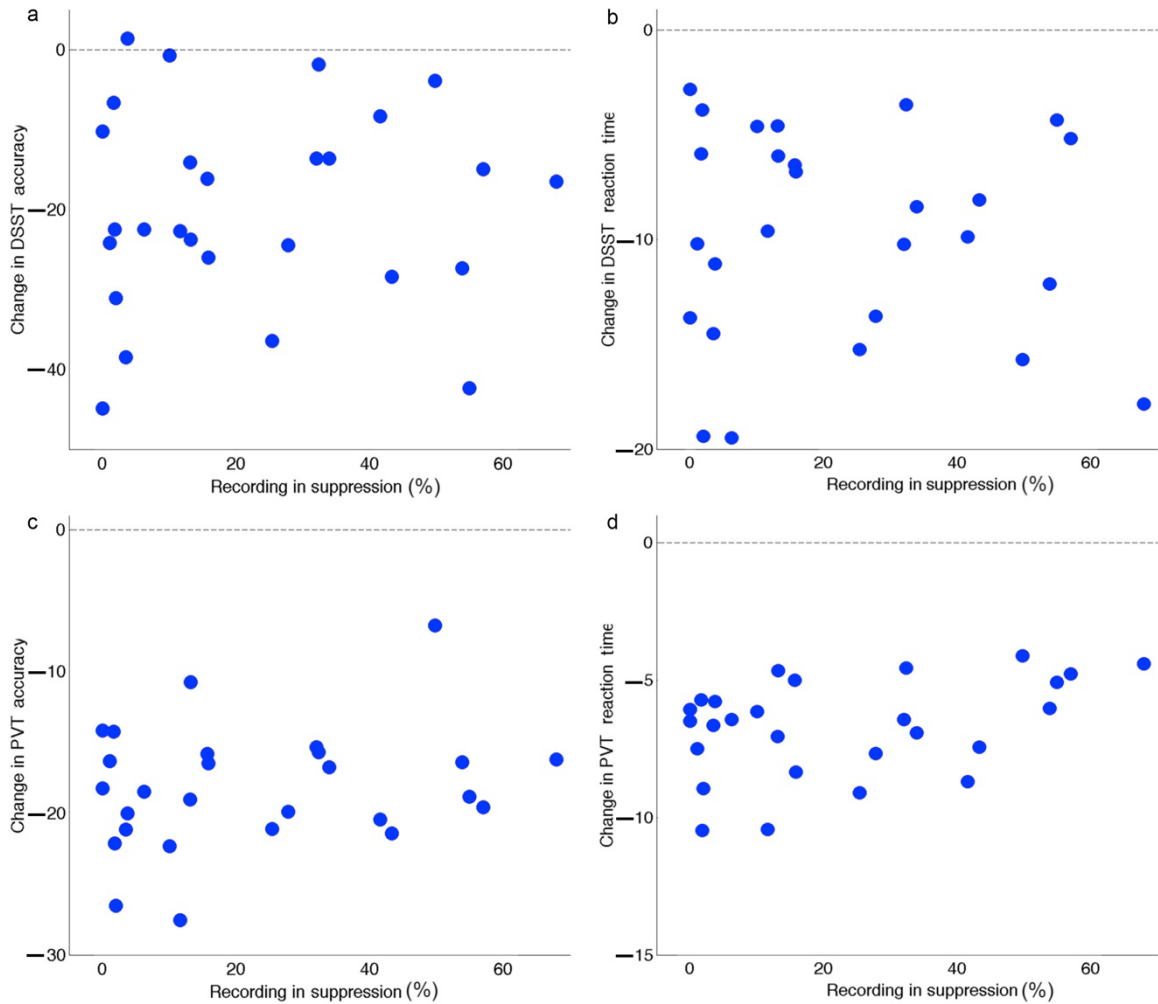


Figure 3.8: Association between amount of EEG suppression on performance speed and accuracy on both the psychomotor vigilance test (PVT) and digit symbol substitution test (DSST). (A - D) The dashed line at zero marks individuals' baseline performance. While most subjects demonstrated impaired performance upon emergence from anesthesia, the degree of this impairment does not appear to be related to the amount of EEG suppression.

CHAPTER 4 – General Discussion

Converging lines of evidence suggest that patterns of brain activity during anesthetic-induced unconsciousness are not fixed. Rather, activity patterns fluctuate between a small number of distinct brain states that are organized via weak, local interactions within the cortex. Despite these local interactions being weak, widespread activity patterns throughout the cortex can be well described in a low-dimensional space. Weak local interactions are a previously underappreciated organizing force for cortical activity patterns.

Three complementary analysis methods show that activity patterns and transition times recorded from the same cortical region are more similar than those recorded simultaneously from different cortical regions. This was true with the notable exception of recordings from cortical layer IV. Given the differential innervation of layer IV, relative to the superficial and infragranular cortical layers, this result alludes to the importance of local communication between neurons within the cortex in organizing brain states and transitions under anesthesia. Further evidence in support of the importance of local communication comes from our results showing that recordings from functionally similar regions are no more similar than those from functionally dissimilar regions. If subcortical structures were responsible for driving state transitions, one would expect to find that recordings collected from bilateral, homologous cortical regions would show more similar activity patterns than recordings from functionally unrelated cortical regions. This was not true in our dataset and implies that the subcortical drivers of cortical activity and state transitions are not the principal drivers of the brain states and transitions we record under anesthesia. The third line of evidence in support of the importance of local, cortical communication comes from our results showing that local communication is necessary

in order for widespread cortical activity patterns to be well described in a low-dimensional space. The shuffled datasets used in Chapter 2 to test for statistical significance were built to specifically test for the importance of local interactions between nearby channels. These shuffled datasets preserved the internal statistics of the channel from which they were generated, by using that channel's transition probabilities. In this way, each individual channel is indistinguishable from the shuffled datasets generated from it. Because these shuffled datasets were generated for each channel individually, they do not preserve the influence that one channel may have on another. For all three of our measures, within- and between-channel comparisons with real data were significantly higher than would be expected by chance. Furthermore, only the real data could be well described in a low dimensional space which demonstrates that, while different regions of cortex may not have the same activity patterns, the activity patterns present in those regions are not completely independent, and the interactions between channels are sufficient to give rise to coherent, global brain states. All together, these results suggest that local communication between cortical neurons are the main organizing mechanism behind the brain states and state transitions that occur under general anesthesia.

States of sleep and those recorded under anesthesia both have pronounced oscillatory activity in the spindle, delta, and slow wave ranges. However, while we show that states under anesthesia are spatially localized, natural sleep is characterized by brain states that engage neurons throughout the thalamocortical network (Dement and Kleitman, 1957; Timo-laria et al., 1970). During sleep, dense, reciprocal connections between the cortex and thalamus are known to be responsible for propagating spindle and delta oscillations (Contreras and Steriade, 1997; Steriade et al., 1991), and corticocortical

communication propagates the slow wave oscillation (Mircea Steriade et al., 1993b). Progressive hyperpolarization of the thalamocortical network over the course of a continuous sleep bout is responsible for the transitions between states of increasing synchrony (Steriade et al., 1991). Additionally, widespread innervation of the cortex by the reticular activating system is responsible for destabilizing states of high synchrony and causing an abrupt transition to a state of more desynchronized activity (Moruzzi and Magoun, 1949). Together, these connections are able to drive transitions and organize coherent oscillatory activity that engages neurons throughout the cortex during sleep.

Anesthetic drugs suppress the neurons in the thalamocortical network. Their strongest effect seems to be on the cortical neurons which disrupts corticocortical communication. However, matrix and core thalamocortical projections are also suppressed (Raz et al., 2014). In this way, anesthetic drugs interfere with key connections responsible for coordinating coherent oscillations throughout the thalamocortical network (Contreras and Steriade, 1997; Mircea Steriade et al., 1993a; Steriade et al., 1991). It is possible that disruption of thalamocortical and corticocortical communication prevents signals that would normally cause transitions between sleep and wake states from spreading throughout the thalamocortical network. While reciprocal connectivity is not required for the generation of spindle or delta oscillations, it is required for their coherent expression throughout the cortex and thalamus (Contreras and Steriade, 1997; Steriade et al., 1991). Anesthetics activate sleep-promoting circuits within the brain, but they disrupt the connections through which the thalamocortical network engages widespread synchrony in firing. The combination of these effects could be an explanation for our observation that activity patterns and transition times are only weakly correlated between cortical regions under anesthesia but that there is greater similarity in nearby regions, regardless

of function. In this case, specific oscillations or activity patterns could initiate spontaneously or as a result of subcortical input, but the ability of this pattern to spread would be impaired. Thereby, rather than the entire thalamocortical network entering a new activity pattern, local interactions stabilize the activity only in a localized region.

In order to know for certain whether or not activity patterns in the thalamus are like those recorded from the cortex under anesthesia, one would need to record from the thalamus directly. While we did not do that, another experiment using very similar methods to our own did record from thalamus and cortex simultaneously and showed distinct brain states with discrete transitions *en route* to emergence (Hudson et al., 2014). When spectra from all simultaneously recorded cortical and thalamic channels were decomposed together using principal component analysis, they show that about 70% of the variance within their dataset can be described by three principal components. This result is aligned with our own data showing very similar results. Given these similarities, an experiment exactly like the one presented here with an additional thalamic electrode would be an exciting future direction to this work. Such an experiment would offer valuable insight into the relationship between transitions and activity patterns recorded in the thalamus and the different cortical layers: in particular layer IV.

Sleep and wake promoting nuclei in the basal forebrain engage in self-excitation and mutual inhibition that is thought to stabilize states of sleep and wakefulness to prevent both from existing in the brain simultaneously (Cho et al., 2017; Donlea et al., 2018; Sara, 2009; Scammell et al., 2017; Schwartz and Roth, 2008). However, there are known exceptions to this boundary between sleep and wake during which spatially restricted regions of cortex can enter a state of sleep. A classic example of this local sleep behavior is observed in cetaceans and other marine mammals (Kendall-Bar et al.,

2019; Lyamin et al., 2008). In these animals, sleep involves one hemi-cortex while the other hemisphere exhibits wake-like activity. Similar phenomena are observed in birds (Rattenborg et al., 2019) and some reptiles (Kelly et al., 2015). In terrestrial mammals such as rodents, local sleep has also been demonstrated (Krueger and Tononi, 2011; Rector et al., 2005; Vyazovskiy et al., 2011). When rats are sleep-deprived, local patches of cortex can spontaneously enter slow wave sleep-like activity patterns while other locations in the cortex continue to exhibit wake-like activity patterns (Vyazovskiy et al., 2011). Such local sleep phenomena may underlie performance decrements observed during drowsiness. In both humans and rats, learning tasks designed to engage specific regions of the brain have been shown to induce spatial differences in slow-wave sleep activity during subsequent sleep bouts (Huber et al., 2004; Vyazovskiy et al., 2000). In humans suffering from NREM parasomnias, NREM-like and wake-like activity patterns can be simultaneously present in different parts of the brain (Mahowald and Schenck, 2005). Altogether, these observations suggest that switch from one brain state to another can occur locally in the context of natural sleep and wake if there are homeostatic or environmental pressures that differentially influence specific cortical regions. This implies that local interactions within cortex may have a stronger influence over activity patterns during sleep and wake than has previously been appreciated.

Our results in Chapter 2 show that brain activity recorded at a single, unchanging anesthetic concentration is not fixed and that activity patterns fluctuate back and forth between a small number of discrete brain states. The work presented in Chapter 3 looked at a more indirect measure of brain state to explore the relationship between brain state and anesthetic depth in humans. In this study, we hypothesized that more time spent in an activity pattern associated with the deepest plane of anesthesia, burst

suppression, would be associated with longer time to emergence. This hypothesis comes from the common assumption that anesthesia can be thought of as a depth from which one must recover back to consciousness. By this logic, more time spent in burst suppression should indicate a deeper plane of anesthesia and, therefore, a greater distance the brain must traverse to achieve emergence. Contrary to this hypothesis, we did not find an association between time spent in burst suppression and time to emergence or performance on cognitive tasks. Our results indicate that the relationship between anesthetic depth and time to emergence is not linear. While it is not possible to collect data from humans to directly test this, it is an exciting possibility that this nonlinearity comes from the stochastic switching between discrete, stable brain states *en route* to emergence similar to those that have been in rats (Hudson et al., 2014).

Hudson et al. found that only certain states are capable of allowing the brain to exit a state of higher synchrony to a state of lower synchrony (Hudson et al., 2014). The brain had to be in one of three hub states to either exit burst suppression and enter a delta-dominated state, to exit from delta to a theta-dominated state, or to emerge to consciousness (Hudson et al., 2014). Entry into a hub state does not guarantee that the brain transitions to a state of more desynchrony, but entry into a hub state is essential for there to be such a transition. Given that many transitions do not necessarily bring the brain closer to achieving emergence, transitions back and forth between states with more or less synchrony could account for why there is hysteresis between induction and emergence from anesthesia.

Additional indirect evidence to support stochastic fluctuations back and forth between different brain states as a potential explanation for the hysteresis between induction and emergence is the variability in time spent in suppression we observed between subjects.

Each subject received identical exposure to anesthesia without confounding factors such as illness or additional pharmaceutical agents. Therefore, the variability in time spent in suppression cannot be explained by experimental factors. Had we found a relationship between time spent in suppression and time to emergence or performance on the cognitive tests, an individual's sensitivity to isoflurane anesthesia could have been an explanation for this variability. However, no such relationship exists. This lack of relationship argues that individual sensitivity is insufficient to explain why some individuals take longer to emerge after identical exposures to anesthesia and leaves open the possibility that stochastic transitions between different brain states is responsible for the between-subject variability we see. This interpretation is in line with other work in zebrafish and mice showing both within- and between-subject variability in responsiveness following identical exposures to anesthesia (McKinstry-Wu et al., 2019). Responses were assayed after allowing time for equilibration and demonstrate stochastic switching between whether or not the animal could respond to stimuli (McKinstry-Wu et al., 2019). Therefore, the stochastic nature of this switching between states of more or less responsiveness during fixed exposure to anesthesia could be the mechanism that gives rise to the anesthetic hysteresis.

Taken together, the work presented in this thesis highlight the importance of local cortical interactions in stabilizing brain activity. The local nature of these interactions gives rise to spatiotemporally complex global states during anesthetic-induced unconsciousness. Activity patterns recorded during these states seem to be influenced by endogenous sleep/wake circuits, but the disruption of widespread connectivity prevents states from propagating throughout the cortex. Stability of brain states and timing of state transitions are governed by local corticocortical interactions. The purpose

of these brain states seems to be to constrain brain activity to a relatively small number of states which allows emergence from anesthesia to occur on a physiologic timescale (Hudson et al., 2014). Fluctuations between states of more or less synchrony is a potential mechanism that underlies the hysteresis between anesthetic induction and emergence whereby the brain must reassemble its networks into a state that can sustain consciousness before emergence may occur. The local and stochastic nature of this reorganization process means that emergence takes longer than induction.

These data have important implications for anesthetic monitoring. They suggest that population-based metrics are insufficient for monitoring anesthetic depth and predicting adverse outcomes such as intraoperative awareness. They also have implications for clinical sleep disorders such as parasomnias which could perhaps be better understood as a disruption in the local mechanisms meant to stabilize states of sleep and wake. Finally, these data provide evidence that greater attention should be paid to local dynamics during basic science studies of sleep and wake.

REFERENCES

- Akrawi WP, Drummond JC, Kalkman CJ, Patel PM. 1996. A Comparison of the Electrophysiologic Characteristics of EEG Burst-Suppression as Produced by Isoflurane, Thiopental, Etomidate, and Propofol. *Journal of Neurosurgical Anesthesiology* **8**.
- Al Ansari M, Dawson A, Conigrave K. 2019. Alcohol: from Mesopotamia to Modern Iraq. *Journal of Ethnicity in Substance Abuse* **20**:343–365. doi:10.1080/15332640.2019.1657541
- Alpert MI, Peterson RA. 1972. On the Interpretation of Canonical Analysis. *Journal of Marketing Research* **9**:7.
- Amzica F. 2009. Basic physiology of burst-suppression. *Epilepsia* **50**:38–39. doi:10.1111/j.1528-1167.2009.02345.x
- Amzica F, Steriade M. 1995. Disconnection of intracortical synaptic linkages disrupts synchronization of a slow oscillation. *J Neurosci* **15**:4658–4677. doi:10.1523/JNEUROSCI.15-06-04658.1995
- Andresen JM, Girard TD, Pandharipande PP, Davidson MA, Ely EW, Watson PL. 2014. Burst Suppression on Processed Electroencephalography as a Predictor of Postcoma Delirium in Mechanically Ventilated ICU Patients: *Critical Care Medicine* **42**:2244–2251. doi:10.1097/CCM.0000000000000522
- Aston-Jones G, Chen S, Zhu Y, Oshinsky ML. 2001. A neural circuit for circadian regulation of arousal. *Nat Neurosci* **4**:732–738. doi:10.1038/89522
- Avanzini G, de Curtis M, Panzica F, Spreafico R. 1989. Intrinsic properties of nucleus reticularis thalami neurones of the rat studied in vitro. *The Journal of Physiology* **416**:111–122. doi:10.1113/jphysiol.1989.sp017752
- Bai D, Pennefather PS, MacDonald JF, Orser BA. 1999. The General Anesthetic Propofol Slows Deactivation and Desensitization of GABAA Receptors. *J Neurosci* **19**:10635–10646. doi:10.1523/JNEUROSCI.19-24-10635.1999
- Ballesteros JJ, Briscoe JB, Ishizawa Y. 2020a. Neural signatures of α 2-Adrenergic agonist-induced unconsciousness and awakening by antagonist. *eLife* **9**:e57670. doi:10.7554/eLife.57670
- Ballesteros JJ, Briscoe JB, Ishizawa Y. 2020b. Neural signatures of α 2-Adrenergic agonist-induced unconsciousness and awakening by antagonist. *eLife* **9**:e57670. doi:10.7554/eLife.57670
- Barann M, Dilger JP, Bönisch H, Göthert M, Dybek A, Urban BW. 2000. Inhibition of 5-HT₃ receptors by propofol: equilibrium and kinetic measurements. *Neuropharmacology* **39**:1064–1074. doi:10.1016/S0028-3908(99)00205-1
- Barann M, Göthert M, Bönisch H, Dybek A, Urban BW. 1997. 5-HT₃ receptors in outside-out patches of N1E-115 neuroblastoma cells: basic properties and effects of pentobarbital. *Neuropharmacology* **36**:655–664.
- Basner M, Dinges DF. 2011. Maximizing Sensitivity of the Psychomotor Vigilance Test (PVT) to Sleep Loss. *Sleep* **34**:581–591. doi:10.1093/sleep/34.5.581

- Basner M, Mollicone D, Dinges DF. 2011. Validity and sensitivity of a brief psychomotor vigilance test (PVT-B) to total and partial sleep deprivation. *Acta Astronautica* **69**:949–959. doi:10.1016/j.actaastro.2011.07.015
- Basner M, Savitt A, Moore TM, Port AM, McGuire S, Ecker AJ, Nasrini J, Mollicone DJ, Mott CM, McCann T, Dinges DF, Gur RC. 2015. Development and Validation of the Cognition Test Battery for Spaceflight. *Aerospace Medicine and Human Performance* **86**:942–952. doi:10.3357/AMHP.4343.2015
- Bialek W, Cavagna A, Giardina I, Mora T, Silvestri E, Viale M, Walczak AM. 2012. Statistical mechanics for natural flocks of birds. *PNAS* **109**:4786–4791. doi:10.1073/pnas.1118633109
- Blain-Moraes S, Lee U, Ku S, Noh G, Mashour GA. 2014. Electroencephalographic effects of ketamine on power, cross-frequency coupling, and connectivity in the alpha bandwidth. *Front Syst Neurosci* **8**. doi:10.3389/fnsys.2014.00114
- Bourassa J, Deschênes M. 1995. Corticothalamic projections from the primary visual cortex in rats: a single fiber study using biocytin as an anterograde tracer. *Neuroscience* **66**:253–263. doi:10.1016/0306-4522(95)00009-8
- Bozdogan H. 1987. Model selection and Akaike's Information Criterion (AIC): The general theory and its analytical extensions. *Psychometrika* **52**:345–370. doi:10.1007/BF02294361
- Brand EJ, Zhao Z. 2017. Cannabis in Chinese Medicine: Are Some Traditional Indications Referenced in Ancient Literature Related to Cannabinoids? *Front Pharmacol* **8**. doi:10.3389/fphar.2017.00108
- Brook K, Bennett J, Desai SP. 2017. The Chemical History of Morphine: An 8000-year Journey, from Resin to de-novo Synthesis. *Journal of Anesthesia History* **3**:50–55. doi:10.1016/j.janh.2017.02.001
- Brown EN, Lydic R, Schiff ND. 2010. General Anesthesia, Sleep, and Coma. *New England Journal of Medicine* **363**:2638–2650. doi:10.1056/NEJMra0808281
- Bruhn J, Bouillon TW, Shafer SL. 2000. Bispectral index (BIS) and burst suppression: Revealing a part of the BIS algorithm. *Journal of Clinical Monitoring and Computing* **16**:593–596. doi:10.1023/A:1012216600170
- Burnham KP, Anderson DR. 2003. Model selection and multimodel inference: a practical information-theoretic approach, Second. ed. New York: Springer Science & Business Media.
- Buzsáki G, Anastassiou C a, Koch C. 2012. The origin of extracellular fields and currents—EEG, ECoG, LFP and spikes. *Nature reviews Neuroscience* **13**:407–20. doi:10.1038/nrn3241
- Buzsaki G, Bickford R, Ponomareff G, Thal L, Mandel R, Gage F. 1988. Nucleus basalis and thalamic control of neocortical activity in the freely moving rat. *J Neurosci* **8**:4007–4026. doi:10.1523/JNEUROSCI.08-11-04007.1988
- Cain SM, Snutch TP. 2010. Contributions of T-type calcium channel isoforms to neuronal firing. *Channels* **4**:475–482. doi:10.4161/chan.4.6.14106

- Canavier CC, Baxter DA, Clark JW, Byrne JH. 1993. Nonlinear dynamics in a model neuron provide a novel mechanism for transient synaptic inputs to produce long-term alterations of postsynaptic activity. *J Neurophysiol* **69**:2252–2257. doi:10.1152/jn.1993.69.6.2252
- Chan MTV, Cheng BCP, Lee TMC, Gin T. 2012. BIS-guided anesthesia decreases postoperative delirium and cognitive decline. *J Neurosurg Anesthesiol* **25**:1.
- Chander D, García PS, MacColl JN, Illing S, Sleight JW. 2014. Electroencephalographic Variation during End Maintenance and Emergence from Surgical Anesthesia. *PLoS ONE* **9**:e106291. doi:10.1371/journal.pone.0106291
- Chemali J, Ching S, Purdon PL, Solt K, Brown EN. 2013. Burst suppression probability algorithms: state-space methods for tracking EEG burst suppression. *J Neural Eng* **10**:056017. doi:10.1088/1741-2560/10/5/056017
- Chen X, Shu S, Bayliss DA. 2005. Suppression of Ih Contributes to Propofol-Induced Inhibition of Mouse Cortical Pyramidal Neurons. *Journal of Neurophysiology* **94**:3872–3883. doi:10.1152/jn.00389.2005
- Cho JR, Treweek JB, Robinson JE, Xiao C, Bremner LR, Greenbaum A, Gradinaru V. 2017. Dorsal Raphe Dopamine Neurons Modulate Arousal and Promote Wakefulness by Salient Stimuli. *Neuron* **94**:1205–1219. doi:10.1016/j.neuron.2017.05.020
- Cimenser A, Purdon PL, Pierce ET, Walsh JL, Salazar-Gomez AF, Harrell PG, Tavares-Stoeckel C, Habeeb K, Brown EN. 2011. Tracking brain states under general anesthesia by using global coherence analysis. *Proceedings of the National Academy of Sciences* **108**:8832–8837. doi:10.1073/pnas.1017041108
- Cirelli C, Bushey D, Hill S, Huber R, Kreber R, Ganetzky B, Tononi G. 2005. Reduced sleep in Drosophila Shaker mutants. *Nature* **434**:1087–1092. doi:10.1038/nature03486
- Civillico EF, Contreras D. 2012. Spatiotemporal properties of sensory responses in vivo are strongly dependent on network context. *Frontiers in Systems Neuroscience* **6**:1–20. doi:10.3389/fnsys.2012.00025
- Clement EA, Richard A, Thwaites M, Ailon J, Peters S, Dickson CT. 2008. Cyclic and sleep-like spontaneous alternations of brain state under urethane anaesthesia. *PLoS ONE* **3**. doi:10.1371/journal.pone.0002004
- Cloostermans MC, van Meulen FB, Eertman CJ, Hom HW, van Putten MJAM. 2012. Continuous electroencephalography monitoring for early prediction of neurological outcome in postanoxic patients after cardiac arrest: A prospective cohort study*. *Critical Care Medicine* **40**:2867–2875. doi:10.1097/CCM.0b013e31825b94f0
- Coleman KA, Mitrofanis J. 1996. Organization of the Visual Reticular Thalamic Nucleus of the Rat. *European Journal of Neuroscience* **8**:388–404. doi:10.1111/j.1460-9568.1996.tb01222.x
- Conley M, Diamond IT. 1990. Organization of the Visual Sector of the Thalamic Reticular Nucleus in Galago. Evidence that the dorsal lateral geniculate and pulvinar nuclei occupy

- separate parallel tiers. *Eur J Neurosci* **2**:211–226. doi:10.1111/j.1460-9568.1990.tb00414.x
- Conley M, Schmechel DE, Diamond IT. 1991. Differential Distribution of Somatostatin-like Immunoreactivity in the Visual Sector of the Thalamic Reticular Nucleus in Galago. *Eur J Neurosci* **3**:237–242. doi:10.1111/j.1460-9568.1991.tb00085.x
- Contreras D, Curró Dossi R, Steriade M. 1993. Electrophysiological properties of cat reticular thalamic neurones in vivo. *The Journal of Physiology* **470**:273–294. doi:10.1113/jphysiol.1993.sp019858
- Contreras D, Steriade M. 1997. State-dependent fluctuations of low-frequency rhythms in corticothalamic networks. *Neuroscience* **76**:25–38. doi:10.1016/s0306-4522(96)00392-2
- Crabtree JW. 1996. Organization in the somatosensory sector of the cat's thalamic reticular nucleus. *J Comp Neurol* **366**:207–222. doi:10.1002/(SICI)1096-9861(19960304)366:2<207::AID-CNE2>3.0.CO;2-9
- Crabtree JW. 1992. The Somatotopic Organization Within the Cat's Thalamic Reticular Nucleus. *European Journal of Neuroscience* **4**:1352–1361. doi:10.1111/j.1460-9568.1992.tb00160.x
- Crabtree JW, Collingridge GL, Isaac JTR. 1998. A new intrathalamic pathway linking modality-related nuclei in the dorsal thalamus. *Nat Neurosci* **1**:389–394. doi:10.1038/1603
- Crabtree JW, Killackey HP. 1989. The Topographic Organization and Axis of Projection within the Visual Sector of the Rabbit's Thalamic Reticular Nucleus. *Eur J Neurosci* **1**:94–109. doi:10.1111/j.1460-9568.1989.tb00777.x
- Cucchiari JB, Uhlrich DJ, Sherman SM. 1991. Electron-microscopic analysis of synaptic input from the perigeniculate nucleus to the A-laminae of the lateral geniculate nucleus in cats. *J Comp Neurol* **310**:316–336. doi:10.1002/cne.903100304
- Dement W, Kleitman N. 1957. The relation of eye movements during sleep to dream activity: an objective method for studying dreaming. *Journal of Experimental Psychology* **53**:339.
- Destexhe A, Contreras D, Sejnowski TJ, Steriade M. 1994. Modeling the control of reticular thalamic oscillations by neuromodulators. *Neuroreport* **5**:2217–2220. doi:10.1097/00001756-199411000-00003
- Donlea JM, Pimentel D, Talbot CB, Kempf A, Omoto JJ, Hartenstein V, Miesenböck G. 2018. Recurrent Circuitry for Balancing Sleep Need and Sleep. *Neuron* **97**:378–389.e4. doi:10.1016/j.neuron.2017.12.016
- Douglas Rodney J., Martin KAC. 2004. Neuronal Circuits of the Neocortex. *Annual Review of Neuroscience* **27**:419–451. doi:10.1146/annurev.neuro.27.070203.144152
- Douglas Rodney J, Martin KAC. 2004. Neuronal circuits of the neocortex. *Annu Rev Neurosci* **27**:419–451.
- Einevoll GT, Kayser C, Logothetis NK, Panzeri S. 2013. Modelling and analysis of local field potentials for studying the function of cortical circuits. *Nature Reviews Neuroscience* **14**:770–785.

- Ermentrout B. 1998. Neural networks as spatio-temporal pattern-forming systems. *Rep Prog Phys* **61**:353–430. doi:10.1088/0034-4885/61/4/002
- Ferron J-F, Kroeger D, Chever O, Amzica F. 2009. Cortical Inhibition during Burst Suppression Induced with Isoflurane Anesthesia. *Journal of Neuroscience* **29**:9850–9860. doi:10.1523/JNEUROSCI.5176-08.2009
- Fisher RS, Engel JJ. 2010. Definition of the postictal state: When does it start and end? *Epilepsy & Behavior* **19**:100–104. doi:10.1016/j.yebeh.2010.06.038
- Fitzpatrick D. 1996. The functional organization of local circuits in visual cortex: insights from the study of tree shrew striate cortex. *Cerebral Cortex* **6**:329–341.
- Fitzpatrick D, Raczkowski D. 1990. Innervation patterns of single physiologically identified geniculocortical axons in the striate cortex of the tree shrew. *Proceedings of the National Academy of Sciences* **87**:449–453.
- Friedman EB, Sun Y, Moore JT, Hung H-T, Meng QC, Perera P, Joiner WJ, Thomas SA, Eckenhoff RG, Sehgal A, Kelz MB. 2010. A Conserved Behavioral State Barrier Impedes Transitions between Anesthetic-Induced Unconsciousness and Wakefulness: Evidence for Neural Inertia. *PLoS One* **5**:e11903. doi:10.1371/journal.pone.0011903
- Fritz BA, Kalarickal PL, Maybrier HR, Muench MR, Dearth D, Chen Y, Escallier KE, Ben Abdallah A, Lin N, Avidan MS. 2016. Intraoperative Electroencephalogram Suppression Predicts Postoperative Delirium. *Anesthesia & Analgesia* **122**:234–242. doi:10.1213/ANE.0000000000000989
- Gao S, Proekt A, Renier N, Calderon DP, Pfaff DW. 2019. Activating an anterior nucleus gigantocellularis subpopulation triggers emergence from pharmacologically-induced coma in rodents. *Nat Commun* **10**:2897. doi:10.1038/s41467-019-10797-7
- Garcia P, Kolesky S, Jenkins A. 2010. General Anesthetic Actions on GABAA Receptors. *CN* **8**:2–9. doi:10.2174/157015910790909502
- Gervasoni D, Lin S-C, Ribeiro S, Soares ES, Pantoja J, Nicolelis MAL. 2004. Global Forebrain Dynamics Predict Rat Behavioral States and Their Transitions. *J Neurosci* **24**:11137–11147. doi:10.1523/JNEUROSCI.3524-04.2004
- Gibbs FA, Gibbs EL, Lennox WG. 1937. Effect on the electro-encephalogram of certain drugs which influence nervous activity. *Arch Intern Med* **60**:54–166.
- Gilbert C, Wiesel T. 1983. Clustered intrinsic connections in cat visual cortex. *J Neurosci* **3**:1116–1133. doi:10.1523/JNEUROSCI.03-05-01116.1983
- Gilbert CD. 1992. Horizontal integration and cortical dynamics. *Neuron* **9**:1–13.
- Gold C, Henze DA, Koch C, Buzsáki G. 2006. On the Origin of the Extracellular Action Potential Waveform: A Modeling Study. *Journal of Neurophysiology* **95**:3113–3128. doi:10.1152/jn.00979.2005
- Goldstein PA. 2015. HCN1 Channels as Targets for Volatile Anesthetics: Coming to the Fore. *Anesthesia & Analgesia* **121**:594–596. doi:10.1213/ANE.0000000000000871

- Hagihira S. 2015. Changes in the electroencephalogram during anaesthesia and their physiological basis. *British Journal of Anaesthesia* **115**:i27–i31. doi:10.1093/bja/aev212
- Halassa MM, Sherman SM. 2019. Thalamocortical Circuit Motifs: A General Framework. *Neuron* **103**:762–770. doi:10.1016/j.neuron.2019.06.005
- Hale PT, Jervie Sefton A, Baur LA, Cottee LJ. 1982. Interrelations of the rat's thalamic reticular and dorsal lateral geniculate nuclei. *Experimental Brain Research* **45**:217–229.
- Hambrecht-Wiedbusch VS, Li D, Mashour GA. 2017. Paradoxical Emergence. *Anesthesiology* **126**:482–494. doi:10.1097/ALN.0000000000001512
- Hao X, Ou M, Zhang D, Zhao W, Yang Y, Liu J, Yang H, Zhu T, Li Y, Zhou C. 2020. The Effects of General Anesthetics on Synaptic Transmission. *CN* **18**:936–965. doi:10.2174/1570159X18666200227125854
- Hara K, Harris RA. 2002. The Anesthetic Mechanism of Urethane: The Effects on Neurotransmitter-Gated Ion Channels. *Anesth Analg* **94**:313–318.
- Harris RM. 1987. Axon collaterals in the thalamic reticular nucleus from thalamocortical neurons of the rat ventrobasal thalamus. *The Journal of Comparative Neurology* **258**:397–406.
- Hartigan JA, Hartigan PM. 1985. The Dip Test of Unimodality. *The Annals of Statistics* **13**:70–84.
- Harting JK, van Lieshout DP, Feig S. 1991. Connectional studies of the primate lateral geniculate nucleus: Distribution of axons arising from the thalamic reticular nucleus of Galago crassicaudatus. *J Comp Neurol* **310**:411–427. doi:10.1002/cne.903100310
- Hemmings HC, Akabas MH, Goldstein PA, Trudell JR, Orser BA, Harrison NL. 2005. Emerging molecular mechanisms of general anesthetic action. *Trends in Pharmacological Sciences* **26**:503–510. doi:10.1016/j.tips.2005.08.006
- Herold KF, Hemmings Jr. HC. 2012. Sodium Channels as Targets for Volatile Anesthetics. *Front Pharmacol* **3**. doi:10.3389/fphar.2012.00050
- Herrera CG, Cadavieco MC, Jago S, Ponomarenko A, Korotkova T, Adamantidis A. 2016. Hypothalamic feedforward inhibition of thalamocortical network controls arousal and consciousness. *Nature Neuroscience* **19**:290–298. doi:10.1038/nn.4209
- Hesse S, Kreuzer M, Hight D, Gaskell A, Devari P, Singh D, Taylor NB, Whalin MK, Lee S, Sleight JW, García PS. 2019. Association of electroencephalogram trajectories during emergence from anaesthesia with delirium in the postanaesthesia care unit: an early sign of postoperative complications. *British Journal of Anaesthesia* **122**:622–634. doi:10.1016/j.bja.2018.09.016
- Hirsch JA, Gallagher CA, Alonso J-M, Martinez LM. 1998. Ascending Projections of Simple and Complex Cells in Layer 6 of the Cat Striate Cortex. *J Neurosci* **18**:8086–8094. doi:10.1523/JNEUROSCI.18-19-08086.1998
- Hodgkin AL, Huxley AF. 1952. A quantitative description of membrane current and its application to conduction and excitation in nerve. *J Physiol* **117**:500–544.

- Hofmeijer J, Tjepkema-Cloostermans MC, van Putten MJAM. 2014. Burst-suppression with identical bursts: A distinct EEG pattern with poor outcome in postanoxic coma. *Clinical Neurophysiology* **125**:947–954. doi:10.1016/j.clinph.2013.10.017
- Hu B, Steriade M, Desche[^]nes M. 1989. The effects of brainstem peribrachial stimulation on perigeniculate neurons: The blockage of spindle waves. *Neuroscience* **31**:1–12. doi:10.1016/0306-4522(89)90026-2
- Huber R, Felice Ghilardi M, Massimini M, Tononi G. 2004. Local sleep and learning. *Nature* **430**:78–81. doi:10.1038/nature02663
- Hudson AE, Calderon DP, Pfaff DW, Proekt A. 2014. Recovery of consciousness is mediated by a network of discrete metastable activity states. *Proceedings of the National Academy of Sciences* **111**:9283–9288. doi:10.1073/pnas.1408296111
- Hudspith MJ. 1997. Glutamate: a role in normal brain function, anaesthesia, analgesia and CNS injury. *British Journal of Anaesthesia* **78**:731–747. doi:10.1093/bja/78.6.731
- Ibrahim AE, Ghoneim MM, Kharasch ED, Epstein RH, Groudine SB, Ebert TJ, Binstock WB, Philip BK, the Sevoflurane Sedation Study Group. 2001. Speed of Recovery and Side-effect Profile of Sevoflurane Sedation Compared with Midazolam. *Anesthesiology* **94**:87–94. doi:10.1097/00000542-200101000-00018
- Iftinca MC. 2011. Neuronal T-type calcium channels: What`s new? **4**:13.
- Ishizawa Y, Ahmed OJ, Patel SR, Gale JT, Sierra-Mercado D, Brown EN, Eskandar EN. 2016a. Dynamics of Propofol-Induced Loss of Consciousness Across Primate Neocortex. *Journal of Neuroscience* **36**:7718–7726. doi:10.1523/JNEUROSCI.4577-15.2016
- Ishizawa Y, Ahmed OJ, Patel SR, Gale JT, Sierra-Mercado D, Brown EN, Eskandar EN. 2016b. Dynamics of Propofol-Induced Loss of Consciousness Across Primate Neocortex. *Journal of Neuroscience* **36**:7718–7726. doi:10.1523/JNEUROSCI.4577-15.2016
- Izhikevich EM. 2007. Dynamical systems in neuroscience: the geometry of excitability and bursting, Computational neuroscience. Cambridge, Mass: MIT Press.
- Jackson MB, Yakel JL. 1995. The 5-HT₃ Receptor Channel. *Annu Rev Physiol* **57**:447–468.
- Jahnsen H, Llinás R. 1984. Ionic basis for the electro-responsiveness and oscillatory properties of guinea-pig thalamic neurones in vitro. *The Journal of Physiology* **349**:227–247. doi:10.1113/jphysiol.1984.sp015154
- Jiang-Xie L-F, Yin L, Zhao S, Prevosto V, Han B-X, Dzirasa K, Wang F. 2019. A Common Neuroendocrine Substrate for Diverse General Anesthetics and Sleep. *Neuron* **102**:1053-1065.e4. doi:10.1016/j.neuron.2019.03.033
- John ER, Prichep LS, Kox W, Valdés-Sosa P, Bosch-Bayard J, Aubert E, Tom M, diMichele F, Gugino LD. 2001. Invariant Reversible QEEG Effects of Anesthetics. *Consciousness and Cognition* **10**:165–183. doi:10.1006/ccog.2001.0507
- Joiner WJ, Friedman EB, Hung H-T, Koh K, Sowcik M, Sehgal A, Kelz MB. 2013. Genetic and Anatomical Basis of the Barrier Separating Wakefulness and Anesthetic-Induced Unresponsiveness. *PLoS Genet* **9**:e1003605. doi:10.1371/journal.pgen.1003605

- Jones BE. 2003. Arousal systems. *Front Biosci* **8**:s438-451. doi:10.2741/1074
- Jones EG. 2009. Synchrony in the interconnected circuitry of the thalamus and cerebral cortex. *Annals of the New York Academy of Sciences* **1157**:10–23.
- Jones EG. 2001. The thalamic matrix and thalamocortical synchrony. *Trends Neurosci* **24**:595–601. doi:10.1016/s0166-2236(00)01922-6
- Jones EG. 1975. Some aspects of the organization of the thalamic reticular complex. *J Comp Neurol* **162**:285–308.
- Katz LC. 1987. Local circuitry of identified projection neurons in cat visual cortex brain slices. *J Neurosci* **7**:1223–1249.
- Kaul HL, Bharti DN. 2002. Monitoring depth of anaesthesia. *Indian Journal of Anaesthesia* **10**.
- Kelly ML, Peters RA, Tisdale RK, Lesku JA. 2015. Unihemispheric sleep in crocodylians? *Journal of Experimental Biology* **218**:3175–3178. doi:10.1242/jeb.127605
- Kelz MB, Sun Y, Chen J, Cheng Meng Q, Moore JT, Veasey SC, Dixon S, Thornton M, Funato H, Yanagisawa M. 2008. An essential role for orexins in emergence from general anesthesia. *Proc Natl Acad Sci U S A* **105**:1309–1314. doi:10.1073/pnas.0707146105
- Kendall-Bar JM, Vyssotski AL, Mukhametov LM, Siegel JM, Lyamin OI. 2019. Eye state asymmetry during aquatic unihemispheric slow wave sleep in northern fur seals (*Callorhinus ursinus*). *PLoS ONE* **14**:1–13. doi:10.1371/journal.pone.0217025
- Kreuz T, Bozanic N, Mulansky M. 2015. SPIKE-Synchronization: a parameter-free and time-resolved coincidence detector with an intuitive multivariate extension. *BMC Neurosci* **16**:P170, 1471-2202-16-S1-P170. doi:10.1186/1471-2202-16-S1-P170
- Krueger JM, Tononi G. 2011. Local Use-Dependent Sleep; Synthesis of the New Paradigm. *Current Topics in Medicinal Chemistry* **11**:2490–2492. doi:10.2174/156802611797470330
- Larsen B, Seitz A, Larsen R. 2000. Recovery of Cognitive Function After Remifentanyl-Propofol Anesthesia: A Comparison with Desflurane and Sevoflurane Anesthesia. *Anesthesia & Analgesia* **90**:168–174. doi:10.1097/00000539-200001000-00035
- Larson EC. 1965. W. T. G. Morton and the Ether Dome. *JAMA* **194**:1151. doi:10.1001/jama.1965.03090230119043
- Lee DD, Seung HS. 1999. Learning the parts of objects by non-negative matrix factorization. *Nature* **401**:788–791. doi:10.1038/44565
- Lee H, Wang S, Hudetz AG. 2020. State-Dependent Cortical Unit Activity Reflects Dynamic Brain State Transitions in Anesthesia. *J Neurosci* **40**:9440–9454. doi:10.1523/JNEUROSCI.0601-20.2020
- Lee U, Ku S, Noh G, Baek S, Choi B, Mashour GA. 2013. Disruption of Frontal–Parietal Communication by Ketamine, Propofol, and Sevoflurane. *Anesthesiology* **118**:1264–1275. doi:10.1097/ALN.0b013e31829103f5
- Leistritz L, Jäger H, Schelenz C, Witte H, Putsche P, Specht M, Reinhart K. 1999. New approaches for the detection and analysis of electroencephalographic burst-suppression patterns in

- patients under sedation. *Journal of Clinical Monitoring and Computing* **15**:357–367. doi:10.1023/A:1009990629797
- Li L, Vlisides PE. 2016. Ketamine: 50 Years of Modulating the Mind. *Front Hum Neurosci* **10**. doi:10.3389/fnhum.2016.00612
- Lindén H, Pettersen KH, Einevoll GT. 2010. Intrinsic dendritic filtering gives low-pass power spectra of local field potentials. *J Comput Neurosci* **29**:423–444. doi:10.1007/s10827-010-0245-4
- Liu J, Lee HJ, Weitz AJ, Fang Z, Lin P, Choy M, Fisher R, Pinskiy V, Tolpygo A, Mitra P, Schiff N, Lee JH. 2015. Frequency-selective control of cortical and subcortical networks by central thalamus. *eLife* **4**:1–27. doi:10.7554/eLife.09215.001
- Lorente de Nó R, Davis L. 1947. *A Study of Nerve Physiology*. New York: Rockefeller Institute for Medical Research.
- Lu J, Sherman D, Devor M, Saper CB. 2006. A putative flip–flop switch for control of REM sleep. *Nature* **441**:589–594. doi:10.1038/nature04767
- Lund JS, Henry GH, Macqueen CL, Harvey AR. 1979. Anatomical organization of the primary visual cortex (area 17) of the cat. A comparison with area 17 of the macaque monkey. *The Journal of Comparative Neurology* **184**:599–618.
- Luo T, Leung LS. 2009. Basal Forebrain Histaminergic Transmission Modulates Electroencephalographic Activity and Emergence from Isoflurane Anesthesia. *Anesthesiology* **111**:725–733. doi:10.1097/ALN.0b013e3181b061a0
- Lyamin OI, Manger PR, Ridgway SH, Mukhametov LM, Siegel JM. 2008. Cetacean sleep: An unusual form of mammalian sleep. *Neuroscience and Biobehavioral Reviews* **32**:1451–1484. doi:10.1016/j.neubiorev.2008.05.023
- Mahowald MW, Schenck CH. 2005. Insights from studying human sleep disorders. *Nature* **437**:1279–1285. doi:10.1038/nature04287
- Maier KL, McKinstry-Wu AR, Palanca BJA, Tarnal V, Blain-Moraes S, Basner M, Avidan MS, Mashour GA, Kelz MB. 2017. Protocol for the Reconstructing Consciousness and Cognition (ReCCognition) Study. *Front Hum Neurosci* **11**:284. doi:10.3389/fnhum.2017.00284
- Mankad S, Michailidis G. 2013. Structural and functional discovery in dynamic networks with non-negative matrix factorization. *Phys Rev E* **88**:042812. doi:10.1103/PhysRevE.88.042812
- Martin KA, Whitteridge D. 1984. Form, function and intracortical projections of spiny neurones in the striate visual cortex of the cat. *J Physiol* **353**:463–504.
- Mashour GA. 2006a. Integrating the Science of Consciousness and Anesthesia: *Anesthesia & Analgesia* **103**:975–982. doi:10.1213/01.ane.0000232442.69757.4a
- Mashour GA. 2006b. Monitoring consciousness: EEG-based measures of anesthetic depth. *Seminars in Anesthesia, Perioperative Medicine and Pain* **25**:205–210. doi:https://doi.org/10.1053/j.sane.2006.09.007

- Mashour GA, Forman SA, Campagna JA. 2005. Mechanisms of general anesthesia: from molecules to mind. *Best Practice & Research Clinical Anaesthesiology* **19**:349–364. doi:10.1016/j.bpa.2005.01.004
- McCormick DA, Pape HC. 1990. Properties of a hyperpolarization-activated cation current and its role in rhythmic oscillation in thalamic relay neurones. *The Journal of Physiology* **431**:291–318. doi:10.1113/jphysiol.1990.sp018331
- McKinstry-Wu AR, Wasilczuk AZ, Harrison BA, Bedell VM, Sridharan MJ, Breig JJ, Pack M, Kelz MB, Proekt A. 2019. Analysis of stochastic fluctuations in responsiveness is a critical step toward personalized anesthesia. *eLife* **8**:e50143. doi:10.7554/eLife.50143
- McLeod DR, Griffiths RR, Bigelow GE, Yingling J. 1982. An automated version of the digit symbol substitution test (DSST). *Behavior Research Methods & Instrumentation* **14**:463–466. doi:10.3758/BF03203313
- Miller KJ, Sorensen LB, Ojemann JG, den Nijs M. 2009. Power-Law Scaling in the Brain Surface Electric Potential. *PLoS Comput Biol* **5**:e1000609. doi:10.1371/journal.pcbi.1000609
- Millett D. 2001. Hans Berger: From Psychic Energy to the EEG. *Perspectives in Biology and Medicine* **44**:522–542. doi:10.1353/pbm.2001.0070
- Milstein J, Mormann F, Fried I, Koch C. 2009. Neuronal Shot Noise and Brownian 1/f² Behavior in the Local Field Potential. *PLoS ONE* **4**:e4338. doi:10.1371/journal.pone.0004338
- Monk TG, Saini V, Weldon BC, Sigl JC. 2005. Anesthetic Management and One-Year Mortality After Noncardiac Surgery. *Anesthesia & Analgesia* **100**:4–10. doi:10.1213/01.ANE.0000147519.82841.5E
- Montero VM. 1983. Ultrastructural identification of axon terminals from the thalamic reticular nucleus in the medial geniculate body in the rat: An EM autoradiographic study. *Exp Brain Res* **51**. doi:10.1007/BF00237870
- Montero VM, Guillery RW, Woolsey CN. 1977. Retinotopic organization within the thalamic reticular nucleus demonstrated by a double label autoradiographic technique. *Brain Research* **138**:407–421. doi:10.1016/0006-8993(77)90681-3
- Montero VM, Scott GL. 1981. Synaptic terminals in the dorsal lateral geniculate nucleus from neurons of the thalamic reticular nucleus: A light and electron microscope autoradiographic study. *Neuroscience* **6**:2561–2577. doi:10.1016/0306-4522(81)90102-0
- Moore JT, Chen J, Han B, Meng QC, Veasey SC, Beck SG, Kelz MB. 2012. Direct Activation of Sleep-Promoting VLPO Neurons by Volatile Anesthetics Contributes to Anesthetic Hypnosis. *Current Biology* **22**:2008–2016. doi:10.1016/j.cub.2012.08.042
- Moruzzi G, Magoun HW. 1949. Brain stem reticular formation and activation of the EEG. *Electroencephalography and Clinical Neurophysiology* **1**:455–473. doi:10.1016/0013-4694(49)90219-9
- Muly EC, Fitzpatrick D. 1992. The morphological basis for binocular and ON/OFF convergence in tree shrew striate cortex. *J Neurosci* **12**:1319–1334.

- Nelson LE, Guo TZ, Lu J, Saper CB, Franks NP, Maze M. 2002. The sedative component of anesthesia is mediated by GABAA receptors in an endogenous sleep pathway. *Nat Neurosci* **5**:979–984. doi:10.1038/nn913
- Nir Y, Staba RJ, Andrillon T, Vyazovskiy VV, Cirelli C, Fried I, Tononi G. 2011. Regional Slow Waves and Spindles in Human Sleep. *Neuron* **70**:153–169. doi:10.1016/j.neuron.2011.02.043
- Nunez PL, Srinivasan R. 2006. *Electric Fields of the Brain: The Neurophysics of EEG*, 2nd ed. Oxford University Press.
- Ohara PT, Lieberman AR. 1985. The thalamic reticular nucleus of the adult rat: experimental anatomical studies. *J Neurocytol* **14**:365–411. doi:10.1007/BF01217752
- Ohara PT, Sefton AJ, Lieberman AR. 1980. Mode of termination of afferents from the thalamic reticular nucleus in the dorsal lateral geniculate nucleus of the rat. *Brain Research* **197**:503–506. doi:10.1016/0006-8993(80)91136-1
- Ohiorhenuan IE, Mechler F, Purpura KP, Schmid AM, Hu Q, Victor JD. 2010. Sparse coding and high-order correlations in fine-scale cortical networks. *Nature* **466**:617–621. doi:10.1038/nature09178
- Ohtahara S, Yamatogi Y. 2003. Epileptic Encephalopathies in Early Infancy With Suppression-Burst: *Journal of Clinical Neurophysiology* **20**:398–407. doi:10.1097/00004691-200311000-00003
- Owen AB, Perry PO. 2009. Bi-cross-validation of the SVD and the nonnegative matrix factorization. *Ann Appl Stat* **3**. doi:10.1214/08-AOAS227
- Pahor AL. 1992. Ear, Nose and Throat in Ancient Egypt. *J Laryngol Otol* **106**:677–687. doi:10.1017/S0022215100120560
- Pan B, Zucker RS. 2009. A General Model of Synaptic Transmission and Short-Term Plasticity. *Neuron* **62**:539–554. doi:10.1016/j.neuron.2009.03.025
- Patel SR, Ballesteros JJ, Ahmed OJ, Huang P, Briscoe J, Eskandar EN, Ishizawa Y. 2020. Dynamics of recovery from anaesthesia-induced unconsciousness across primate neocortex. *Brain* **143**:833–843. doi:10.1093/brain/awaa017
- Pettersen KH, Hagen E, Einevoll GT. 2008. Estimation of population firing rates and current source densities from laminar electrode recordings. *J Comput Neurosci* **24**:291–313. doi:10.1007/s10827-007-0056-4
- Pinault D, Bourassa J, Deschênes M. 1995. Thalamic reticular input to the rat visual thalamus: a single fiber study using biocytin as an anterograde tracer. *Brain Research* **670**:147–152.
- Pinault D, Deschênes M. 1998. Projection and innervation patterns of individual thalamic reticular axons in the thalamus of the adult rat: A three-dimensional, graphic, and morphometric analysis. *J Comp Neurol* **391**:180–203. doi:10.1002/(SICI)1096-9861(19980209)391:2<180::AID-CNE3>3.0.CO;2-Z
- Pinault D, Smith Y, Deschênes M. 1997. Dendrodendritic and Axoaxonic Synapses in the Thalamic Reticular Nucleus of the Adult Rat. *J Neurosci* **17**:3215–3233. doi:10.1523/JNEUROSCI.17-09-03215.1997

- Poulet JFA, Petersen CCH. 2008. Internal brain state regulates membrane potential synchrony in barrel cortex of behaving mice. *Nature* **454**:881–885. doi:10.1038/nature07150
- Purpura DP. 1968. Role of synaptic inhibition in synchronization of thalamocortical activity. *Prog Brain Res* **22**:107–122. doi:10.1016/s0079-6123(08)63499-8
- Quairiaux C, Megevand P, Kiss JZ, Michel CM. 2011. Functional Development of Large-Scale Sensorimotor Cortical Networks in the Brain. *Journal of Neuroscience* **31**:9574–9584. doi:10.1523/JNEUROSCI.5995-10.2011
- Radtke FM, Franck M, Lendner J, Krüger S, Wernecke KD, Spies CD. 2013. Monitoring depth of anaesthesia in a randomized trial decreases the rate of postoperative delirium but not postoperative cognitive dysfunction. *BJA: British Journal of Anaesthesia* **110**:i98–i105. doi:10.1093/bja/aet055
- Rampil IJ, Sasse FJ, Smith NT, Hoff BH, Flemming DC. 1980. Spectral edge frequency: A new correlate of anesthetic depth. *Anesthesiology* **53**:S12.
- Rattenborg NC, Meij JVD, Beckers GJL, Lesku JA. 2019. Local aspects of avian non-rem and rem sleep. *Frontiers in Neuroscience* **13**:1–16. doi:10.3389/fnins.2019.00567
- Raz A, Grady SM, Krause BM, Uhlrich DJ, Manning KA, Banks MI. 2014. Preferential effect of isoflurane on top-down vs. bottom-up pathways in sensory cortex. *Frontiers in Systems Neuroscience* **8**:191. doi:10.3389/fnsys.2014.00191
- Rector DM, Topchiy IA, Carter KM, Rojas MJ. 2005. Local functional state differences between rat cortical columns. *Brain Research* **1047**:45–55. doi:10.1016/j.brainres.2005.04.002
- Reitz SL, Wasilczuk AZ, Beh GH, Proekt A, Kelz MB. 2021. Activation of Preoptic Tachykinin 1 Neurons Promotes Wakefulness over Sleep and Volatile Anesthetic-Induced Unconsciousness. *Current Biology* **31**:394-405.e4. doi:10.1016/j.cub.2020.10.050
- Rikhye RV, Gilra A, Halassa MM. 2018. Thalamic regulation of switching between cortical representations enables cognitive flexibility. *Nat Neurosci* **21**:1753–1763. doi:10.1038/s41593-018-0269-z
- Rose J, Weiser TG, Hider P, Wilson L, Gruen RL, Bickler SW. 2015. Estimated need for surgery worldwide based on prevalence of diseases: a modelling strategy for the WHO Global Health Estimate. *The Lancet Global Health* **3**:S13–S20. doi:10.1016/S2214-109X(15)70087-2
- Saczynski JS, Marcantonio ER, Quach L, Fong TG, Gross A, Inouye SK, Jones RN. 2012. Cognitive Trajectories after Postoperative Delirium. *New England Journal of Medicine* **367**:30–39. doi:10.1056/NEJMoa1112923
- Sanchez-Vives MV, McCormick DA. 2000. Cellular and network mechanisms of rhythmic recurrent activity in neocortex. *Nature Neuroscience* **3**:1027–1034. doi:10.1038/79848
- Saper CB, Fuller PM, Pedersen NP, Lu J, Scammell TE. 2010. Sleep State Switching. *Neuron* **68**:1023–1042. doi:10.1016/j.neuron.2010.11.032
- Saper CB, Lu J, Chou TC, Gooley J. 2005. The hypothalamic integrator for circadian rhythms. *Trends in Neurosciences* **28**:152–157. doi:10.1016/j.tins.2004.12.009

- Sara SJ. 2009. The locus coeruleus and noradrenergic modulation of cognition. *Nature Reviews Neuroscience* **10**:211.
- Särkelä M, Mustola S, Seppänen T, Koskinen M, Lepola P, Suominen K, Juvonen T, Tolvanen-Laakso H, Jäntti V. 2002. Automatic analysis and monitoring of burst suppression in anesthesia. *Journal of Clinical Monitoring and Computing* **17**:125–134. doi:10.1023/A:1016393904439
- Scammell TE, Arrigoni E, Lipton J. 2017. Neural circuitry of wakefulness and sleep. *Neuron* **93**:747–765. doi:10.1016/j.physbeh.2017.03.040
- Schiff ND. 2008. Central thalamic contributions to arousal regulation and neurological disorders of consciousness. *Annals of the New York Academy of Sciences* **1129**:105–118. doi:10.1196/annals.1417.029
- Schneidman E, Berry MJ, Segev R, Bialek W. 2006. Weak pairwise correlations imply strongly correlated network states in a neural population. *Nature* **440**:1007–1012. doi:10.1038/nature04701
- Schomer DL, Lopes da Silva FH. 2018. *Niedermeyer’s Electroencephalography: Basic Principles, Clinical Applications, and Related Fields*, 7th ed. Oxford University Press.
- Schwartz JRL, Roth T. 2008. Neurophysiology of sleep and wakefulness: Basic science and clinical implications. *Current Neuropharmacology* **6**:367–378. doi:10.1080/10580530.2014.958342
- Seeman P. 1972. The membrane actions of anesthetics and tranquilizers. *Pharmacological Reviews* **24**:583–655.
- Self MW, Kerkoerle T van, Supèr H, Roelfsema PR. 2013. Distinct roles of the cortical layers of area V1 in figure-ground segregation. *Current biology* **23**:2121–2129. doi:10.1016/j.cub.2013.09.013
- Sessler DI, Sigl JC, Kelley SD, Chamoun NG, Manberg PJ, Saager L, Kurz A, Greenwald S. 2012. Hospital Stay and Mortality Are Increased in Patients Having a “Triple Low” of Low Blood Pressure, Low Bispectral Index, and Low Minimum Alveolar Concentration of Volatile Anesthesia. *Anesthesiology* **116**:1195–1203. doi:10.1097/ALN.0b013e31825683dc
- Soehle M, Dittmann A, Ellerkmann RK, Baumgarten G, Putensen C, Guenther U. 2015. Intraoperative burst suppression is associated with postoperative delirium following cardiac surgery: a prospective, observational study. *BMC Anesthesiol* **15**:61. doi:10.1186/s12871-015-0051-7
- Solt K, Cotten JF, Cimenser A, Wong KFK, Chemali JJ, Brown EN. 2011. Methylphenidate Actively Induces Emergence from General Anesthesia. *Anesthesiology* **115**:791–803. doi:10.1097/ALN.0b013e31822e92e5
- Stecker MM, Cheung AT, Pochettino A, Kent GP, Patterson T, Weiss SJ, Bavaria JE. 2001. Deep hypothermic circulatory arrest: I. Effects of cooling on electroencephalogram and evoked potentials. *The Annals of Thoracic Surgery* **71**:14–21. doi:10.1016/S0003-4975(00)01592-7

- Steinberg EA, Wafford KA, Brickley SG, Franks NP, Wisden W. 2015. The role of K2P channels in anaesthesia and sleep. *Pflugers Arch - Eur J Physiol* **467**:907–916. doi:10.1007/s00424-014-1654-4
- Steriade M. 2004. Acetylcholine systems and rhythmic activities during the waking--sleep cycle. *Prog Brain Res* **145**:179–196. doi:10.1016/S0079-6123(03)45013-9
- Steriade M, Amzica F. 1998. Slow sleep oscillation, rhythmic K-complexes, and their paroxysmal developments. *Journal of Sleep Research* **7**:30–35. doi:10.1046/j.1365-2869.7.s1.4.x
- Steriade Mircea, Amzica F, Contreras D. 1994. Cortical and thalamic cellular correlates of electroencephalographic burst-suppression. *Electroencephalography and Clinical Neurophysiology* **90**:1–16. doi:10.1016/0013-4694(94)90108-2
- Steriade M., Amzica F, Contreras D. 1994. Cortical and thalamic cellular correlates of electroencephalographic burst-suppression. *Electroencephalography and Clinical Neurophysiology* **90**:1–16. doi:10.1016/0013-4694(94)90108-2
- Steriade M., Amzica F, Nunez A. 1993. Cholinergic and noradrenergic modulation of the slow (approximately 0.3 Hz) oscillation in neocortical cells. *Journal of Neurophysiology* **70**:1385–1400. doi:10.1152/jn.1993.70.4.1385
- Steriade M, Apostol V, Oakson G. 1971. Control of unitary activities in cerebellothalamic pathway during wakefulness and synchronized sleep. *Journal of Neurophysiology* **34**:389–413. doi:10.1152/jn.1971.34.3.389
- Steriade M, Deschênes M. 1987. Inhibitory processes in the thalamus. *The Journal of Mind and Behavior* **8**:559–571.
- Steriade M, Deschenes M. 1984. The thalamus as a neuronal oscillator. *Brain Res* **320**:1–63.
- Steriade M, Deschenes M, Domich L, Mulle C. 1985. Abolition of spindle oscillations in thalamic neurons disconnected from nucleus reticularis thalami. *Journal of Neurophysiology* **54**:1473–1497. doi:10.1152/jn.1985.54.6.1473
- Steriade M, Dossi R, Nunez A. 1991. Network modulation of a slow intrinsic oscillation of cat thalamocortical neurons implicated in sleep delta waves: cortically induced synchronization and brainstem cholinergic suppression. *J Neurosci* **11**:3200–3217. doi:10.1523/JNEUROSCI.11-10-03200.1991
- Steriade M, Jones EG, Llinás RR. 1990. Thalamic oscillations and signaling. New Jersey: John Wiley & Sons.
- Steriade M, Llinás RR. 1988. The functional states of the thalamus and the associated neuronal interplay. *Physiological Reviews* **68**:649–742. doi:10.1152/physrev.1988.68.3.649
- Steriade M, McCarley RW. 1990. Brainstem Control of Wakefulness and Sleep. Boston, MA: Springer.
- Steriade Mircea, McCormick DA, Sejnowski TJ. 1993a. Thalamocortical Oscillations in the Sleeping and Aroused Brain. *Science* **262**:679–685. doi:10.1126/science.8235588

- Steriade Mircea, Nunez A, Amzica F. 1993b. A novel slow (< 1 Hz) oscillation of neocortical neurons in vivo: depolarizing and hyperpolarizing components. *J Neurosci* **13**:3252–3265. doi:10.1523/JNEUROSCI.13-08-03252.1993
- Strogatz SH. 2015. *Bifurcations Nonlinear Dynamics and Chaos: With Applications to Physics, Biology, Chemistry, and Engineering*. Boca Raton: CRC Press. pp. 45–94.
- Sullivan R. 1996. The identity and Work of the Ancient Egyptian Surgeon. *J R Soc Med* **89**:467–473. doi:10.1177/014107689608900813
- Takahashi K, Lin JS, Sakai K. 2009. Characterization and mapping of sleep-waking specific neurons in the basal forebrain and preoptic hypothalamus in mice. *Neuroscience* **161**:269–292. doi:10.1016/j.neuroscience.2009.02.075
- Tang A, Jackson D, Hobbs J, Chen W, Smith JL, Patel H, Prieto A, Petrusca D, Grivich MI, Sher A, Hottowy P, Dabrowski W, Litke AM, Beggs JM. 2008. A Maximum Entropy Model Applied to Spatial and Temporal Correlations from Cortical Networks In Vitro. *J Neurosci* **28**:505–518. doi:10.1523/JNEUROSCI.3359-07.2008
- Tassonyi E, Charpentier E, Muller D, Dumont L, Bertrand D. 2002. The role of nicotinic acetylcholine receptors in the mechanisms of anesthesia. *Brain Research Bulletin* **57**:133–150. doi:10.1016/S0361-9230(01)00740-7
- Thomas SA, Matsumoto AM, Palmiter RD. 1995. Noradrenaline is essential for mouse fetal development. *Nature* **374**:643–646. doi:10.1038/374643a0
- Thomson DJ. 1982. Spectrum estimation and harmonic analysis. *Proc IEEE* **70**:1055–1096. doi:10.1109/PROC.1982.12433
- Timofeev I, Grenier F, Steriade M. 2004. Contribution of Intrinsic Neuronal Factors in the Generation of Cortically Driven Electrographic Seizures. *Journal of Neurophysiology* **92**:1133–1143. doi:10.1152/jn.00523.2003
- Timofeev I, Steriade M. 1996. Low-frequency rhythms in the thalamus of intact-cortex and decorticated cats. *J Neurophysiol* **76**:4152–4168. doi:10.1152/jn.1996.76.6.4152
- Timo-laria C, Negràò N, Schmidek WR, Hoshino K, de Menezes CEL, da Rocha TL. 1970. Phases and states of sleep in the rat. *Physiology & Behavior* **5**:1057–1062. doi:10.1016/0031-9384(70)90162-9
- Tkačik G, Marre O, Amodei D, Schneidman E, Bialek W, li MJB. 2014. Searching for Collective Behavior in a Large Network of Sensory Neurons. *PLOS Computational Biology* **10**:e1003408. doi:10.1371/journal.pcbi.1003408
- Tkačik G, Schneidman E, Berry II MJ, Bialek W. 2006. Ising models for networks of real neurons. *arXiv:q-bio/0611072*.
- Usrey WM, Fitzpatrick D. 1996. Specificity in the axonal connections of layer VI neurons in tree shrew striate cortex: evidence for distinct granular and supragranular systems. *The Journal of Neuroscience* **16**:1203–1218.
- Usrey WM, Muly EC, Fitzpatrick D. 1992. Lateral geniculate projections to the superficial layers of visual cortex in the tree shrew. *The Journal of Comparative Neurology* **319**:159–171.

- Vacanti CJ, Van Houten RJ, Hill RC. 1970. A statistical analysis of the relationship of physical status to postoperative mortality in 68,388 cases. *Anesthesia & Analgesia* **49**:564–566.
- Vazey EM, Aston-Jones G. 2014. Designer receptor manipulations reveal a role of the locus coeruleus noradrenergic system in isoflurane general anesthesia. *Proc Natl Acad Sci U S A* **111**:3859–3864. doi:10.1073/pnas.1310025111
- Velayos JL, Jiménez-Castellanos Jr. J, Reinoso-Suárez F. 1989. Topographical organization of the projections from the reticular thalamic nucleus to the intralaminar and medial thalamic nuclei in the cat. *The Journal of Comparative Neurology* **279**:457–469.
- Victor JD, Drover JD, Conte MM, Schiff ND. 2011. Mean-field modeling of thalamocortical dynamics and a model-driven approach to EEG analysis. *PNAS* **108**:15631–15638. doi:10.1073/pnas.1012168108
- Vutskits L, Xie Z. 2016. Lasting impact of general anaesthesia on the brain: mechanisms and relevance. *Nat Rev Neurosci* **17**:705–717. doi:10.1038/nrn.2016.128
- Vyazovskiy V, Borbely AA, Tobler I. 2000. Unilateral vibrissae stimulation during waking induces interhemispheric EEG asymmetry during subsequent sleep in the rat. *J Sleep Res* **9**:367–371. doi:10.1046/j.1365-2869.2000.00230.x
- Vyazovskiy VV, Olcese U, Hanlon EC, Nir Y, Cirelli C, Tononi G. 2011. Local sleep in awake rats. *Nature* **472**:443–447. doi:10.1038/nature10009
- Warnaby CE, Sleight JW, Hight D, Jbabdi S, Tracey I. 2017. Investigation of Slow-wave Activity Saturation during Surgical Anesthesia Reveals a Signature of Neural Inertia in Humans. *Anesthesiology* **127**:645–657. doi:10.1097/ALN.0000000000001759
- Watson PL, Shintani AK, Tyson R, Pandharipande PP, Pun BT, Ely EW. 2008. Presence of electroencephalogram burst suppression in sedated, critically ill patients is associated with increased mortality: *Critical Care Medicine* **36**:3171–3177. doi:10.1097/CCM.0b013e318186b9ce
- Wickelgren WA. 1977. Speed-accuracy tradeoff and information processing dynamics. *Acta Psychologica* **41**:67–85. doi:10.1016/0001-6918(77)90012-9
- Witten IH, Frank E, Hall MA. 2011. Data mining: practical machine learning tools and techniques, 3rd ed. ed, Morgan Kaufmann series in data management systems. Burlington, MA: Morgan Kaufmann.
- Woodcock TE, Murkin JM, Farrar JK, Tweed WA, Guiraudon GM, McKenzie FN. 1987. Pharmacologic EEG Suppression during Cardiopulmonary Bypass. *Anesthesiology* **67**:218–224. doi:10.1097/00000542-198708000-00011
- Yael D, Vecht JJ, Bar-Gad I. 2018. Filter-Based Phase Shifts Distort Neuronal Timing Information. *Eneuro* **5**:ENEURO.0261-17.2018. doi:10.1523/eneuro.0261-17.2018
- Yu S, Huang D, Singer W, Nikolic D. 2008. A small world of neuronal synchrony. *Cereb Cortex* **18**:2891–2901. doi:10.1093/cercor/bhn047
- Zhang Y, Laster MJ, Hara K, Harris RA, Li EIE, Stabernack CR, Sonner JM. 2003. Glycine Receptors Mediate Part of the Immobility Produced by Inhaled Anesthetics. *Anesthetic Pharmacology* **96**:97–101.

- Zhang Z, Ferretti V, Güntan İ, Moro A, Steinberg EA, Ye Z, Zecharia AY, Yu X, Vyssotski AL, Brickley SG, Yustos R, Pillidge ZE, Harding EC, Wisden W, Franks NP. 2015. Neuronal ensembles sufficient for recovery sleep and the sedative actions of $\alpha 2$ adrenergic agonists. *Nat Neurosci* **18**:553–561. doi:10.1038/nn.3957
- Zhao P, Yu X, Kagemoto Y. 2018. Was Mafeisan an Anesthetic in Ancient China? *Journal of Anesthesia History* **4**:177–181. doi:10.1016/j.janh.2018.01.009
- Zhou W, Cheung K, Kyu S, Wang L, Guan Z, Kurien PA, Bickler PE, Jan LY. 2018. Activation of orexin system facilitates anesthesia emergence and pain control. *Proc Natl Acad Sci USA* **115**:E10740–E10747. doi:10.1073/pnas.1808622115
- Zilles K, Palomero-Gallagher N. 2017. Multiple Transmitter Receptors in Regions and Layers of the Human Cerebral Cortex. *Front Neuroanat* **11**:78. doi:10.3389/fnana.2017.00078